Università degli Studi di Firenze
XXI PhD Course in Chemical Sciences

Interactions of Nucleolipids with Oligonucleotides

Silvia Milani

Tutor: Prof. Piero Baglioni

PhD Thesis
University of Florence
2008

PhD Coordinator:
Prof. Gianni Cardini

Prof. Giacomo Martini

CHIM02- Physical Chemistry

A mio Marito

Index

INTRODUCTION **v**

Bibliography viii

PART I

Chapter 1 **1**

Membranes **1**

1.1 Phase Behaviour of the Lipid Bilayers 1
1.2 Structural parameters 5
1.3 Fluctuations in Membranes 6
1.4 Hydration of lipid Membranes 7

Bibliography 10

Chapter 2 **13**

Nucleolipid Membranes: Pure and Mixed **13**

2.1 Structural Investigation of Bilayers Formed by 1-Palmitoyl-2-Oleoylphosphatidylnucleosides 14
2.2 Mixed POPA/POPU Membranes: Molecular Recognition between Base-Complementary Lipids 24
2.3 Effect of "Helper Lipid" in Nucleolipid Membrane 32

Bibliography 42

Chapter 3 **45**

A new paradigm: Nucleolipoplexes **45**

3.1 Nucleolipids Bilayers-Nucleic Acids Interactions 46
3.1.1. Single strand DNA interaction with Nucleolipids Membranes 57
3.2 Intercalation of Single Strand Oligonucleotides in-between POPN:POPC membranes 60

Bibliography 66

PART II

Chapter 4 69

Liposomes as Therapeutic delivery Vehicles 69
4.1 Classification and Preparation of liposomes 70
4.2 Cationic Liposomes-DNA Complexes 72
4.3 Cytotoxicity issues applicable to lipoplexes in gene-therapy 74
4.4 Other Liposomes Delivery Systems for DNA transfer 76
Anionic Liposomes 76
Zwitterionic Liposomes 76
Stabilized plasmid-lipid particles (SPLP) 77

Bibliography 78

Chapter 5 81

Hybrid Structures between Nucleolipid liposomes and Oligonucleotides 81
5.1 Effect of Buffer on Nucleolipids/Polynucleotides interaction 81
TRIS Buffer 83
TRIS/KCl Buffer 93
Phosphate Buffer 98
5.2 Effect of Oligonucleotides length on POPA liposomes 104
5.3 A Cryo-TEM investigation on Oligonucleotides and Nucleolipids Mixtures in solution 108

Bibliography 115

Chapter 6 117

Complexes between Nucleolipid/liposomes and DNA 117
6.1 Structural and Spectroscopic investigation on Nucleolipids liposomes and ds-DNA 118
6.1.1 Circular Dichroism on 50dAdT double strand 125
6.1.2 Detecting ds-DNA with molecular probes 127
6.2 Nuclolipoplexes by Optical Microscopy 128

Bibliography 132

PART III

Chapter 7 133

Material and Methods **133**
7.1 Materials 133
7.2 Sample preparation 134
7.3 Methods 136
7.3.1 Small Angle X-ray (SAXS and SAXD) 136
7.3.2 Neutron Diffraction Data Acquisition and Data Analysis 137
7.3.3 Light Scattering 138
7.3.4 Fourier Transform Infrared Spectroscopy (FTIR) 139
Transmission 139
FTIR Linear Dichroism 139
7.3.5 UV and Circular Dichroism 141
7.3.6 Cryo-TEM and Optical Microscopy 142
7.3.7 Differential Scanning Calorimetry (DSC) 142
Bibliography 143

Chapter 8 **145**

Concluding Remarks **145**
Bibliography 148

ACKNOWLEDGEMENTS **149**

Introduction

Phospholiphids, the scaffolding units of biological membranes, are naturally designed to divide cells from the rest of the environment and to segregate processes and components, using weak interactions that nonetheless lead to stable and functional structures. Chemists have soon realized that this fascinating ability of self-assembling, which occurs in living systems, could be reproduced and utilized. A great deal of surfactants were thus synthesized and a new science, Soft Matter, started up in investigating their properties and rich phase diagrams in aqueous solutions. Afterwards, scientists observed that even proteins and nucleic acids self-organize through weak interactions, which take place among a limited number of rather simple building blocks (i.e., amino acids and nucleic bases), leading eventually to mesoscopic structures. Many efforts have been devoted to mimic Nature's strategies and reproduce this kind of *bottom-up* approach in artificial systems. As a result, a "second generation" of amphiphilic self-assemblies has been modelled, where a chemical motif with precise functional properties or responsivity to external stimuli, was included in the amphiphilic polar heads. The ability to exploit self-organization of such functional molecular building blocks and the possibility to impart tuneable, responsive properties on the resulting aggregates has led to a dramatic growth in the activity and understanding of these self-assembled supramolecular structures[1-4]. Among biologically-inspired examples, peptide-amphiphiles[5] and oligonucleotide-amphiphiles[6-8] represent the most interesting and recent cases. In particular, these latter molecules join the self-assembly capability of lipids with the molecular recognition properties of nucleic acids, pointing out a potential further route to control auto-organization. The possibility to integrate nucleic acid motifs into amphiphilic molecules can lead to the formation of hybrid systems of such bio-inspired molecules with biopolymers (nucleic acids, proteins and so on). Therefore, it is possible to figure out the formation of extremely complex and fascinating structures with possible applications in many sectors. DNA-like nanofibers were, for example, formed by the interaction of thymidine bolaamphiphiles (a nucleotide with two thymine connected *via* an aliphatic spacer) with complementary oligoadenylic acid template[9], showing direct evidence for the formation of multiple hydrogen bonds between base pairs. DNA complexation by neutral nucleoside base amphiphiles[10] was also achievable thanks to the amphiphilic character of the molecule and the phosphate-sugar interactions. Remarkably, the uridine moiety attached to the polar head is involved in the stabilization of the complex itself. Supramolecular duplex *via* canonical Watson-Crick base paring were found by interaction of oligonucleotide-amphiphiles[11,12] with complementary nucleic acid strands as well, when the amphiphile is anchored into a membrane, indicating future strategies for antisense oligonucleotides gene-therapy or fabrication of efficient DNA-arrays.

In this scenario, where the regulation of the auto-organization and the understanding of the formation of these fascinating complex supramolecular structures is widely in progress, this study deals with nucleolipid derivatives; that is a class of molecules where the monomeric base of a nucleotide is attached to a lipidic double chain skeleton. Therefore, these amphiphilic molecules reproduce the chemistry and the same charge of DNA monomers, so representing a further challenge with respect to the previous mentioned systems regarding the nucleic acids interaction.

It has been reported that nucleolipids are able to exhibit molecular recognition by H-bond and π-stacking between complementary bases of different derivatives. It has been showed that actually the molecular recognition capability is triggered by the self-assembly and affects structural features of these aggregates: amphiphilic systems made of mixed "complementary" nucleolipids show deviations from ideal behaviour[13-15].

The main novelty and the aim of this study are to highlight, by means of the characterization of hybrid systems nucleolipid/oligonucleotides, how it is possible to modulate the aggregate morphology thanks to self-assembly and molecular recognition abilities both of nucleolipids and oligonucleotides. This goal can be accomplished investigating the rich phase behaviour of these aggregates. Furthermore, obtaining hybrid systems between negatively charged nucleolipids and oligonucleotides, it allows imagining future applications in other sectors, such as medical and pharmacological field.

In the last decades much attention has been devoted to the development of non-viral vectors to employ in gene therapy[16-18]. The motivation consists in finding drug delivery systems that can be less dangerous for human health and less cytotoxic for cells. Among the several non-viral DNA carriers, surfactants/DNA systems represent the most relevant class. However, cationic liposomes/DNA[19], commonly known as lipoplexes, are the most studied vehicles for DNA delivery and release, since some pioneering studies showed the formation of complexes with DNA. The driving force for complexation is charge interaction between negative DNA and cationic lipid headgroup. Many questions and concerns regarding their transfection efficiency and toxicity still stir debate and limit lipoplexes' applicability *in-vivo*. From a physico-chemical point of view, the major point to be addressed is a precise control of lipoplex size and stability with respect to aggregation and to the eventual precipitation. Besides the intrinsic toxicity of cationic amphiphiles, the size and charge of lipoplexes determine cell membrane crossing and DNA delivery into the cell nucleus. At this regard, aggregates with nucleolipids/DNA potentially represent alternative and less toxic lipid-based delivery systems for DNA. These assemblies provide negatively charged interfaces decorated with nucleic motifs that can complex complementary nucleic acid strands using, as driving force, molecular recognition instead of electrostatic interactions. In a recent investigation[20], it has been shown that globular micelles composed of 1,2-dioctanoyl-phosphatidyl-adenosine interact with complementary RNA single strands (ss-polyUridylic acid) forming a new hexagonal phase where the nucleic acids is confined amongst cylindrical micelles. This provides a proof-of-principle that complexation is

possible notwithstanding the same charge of both partners (i.e. lipid assembly and nucleic acid).

In this work the investigation has been focused on zero-curvature assemblies. Given the widespread use of these assemblies as drug-delivery devices, this research represents a further contribution towards the application of such supramolecular structures in biomedical field.

Nucleolipid membranes, formed by 1-Palmitoyl-2-Oleoylphosphatidyl-Nucleosides, POPN, have been studied with and without oligonucleotides. The effect of the water content, the length of the oligonucleotides, the difference in nucleolipids derivatives, the nucleolipids concentration and the presence of other lipids (i.e., neutral lipid) in determining either the interactions with nucleic acids or the morphology of the aggregates will be presented, analyzed and discussed throughout the manuscript.

Bibliography

(1) Luk, Y. Y.; Abbott, N. L. *Current Opinion in Colloid & Interface Science* **2002**, *7*, 567-275.

(2) Bonini, M.; Berti, D.; Di Meglio, J. M.; Almgren, M.; Teixeira, J.; Baglioni, P. *Soft Matter* **2005**, *6*, 444-454.

(3) Ambrosi, M.; Fratini, E.; Alfredsson, V.; Ninham, B. W.; Giorgi, R.; Lo Nostro, P.; Baglioni, P. *J. Am. Chem. Soc.* **2006**, *128*, 7209-7214.

(4) Berti, D.; Baglioni, P. *Current Opinion in Colloid & Interface Science* **2006**, *110*, 74-78.

(5) Tu, R. S.; Tirrell, M. *Advanced Drug Delivery Reviews* **2004**, *56*, 1537-1563.

(6) Rosemeyer, H. *Chemistry & Biodiversity* **2005**, *2*, 977-1063.

(7) Berti, D. *Current Opinion in Colloid & Interface Science* **2006**, *11*, 74-78.

(8) Gissot, A.; Camplo, M.; Grinstaff, M. W.; Barthelemy, P. *Org. Biomol. Chem.* **2008**, *6*, 1324-1333.

(9) Iwaura, R.; Yoshida, K.; Mitsutoshi, M.; Ohnishi-Kameyama, M.; Yoshida, M.; Shimizu, T. *Angew. Chem. Int. Ed.* **2003**, *42*, 1009-1012.

(10) Arigon, J.; Prata, M.; Grinstaff, M. W.; Barthelemy, P. *Bioconjugate Chem.* **2005**, *16*, 864-872.

(11) Bunge, A.; Kurz, A.; Windeck, A. K.; Korte, T.; Flasche, W.; Liebscher, J.; Herrmann, A.; Huster, D. *Langmuir* **2007**, *23*, 4455-4464.

(12) Kurz, A.; Bunge, A.; Windeck, A. K.; Rost, M.; Flasche, W.; Arbuzova, A.; Strohbach, D.; Mueller, S.; Liebscher, J.; Huster, D.; Herrmann, A. *Angew. Chem.-Int. Edit.* **2006**, *45*, 4440-4444.

(13) Berti, D.; Bonaccio, S.; Barsacchi-Bo, G.; Luisi, P. L.; Baglioni, P. *J. Phys. Chem. B* **1998**, *102*, 303-308.

(14) Berti, D.; Barbaro, P.; Bucci, I.; Baglioni, P. *J. Phys. Chem. B* **1999**, *103*, 4916-4922.

(15) Berti, D.; Baldelli Bombelli, F.; Fortini, F.; Baglioni, P. *J. Phys. Chem. B* **2007**, *111*, 11734-11744.

(16) Li, S.; Huang, L. *Gene Therapy* **2000**, *7*, 31-34.

(17) Cotten, M.; Wagner, E. *Curr. Opin. Biotech.* **1993**, *4*, 705-710.

(18) Mahato, R. I.; Kim, S. W. *Pharmaceutical Perspectives of Nucleic Acid-Based Therapeutics*; Taylor and Francis: London and New York, 2002.

(19) Felgner, L. P.; Gadek, R. T.; Holm, M.; Roman, R.; Chan, W. H.; Wenz, M.; Northrop, P. J.; Ringold, M. G.; Danielsen, M. *Proc. Natl. Acad. Sci.* **1987**, *84*, 7413-7417.

(20) Banchelli, M.; Berti, D.; Baglioni, P. *Angew. Chem.* **2007**, *47*, 3070 –3073.

PART I

Chapter 1

Membranes

Lipids adopt a wealth of shapes and structures depending on the water amount and on their chemical formula. A reason of their rich phase diagram can be found in hydrophilic and hydrophobic properties of the molecules, that is a balance between size and energy of their polar headgroup and tail. Physically speaking, this concept was proposed as the "molecular packing parameter" by Israelachvili, Mitchell and Ninham[1]. They demonstrated how size and shape of the aggregate at the equilibrium can be predicted from a combination of geometrical considerations and thermodynamic parameters. The packing parameter is defined as $v/a_0 l_c$ where l_c is the chain length, v is the volume of the chain and a_0 is the area at the water hydrocarbon interface. When the packing parameter is 1, the morphology of the lipid assembly is called lamellar phase (sketched in Figure1.1).

Lamellar phases of lipids were deeply studied due to the similarity with biological membranes determining their behaviour in function of the temperature, pH, ionic strength, pressure and water uptake.

1.1 Phase Behaviour of the Lipid Bilayers

Lamellar phases or bilayer phases can be found in Nature under physiological conditions mainly in liquid crystalline status (L_α). In this fluid phase, the lipid molecule tails are free and in general the area for polar head, which is the surface area occupied by a single polar head in the assembly, is large due to the chain mobility. This status is established by the amount of water (or water solvent) imbibed within the lamella and by temperature. However, the exact number of water molecules and the temperature at which the lamellar morphology occurs, are two parameters dependent on the molecular formula of the lipid itself.

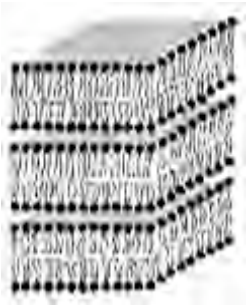

Figure1.1 Example of lamellar phase.

It is known that several categories of lipid exist: glycerolipids, glycerophospholipids, sphingolipids, sterol lipids, saccharolipids and fatty acids. All these lipids can be classified by their bulk behaviour in water. There are lipids as cholesterol - the more biologically relevant sterol lipid - that does not imbibe water at all. These lipids, indeed, do not form bilayers by themselves, even though they can intercalate into the membrane and influence its properties, stiffening the lamellae. Other lipids are also insoluble, but they can swell in water to form ordered mosophases. Many important components of cellular membranes belong to the former category, such as long-chain phosphatidylcholines, phosphatidylethaonamines, phostidylserine and sphingomyelin. All these lipids form lamellar phases, but having different molecular formula - different degree of chain unsaturation and charge - arrange in L_α membranes at different temperature and different water amount. From the previous sentence it is possible to infer that lipids are invariably polymorphic[2-4]; that is, the dynamic and organization of lamellar structure can vary, as presented below and illustrated in Figure1.2.

Most phospholipids form crystalline lamellar phases L_c at sufficiently low temperatures and/or hydration degree. These phases exhibit both long and short range order in three dimensions and are therefore true crystals. Generally, to observe this phase the lipids have to be kept frozen for long time. In this state, lipid chains are tightly packed and the rotation around their axis has severe restrictions. At low temperature lipids are usually in so-called the L_β gel-like phase. In this state the hydrocarbon chains exist predominantly in their rigid, extended, all-*trans* conformation. Increasing the temperature, the alkyl chains remain in an all-*trans* configuration while the headgroup dipole becomes disordered. When the area of the lipid headgroup exceeds twice that of the chain, the lipid tails tilt. This phase is still a gel phase, but is usually labelled $L_{\beta'}$. Moreover, when the tilting becomes too large, the so-called interdigitated $L_{\beta 1}$ phase may occur. In these phases the chain can slightly and slowly rotate.

Before the L_α phase it is sometimes possible to observe the ripple phase, $P_{\beta'}$[5]. In this phase the degree of *gauche* conformers is intermediate between the gel and the liquid crystalline phases. The origin is the different mobility of the polar headgroup, which bond new water molecules during the transition from gel to liquid crystalline phase. This phase has never been observed for unsaturated lipids. The reason is that the rippling in the lamellae is due to the tendency of the polar lipid

headgroup to achieve a certain degree of fluidity and solvation whilst the hydrocarbon chains remain ordered. Therefore, lamellar phase of this kind may be observed only if the polar headgroup are sufficiently hydrophilic and hydrated and if the inter-chain packing is sufficiently weak[6].

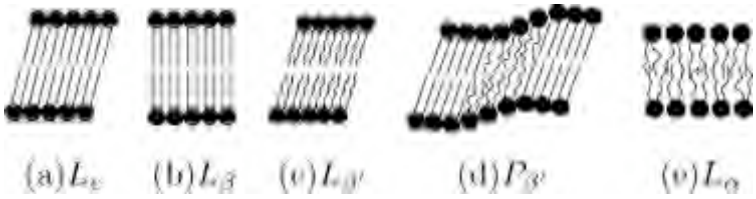

Figure1.2. Phase Structures of Lipids: crystalline L_c, untilted gel L_β, tilted gel $L_{\beta'}$, ripple phase $P_{\beta'}$ and liquid crystallone L_α.

From a biological point of view, the L_α, where the increased cross-sectional area can favour the diffusion of proteins, is surely the most interesting. For this reason the phase transition, termed the main phase transition, involving the conversion of a relatively ordered chain to a disordered liquid crystalline bilayer, has been intensively studied by means of several thecniques[7-10]. The temperature, at which this transition occurs, is called melting temperature (T_m).

The hydrocarbon chain melting is accompanied by a pronounced lateral expansion and usually the bilayer thickness decreases during the transition because of the increased volume of the molecules. The effects of the molecular formula and composition are thus enormous. The chain length is surely one of the most relevant parameters that have to be taken into account looking at this temperature. T_m usually increases with increased number of carbon atoms in the lipid chain. However, this increasing is not linear and it is also dependent on the number of unsaturations and branchings of the lipid chain. One single double bond in a chain may drop considerably the melting temperature and also the position of this bond in the chain has a noteworthy role in determining the decreasing of temperature transition. Although the study of the effect of the chain length on the melting temperature is complex, there are papers and reviews that permitted to trace back a prediction of the T_m[11,12]. On the other hand, an evaluation of the influence of the polar headgroup on thermotropic features of the bilayers is not an easy task. In general, it needs to allow for the size and polarity of the headgroup as well as the capability for forming hydrogen bonds. All these parameters are actually linked to the molecular packing parameters and to the hydrophilic properties that determine the membrane structure. Therefore, it is obvious that the headgroup size can affect the transition temperature. If the cross sectional area of the lipid headgroup is small the gel phase should be stabilized because of closer interactions among the chains. This should result in relatively higher phase transition temperature. However, this simple rule may change because of other factors. The charge can enhance or ease the interaction with other species as solvent molecules or ions and can even suppress the influence of other physical factor, such as headgroup size. For example DPPS (1,2-Dipalmitoyl-sn-Glycero-3-Phospho-L-Serine) has the main transition

temperature at 55ºC for physiological pH, when it is negatively charged, whereas its transition temperature decreases considerably introducing a further negative charge (32ºC). However, this lipid melts at higher temperatures than the neutral DPPC (1,2-dipalmitoyl-sn-glycero-3-phosphocholine), showing ability to interact by hydrogen bonds, which increase the stability of the gel phase and consequently raise the temperature[13,14].

Finally, the effect of the hydrogen bond is hard to predict and it is related to other factors (i.e. hydration). In fact, especially for fully hydrated membranes the lipid polar headgroups would rather interact with the solvent than hydrogen bond with each other.

As already mention and discussed below, hydration is one of the most important parameters that determines the kind of lamellar phase. Since increasing the hydration, the number of water molecules bounded to the polar headgroups grows - determining a different mobility or different arrangement of the polar head within the lamellae - increasing the water content usually tends to lower the chain transition temperature[15].

Among the numerous experimental techniques, Differential Scanning Calorimetry and Differential thermal Analysis have had a key role in characterizing the polymorphic behaviour of the lipid membranes[7,16,17]. The information, achievable by DSC and DTA analysis, are enthalpy, number of cooperation units and of course T_m. Observing the shape of the thermal peaks and its width at half-height, the sharpness of a phase transition can be measured. This can permit to determine the van't Hoff enthalpy as:

$$\Delta H_{vH} \simeq 4RT_m^{\,2} / \Delta T_{1/2} \qquad (1.1)$$

The ratio between $\Delta H_{vH} / \Delta H_{meas}$ (where ΔH_{meas} indicates the experimental value) gives a numerical evaluation of the cooperation among the lipid molecules in a bilayer, and it is named *number of cooperation unit*, CU. For a completely cooperative transition of an absolutely pure substance this parameter should be infinite, while for a non-cooperative process this ratio should approach the unit. Therefore, only a sharp and symmetric thermal peak should pop up during the gel-liquid crystalline transition for pure systems. Nonetheless, there are many cases in which the polar headgroup heterogeneity or the bilayers defects produce broad peaks.

The melting temperature can be determined also by means of other techniques, for example examining the bilayers spacing trend in a diffraction temperature scan. Even infrared spectroscopy measurements can yield information on the molecular packing in membranes and consequently provide details upon the polymorphic behaviour of the lipids[9,18-21]. Analysing a single spectrum, it is possible not only to determine the melting temperature, but also to measure the amount of imbibed water due to the infrared sensitivity for this molecule.

CH stretching vibrations give rise to bands between 3100-2800 cm^{-1}. These vibrations due to the bonds, located along all the lipid chain, shift in frequency in dependence of the molecular packing and/or the type of lamellar phase. In gel-like

lamellae, CH_2 stretching vibrations are located at 2918 and 2850 cm^{-1} for anti-symmetric and symmetric stretch respectively. The same vibrations are shifted towards higher frequencies, lower wavelengths (i.e. 2924 and 2852 cm^{-1}) when the L_α phase occurs. That corresponds to an abrupt band broadening, too. Even if the ripple phases do not induce huge structural packing transformation, it is possible to identify it from differences in the CH bending or by analysing the CH stretching trend with respect to the expected one for $L_{\beta'}$-L_α transition. C=O stretching mode can be analyzed as well as the CH modes. This bond is comprised of, at least, two different contributes assigned to *sn-1* (~1742 cm^{-1}) and *sn-2* (~1727 cm^{-1}) C=O groups. In this case increasing the temperature, the intensity of the *sn-1* bands and *sn-2* bands change, while there are no frequency shifts.

Moreover, infrared measurements permit to gather information on the number of *trans-gauche* conformers by study of CH_2 wagging motions in the region between 1180-1330 cm^{-1}[22-26].

1.2 Structural parameters

Considering the sketch of neighbouring bilayers depicted in Figure1, the first parameter that it is possible to define describing the structure, is the lattice spacing or the bilayer spacing, d. This parameter indicates the distance between two lamellae or better the space occupied by a bilayer and its hydration water. More relevant than the bilayer spacing are the parameters that it is possible to derive from; that is the bilayer thickness d_b and the water thickness d_w. These values are easily obtained by knowing the bilayer spacing and the volume fraction of the lipid:

$$d_b = d \cdot \phi_L \tag{1.2}$$

$$d = d_b - d_w \tag{1.3}$$

The bilayer thickness includes contributions from both hydrophilic and hydrophobic parts and so the next refinement level is to divide the bilayer into hydrocarbon thickness d_c and headgroup thickness d_h. All these parameters indicate the size of the lipid in between the lamellae, but there are other parameters that have to be considered and that are fundamental in describing lipid behaviour: the Surface Area per molecule, the Volume per molecule and the number of water molecules for lipid.

The Area, A, is related to thickness as two factors of the volume, V, as proposed by Luzzati in the simplest description of the bilayer[27]. However, to obtain correct values could be a challenge. This simple model, indeed, does not take in account the membrane fluctuations and furthermore d_b, as above defined, is based on a correct measurement of the water imbibed. Apart from possible errors in weighting, the amount of water obtained by gravimetric methods assume that all the water added to the system goes in between the lipid bilayers that are neatly stacked in regular one-dimensional arrays. The membranes, though, may have defects, which may hinder the correct water measurement, overestimating A. One indication

that there was problem with gravimetric method was that many studies came up with dissimilar values of the calculated number of water molecules. Even for the gel phase of DPPC, the Area varied from about 50 to 54Å^2; similar variations were obtained for L_α phases of DPPC, DMPC (1,2-dimyristoyl-sn-glycero-3-phosphocholine) and DOPC (1,2-dioleoyl-sn-glycero-3-phosphocholine)[28,29].

Two are the main experimental techniques for studying long-range order of membranes: Neutron and X-ray diffraction. Although electron diffraction has been employed to characterize lipid systems, one of the disadvantages is the necessity to work in vacuum to minimize the air scattering and of course the inability of the X-ray to distinguish the chain where electron density is relatively small. Neutron diffraction, for these reasons, has several extremely important advantages, namely the possibility of contrast variation.

NMR is and has been also used to study these systems, in particular fluid phases. The order parameter is related to the quadrupole splitting due to the fast rotation of the lipids molecules around their long axes that causes an averaging of nonaxial symmetric component of the interaction tensor. Measurements of the order parameter have provided a variety of values for Area as many as the diffraction methods.

Recently, a different way to use NMR to obtain *A* has been proposed. This is based on magic angle spinning measurements of the water proton signal, which has a different chemical shift depending upon whether the water is in bulk or it interacts with bilayers. Using this technique one should obtain the number of water molecules for lipid, which can be then used to obtain *A*[30-32].

There are many techniques to measure lipid volume: differential densimetry, differential weight, dilatometry. However, lipid volume may be calculated by $Ad_b = 2V_L$. Furthermore, estimates of the volumes of all the component groups have been obtained from computer simulations for DPPC, DOPC and POPC[33].

1.3 Fluctuations in Membranes

A stack of lipid bilayers can be labelled as one-dimensional (1D) array of two-dimensional fluids (2D). It is known, as stressed by de Gennes, that dimensionality is a crucial issue in studying order/disorder of a system. The order/disorder properties of a system are described by the correlations between system's building blocks. In particular, crystalline structures are described by the positional correlation functions. In a true crystal there is a long-range correlation, which means defined patterns of diffraction. On the other hand, fluids have short-range correlations and most of the scattering is diffuse. A typical diffraction pattern for liquid bilayers is therefore visible only at wide angle, where sizes are related to the intra-bilayers correlations. This said, the bilayers gives also low-angle scattering peaks due to their inter-bilayer correlation.

Due to the long and short range order properties, bilayers are not properly described by the Debye-Waller theory of the crystal scattering, whilst the quasi-long-range order holds. This long range order can be destroyed by fluctuactions;

therefore pair correlation function diverge logarithmically instead of remaining bonded as in a crystal.

Two kinds of fluctuations are then possible for liquid bilayers[34,35]: a short-range fluctuation that may affect only one single bilayer and a long-range fluctuation, which has an effect on all the bilayers. The latter kind of fluctuations are related to the change of the position with respect to the centre of the bilayers. This phenomenon needs high brilliance synchrotron X-ray diffraction to collect high quality data to be analysed[36-38].

The most important parameter in the theory of the scattering used to describe the former fluctuations is the Caillé's parameter:

$$\eta = \kappa_B T q^2 \Big/ 8\pi\sqrt{BK_c} \qquad (1.4)$$

where κ_B is the Boltzman's constant, q is the scattering vector, B is the compression modulus and K_c is the bending modulus for the stacks of bilayers. Large values of η causes a broadening of scattering peaks tails that behave asyntotically as $|q-q_h|^{-1+\eta}$ [39,40]. This means that this tail width increases with the diffraction order (h). Moreover, because of lipid polymorphism the fluctuations become higher in relation to temperature and composition of the membrane.

By and large, high order diffraction peaks disappear due to these effects and only a diffuse scattering is detectable.

1.4 Hydration of lipid Membranes

Water has a notable role in determining the geometry of lamellar phase, but how can water affect bilayers and which amount of water may be uptaken by different lipids?

It was stressed mainly by neutron diffraction thanks to the different scattering length between deuterium and hydrogen, that water usually does not penetrate in the chain region, even though water molecules can overlap with the headgroup molecules and diffuse across the bilayer[41]. This is a key point because the water depth was demonstrated to be a critical parameter in determining the organization and in understanding the properties of the membrane (i.e., proteins functionality and distribution of non-electrolytes)[42]. However, the total number of water molecules as well as the number of water molecules that interact with the polar head are inevitably related to the kind of lipid. For example, these numbers are deeply linked with the trend of the bilayer spacing and thickness. Thus, for neutral lipid bilayers it is possible to find that the bilayers spacing reaches a limiting value upon increasing water content. That is, neutral lipids can imbibe only a neat number of water molecules in between the lamellae, beyond that value any additional water molecule forms an excess of fluid phase. On the other hand, charged lipids do not show the previous trend, but can swell indefinitely. The reason of this different behaviour is

based on the fact that hydration process is a balance of several effects that regard both *inter*-bilayer (interaction perpendicular to the plane of the bilayer) and *intra*-bilayer (interaction in the plane of the bilayers) forces. In excess of water, several attractive and repulsive forces rule the equilibrium distance between adjacent bilayers. The hydration, steric, electrostatic and fluctuation forces are repulsive whereas the Van der Waals and intermolecular bonding are attractive components.

The hydration repulsion relies on the binding, polarization and reorganization of water molecules near the surface of the bilayers and follows the form:

$$P_h = P_0 \exp\left(-\frac{d}{\lambda}\right) \qquad (1.5)$$

where λ is the decay length that is dependent on the solvent packing. The electrostatic pressure described by the Gouy-Chapman double layers theory explains the infinite swelling of charged lipids. In this case the electrostatic force overwhelms any long-range attractive force, mainly the Van der Waals pressure. It was found that also neutral lipids containing various divalent cations can swell infinitely. This behaviour was explained by the fact that cations could bind the phosphate moiety and therefore an electrostatic repulsion pressure is added to the bilayers, like for naturally charged membranes.

In the previous paragraph, fluctuations give rise to a force that break down the order of bilayers, thereby it is repulsive. This force is inversely proportional to the bending modulus and to the fluid space between the lamellae. This implies that the fluctuations are negligible in gel phase compared to hydration pressure, whereas for fluid phase fluctuation effects are dominant. The presence of fluctuation forces explains also why liquid crystalline phases imbibe more water than crystalline bilayers do. Moreover, the fluctuations could also clarify why preparation method strongly influences the maximum water content for neutral lipids. Different amounts of water were found for membranes that absorbed water from fixed relative humidity atmosphere or from a bulk aqueous phase. Well-ordered stacks of multibilayers contain less energetically induced undulation that lamellae obtained by vigorous vortex mixing of the powder and water. This difference in undulation accounts for their higher water uptake.

Sometimes it happens, though, that hydration cannot be explained solely in terms of the previous contributions. Phosphatidylserine bilayers containing Li^+ or divalent cations, in fact, imbibe only a small amount of water. That was discussed in terms of specific binding of the hydrophilic cation on the serine headgroup, which might withdraw the solvation[43]. More challenging is the case for phosphatylethanolamine bilayers. This membrane was found to have a little fluid space in comparison with their charge. The more reliable hypothesis was thought to be a strong hydrogen-bond between opposite bilayers[44].

The effect on morphology of lipid bilayers was studied by dehydration experiments. These investigations showed that the subtraction of water does not determine a dramatic change of the bilayer morphology in the first stage, corresponding to no or minor modifications in the bilayers thickness. On the other

hand, huge variations of morphology are originated from further dehydration. When additional water molecules are subtracted from the headgroup region, the area for polar headgroup decreases and the bilayer thickness increases. Taking away a considerable volume, about 30 $Å^3$ for water molecules, from the polar headgroup determines a squeezing of the hydrocarbon chain, rising the melting temperature transition[45].

Bibliography

(1) Isrealachvili, j.; Mitchell, D. J.; Ninham, B. W. *J. Chem. Soc. Faraday Trans.* **1976**, *72*, 1525.

(2) Seddon, J. M.; Templer, R. H. In *Handbook of Biological Physics*; Lipowsky, L.; Sackmann, E., Eds.; Elsevier, 1995; Vol. 1, pp 97-160.

(3) Blume, A. *Thermochimica Acta* **1991**, *193*, 299-347.

(4) Seddon, J. M.; Cevc, G. In *Phospholipids Handbook*; Cevc, G., Ed.; Marcel Dekker, 1993; pp 403-433.

(5) Kodama, M.; Kuwabara, M.; Seki, S. *Biochim. Biophys. Acta* **1982**, *689*, 567-570.

(6) Cevc, G. *Biochim. Biophys. Acta* **1991**, *1062*, 59-69.

(7) McElhaney, R. *Chem. Phys. Lipids* **1982**, *30*, 229-259.

(8) Lewis, N. A. H. R.; McElhaney, R. In *The Structure of Biological Membrane*; Yeagle, Ed.; CRC Press, 1992.

(9) Casal, L. H.; Mantsch, H. H. *Biochim. Biophys. Acta* **1984**, *779*, 381-401.

(10) Seddon, J. M.; Harlos, H.; Marsh, D. *J. Biol. Chem.* **1983**, *258*, 3850-3854.

(11) Cevc, G. *Biochemistry* **1987**, *26*, 6305-6310.

(12) Cevc, G. *Biochemistry* **1991**, *30*, 7186-7193.

(13) Cevc, G.; Watt, a.; Marsh, D. *Biochemistry* **1981**, *20*, 4955-4965.

(14) MacDonald, C. R.; Simon, A. S.; Bear, E. *Biochemistry* **1976**, *15*, 885-891.

(15) Cevc, G.; Marsh, D. *Biophys.J.* **1985**, *47*, 21-31.

(16) Bach, D. In *Biomembrane Structure and Function*; Chapman, D., Ed.; Verlag Chemie GmbH, 1984; pp 1-41.

(17) Blume, A. *Thermochimica Acta* **1991**, *193*, 299-347.

(18) Mendelsohn, R.; Snyder, R. In *Biological Membranes*; Merz, K.; Roux, B., Eds.; Birkhäuser, 1996; pp 145-174.

(19) Tamm, K. L.; Tatulian, A. S. *Quaternary Reviews of Biophysics* **1997**, *30*, 365-429.

(20) Lis, L. J.; McAlister, M.; Fuller, N.; Rand, R. P.; Parsigian, V. A. *Biophys. J.* **1982**, *37*, 657-666.

(21) Ruocco, M. J.; Shipley, G. G. *Biochim. Biophys. Acta* **1982**, *691*, 309-320.

(22) Tuchtenhagen, J.; Ziegler, W.; Blume, A. *Eu. Biophys. J.* **1994**, *23*, 323-335.

(23) Davies, A. M.; Hubner, W.; Blume, A.; Mendelsohn, R. *Biophys. J.* **1992**, *63*, 1059-1062.

(24) Ziegler, W.; Blume, A. *Spectrochimica Acta Part A* **1995**, *51*, 1763-1778.

(25) Casal, L. H.; McElhaney, R. *Biochemistry* **1990**, *29*, 5423-5427.

(26) Senak, L.; Davies, A. M.; Mendelsohn, R. *J. Phys. Chem.* **1991**, *95*, 2565-2571.

(27) Luzzati, V.; Husson, F. *J. Cell. Biol.* **1962**, *12*, 207-219.

(28) Nagle, F. J.; Tristram-Nagle, S. *Biochim. Biophys. Acta* **2000**, *779*, 381-401.
(29) Rand, R. P.; Parsigian, V. A. *Biochim. Biophys. Acta* **1989**, *988*, 351-376.
(30) Koenig, B. W.; Strey, H. H.; Gawrisch, K. *Biophys. J.* **1997**, *73*, 1954-1966.
(31) Zhou, Z.; Sayer, B. G.; Hughes, D. W.; Stark, R. E.; Epand, R. M. *Biophys. J.* **1999**, *76*, 387-399.
(32) Nagle, F. J.; Liu, Y.; Tristram-Nagle, S.; Epand, R. M.; Stark, R. E. *Biophys. J.* **1999**, *77*, 2062-2065.
(33) Armen, R. S.; Uitto, O. D.; Feller, S. E. *Biophys. J.* **1998**, *75*, 734-744.
(34) Zhang, R.; Sun, W.; Tristram-Nagle, S.; Headrick, R. L.; Suter, M. R.; Nagle, F. J. *Phys. Rev. Letter* **1995**, *74*, 2832-2835.
(35) Zhang, R.; Suter, M. R.; Nagle, F. J. *Phys. Rev. E* **1994**, *50*, 5047-5060.
(36) Safinya, R. C.; Roux, D.; Smith, S. G.; Sinha, K. S.; Dimon, P.; Clark, N. A.; Bellocq, A. M. *Phys. Rev. Letter* **1986**, *57*, 2718-2721.
(37) Petrache, H.; Gouliaev, N.; Tristram-Nagle, S.; Zhang, R.; Suter, M. R. *Phys. Rev. E* **1998**, *57*, 7014-7024.
(38) Coldren, A. B.; Warriner, H.; van Zanten, R.; Zasadzinski, A. J. *Langmuir* **2006**, *22*, 2474-2481.
(39) Sornette, D.; Ostrowsky, N. In *Micelles, Membranes, Microemulsion and Monolayers*; Gelbart, M. W.; Ben-Shaul, A.; Roux, D., Eds.; Sringer-Verlag pp 251-302.
(40) Roux, D.; Safinya, R. C.; Nallet, F. In *Micelles, Membranes, Microemulsion and Monolayers*; Gelbart, M. W.; Ben-Shaul, A.; Roux, D., Eds.; Sringer-Verlag Vol. 303-346.
(41) McIntosh, J. T.; Magid, D. A. In *Phospholipids Handbook*; Cevc, G., Ed.; Marcel Dekker pp 553-577.
(42) Simon, A. S.; McIntosh, J. T. *Methods in Enzimology* **1986**, *127*, 511-521.
(43) Hauser, H.; Shipley, G. G. *Biochemistry* **1983**, *22*, 2171-2178.
(44) Rand, R. P.; Fuller, N.; Parsigian, V. A.; Rau, C. D. *Biochemistry* **1988**, *27*, 7711-7722.
(45) McIntosh, J. T.; Magid, D. A.; Simon, A. S. *Biochemistry* **1987**, *26*, 7325-7332.

Chapter 2

Nucleolipid Membranes: Pure and Mixed

Hybrids molecules composed of two or more molecular moieties are present both in Nature and in synthetic chemistry. In Nature, one of the most beautiful examples is certainly the nucleic acid double strand, DNA. This molecule made up from a stack of nucleic bases (purine and pyrimidine) attached by means of a sugar phosphate backbone is regulated by molecular recognition energies, namely hydrogen bond and stacking between complementary bases. However, base recognition can be displayed only if the bases are attached to a covalent supramolecular structure. This concept has inspired the design of a variety of hybrid molecules, called nucleolipids, which are nucleic acid bases or oligonucleotides anchored to a lipid skeleton. The lipid capability of self-organization can favour molecular recognition between the bases in the lipid assembly as well as the interaction with DNA or RNA. Therefore, the rationale is to employ this kind of molecules in gene-delivery or other biomedical or pharmaceutical application.

Among the several classes of nucleolipids recently reviewed by Rosemeyer[1], this thesis deals with phosphathidylnucleosides. They belong to a new class of anionic lipid surfactants, having a double chain and a glycerol backbone. The complex behaviour of lipids that was briefly described in the previous chapter justifies an extended study on the phase diagram of this molecule. Moreover, thinking about nucleic base polar head that meaningfully may alter lipid aggregation, the necessity of a chemical physical characterization becomes mandatory.

The following paragraphs will examine those nucleolipids that assemble in lamellar phases thanks to their long hydrocarbon tails, reviewing the swelling behaviour of nucleolipid membranes. Moreover, the role of different kinds of polar headgroup will be highlighted in terms of alteration of the bilayer structural properties. The effect of other lipid upon the nucleolipid bilayers organization will be also investigated.

2.1 Structural Investigation of Bilayers Formed by 1-Palmitoyl-2-Oleoylphosphatidylnucleosides

1-Palmitoyl-2-Oleoylphosphatidylnucleosides (POPN) have two hydrocarbon chains with a sufficient length to guarantee bilayer assembly. The spectroscopic properties of long chain derivatives, assembled as liposomes in phosphate buffer, indicated base interactions through stacking and H-bonding modes[2,3]. Therefore, to check the structural characteristics of these bilayers and to understand better the mutual orientation of the bases in the assembly, a study of these aggregates in a low water content regime has been performed.

The lipids investigated were POP-Adenosine and POP-Uridine (Figure 2.1). The choice of unsaturated derivatives was straightforward since, as recalled in the previous chapter, the incorporation of *cis* double bond into a saturated lipid chain drastically lowers the main phase transition. Thus, these bilayers are expected to be in liquid crystalline state at room and/or physiological temperature; where wider functionality for medical and pharmaceutical applications in view of possible interactions with oligonucleotides, can be envisaged.

These molecules differ from their synthetic precursor POPC (1-Palmitoyl-2-Oleoyl-sn-glycero-3-Phosphocholine) in the nature of their polar headgroup and of course in charge.

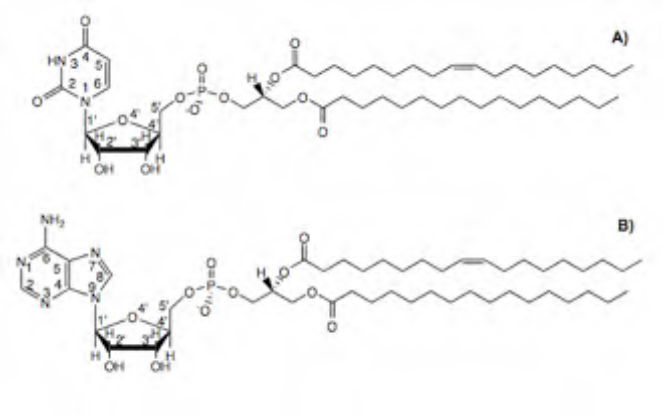

Figure2.1. Schematic drawing of the molecular structure of 1-Palmitoyl-2-Oleoyl-sn-glycero-3-Uridine (A) 1-Palmitoyl-2-Oleoyl-sn-glycero-3-Adenosine (B).

Charge is a relevant parameter; the electrostatic forces determine the lyotropic behaviour of membranes. Therefore, the expected trend for POPA and POPU, anionic lipids, is an unlimited swelling, whereas for POPC, zwitterionic lipid, a swelling limit is expected. However, speaking of lipids and in particular about lipids that have such particular a polar head, other forces should be taken in account in addition to the energies discussed in chapter1. From this point of view, POPA and POPU not only differ from POPC, but also one from the other.

SAXD and gravimetric experiments showed that the water uptake for the two derivatives is different. This dissimilarity was found irrespective of the preparation method, whether sample was obtained from powder or evaporation from organic solvent. In the first method, pastes were obtained weighting the correct amount of water, which was added directly to lipid powder and homogenized by mechanical agitation. In the second, stacks of lamellae were prepared spreading lipids dissolved in an organic solvent mixture over a solid support, drying and then re-hydrating them in controlled relative humidity. Preparation methods indeed can produce a different amount of undulations within the membranes, in particular when an excess of water is considered, producing subtle variations. However, this phenomenon does not explain why POPA lamellar phases always result less hydrated then POPU bilayers.

Gravimetric experiments performed on re-hydrated films resulted in 17±3 water molecules for POPU and only 9±3 for POPA lamellae. This different behaviour in water uptake was encountered both for ammonium and for sodium nucleolipid salts, highlighting no particular effect of the nature of the counter-ion on the lamellar phase behaviour. SAXD experiments performed on the sodium salts allow us to evaluate a number of water molecules in the "full hydration" condition in good agreement with the number obtained for the ammonium derivatives by gravimetric measurements (Table 2.1). Moreover, SAXD experiments show a trend of the observed smectic period for POPU lamellae that increases in value with the water content, whereas POPA membrane smectic thickness followed an asymptotic trend that resemble neutral lipid rather than anionic lipid one (Figure2.2).

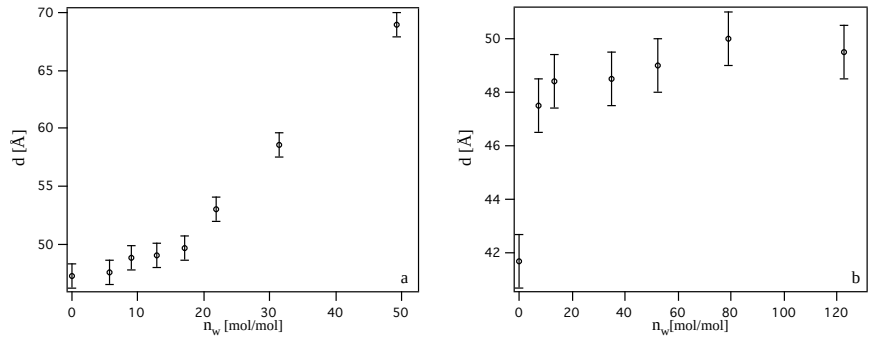

Figure2.2. Bilayers spacings d versus the number of water molecules n_w for POPU/Na^+ (a) and POPA/Na^+ (b) lamellar phases.

Beside the fact that POPA lamellae imbibe by far less water than POPU does, this amount is also smaller than the one found for POPC (n_w = 10) bilayers where lack of the charge should favour the interaction and then stabilization of mulilamellar stacks. Since the acyl chains are the same, we can attribute any deviation to different steric hindrance and to interactions at the interface region of the membranes. Following this logic any differences between POPA and POPU should be explained in view of possibly "attractive" interaction between patterns. A reasonable working hypothesis for explaining such peculiar behaviour might be

related to the stacking constant of the adenosine motif. It is well known from NMR experiments that stacking interactions among nucleic bases follow the trend *purine-purine* > *purine-pyrimidine* > *pyrimidine-pyrimidine*[4,5]. This might cause favourable interactions that could partially oppose double-layer repulsion and hinder interbilayer water insertion for POPA lamellar phase.

Table2.1. Bilayer spacing versus water content as determined by SAXS

Lipid/water % [w/w]	n_w	POPA/Na^+ d[Å]	POPU/Na^+ d[Å]
dry	0±2	41.7±0.5	47.0±0.5
0.10	7±2	47.5±0.5	47.5±0.5
0.15	9±2	48.0±0.5	48.5±0.5
0.20	13±2	48.5±0.5	49.0±0.5
0.25	17±2	#	49.7±0.5
0.30	22±2	48.7±0.5	50.0±0.5
0.40	34±2	48.5±0.5	58.5±0.5
0.50	51±2	49.0±0.5	69.0±0.5
0.60	79±2	50.0±0.5	#
0.70	123±2	49.5±0.5	#

Beside this noteworthy difference in the water-binding capability, which may be misleading to attribute to a single physico-chemical property without considering further aspects, neutron diffraction rocking scans reveal an almost powder-like nature of POPA membranes. This behaviour of the POPA bilayers not to form well-aligned stacks, was found for sodium and ammonium salts and with all the preparation methods that we used to improve the number of diffraction orders. On the other hand, POPU membranes always arrange in well-ordered arrays of stacked bilayers. For these membranes, the neutron diffraction experiments reveal at least five orders in every condition (e.g., temperature, sample preparation), as shown in Figure 2.3 for lamellae obtained by lipid hydration from vapour phase at 37ºC for three different contrast variations. The mosaicity - lipid bilayer orientation with respect to the surface normal determined by the quartz support - of POPU membranes was about 0.2º comparable to or at least better than the 0.5º obtained for POPC bilayers in the same experimental condition[6].

Due to the high quality of the data and number of observed reflections, it is possible to obtain the scattering length density profile along the normal to the membrane plane through the Fourier synthesis from the structure factor at 0% D_2O for POPU lamellar phase. The bilayers spacing measured is 51Å for POPU/NH_4^+ at ~26% water content, which indicates full hydration and corresponds to the hydration degree after equilibration in the neutron diffraction can.

This profile reported in Figure 2.4 represents the elementary cell of one bilayer plus its hydration shell. The water content is centred at the edges of the diagram, while the two maxima typically correspond to the glycerol backbone; that is, the lipid headgroup. In this case a calculation of the scattering length density for all the sub-groups of POPU, allows assigning the highest value of the profile (±17 Å) to the carbonyl groups, as represented in Figure 2.5. The correlation for the scattering length density of the uridine derivative was evaluated by considering the

contributions of the different sub-molecular fragments as separated by sharp interfaces. The minimum in the profile (at 25.5 Å) is the representation of the terminal methyl groups of the phospholipids and its appearance rules out any interdigitation in the lipid bilayer.

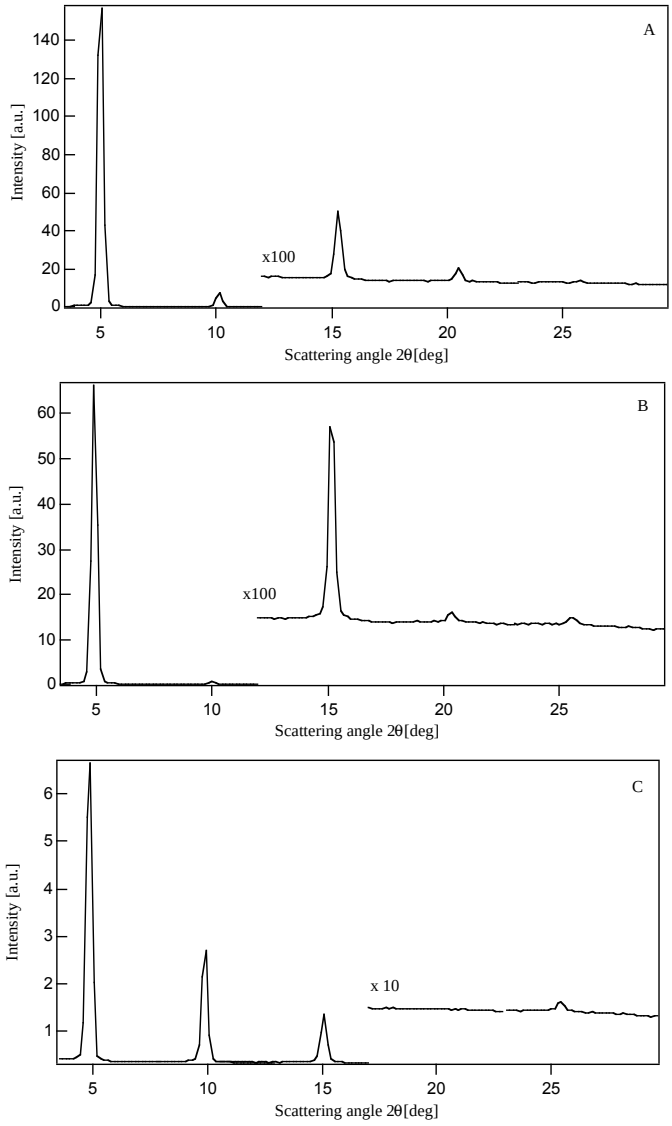

Figure2.3. Diffraction patterns of POPU bilayers 100% D_2O (A), 50% D_2O (B) and 100% H_2O (C).

In agreement with Luzzati method, a bilayer thickness of 38.5 Å was determinated, knowing the actual volume fraction of the lipids. This parameter permits to evaluate the Area for polar headgroup, if the molecular volume is known. This volume was obtained summing all the submolecular fragment volumes as

determined by Armen et al. through molecular dynamics simulation[7]. In this approximation, the Volume of POPU molecule resulted around 1349 Å^3. Subsequently the POPU area for polar head results ~72 Å^2, noticeably higher than POPC (~58 Å^2)[6] in fully hydrated lamellar phases. This is likely due to the increased bulkiness of the nucleolipid polar heads in terms of steric hindrance and Coulombic repulsion.

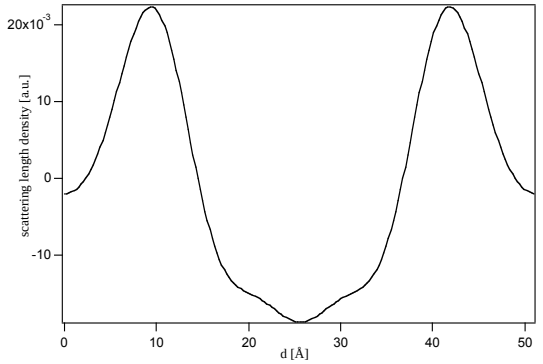

Figure2.4. Experimental scattering length density profiles at 0% D_2O from diffraction data of POPU membranes.

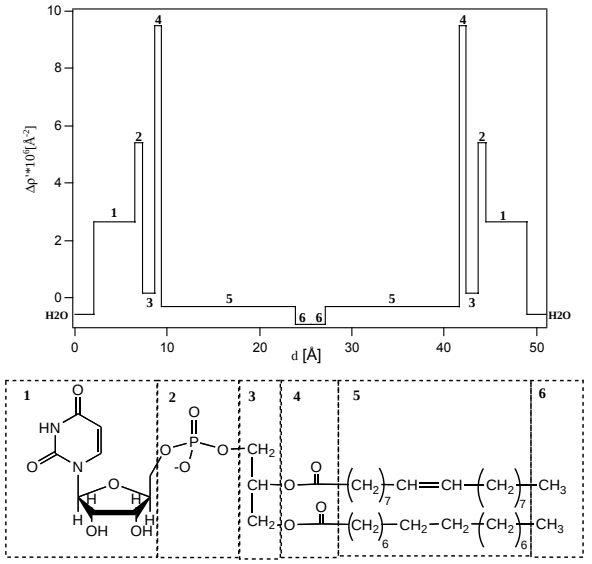

Figure2.5. Calculated scattering-length profile evaluated by considering the contributions of the different sub-molecular fragments as separated by sharp interfaces.

As already mentioned, POPA lamellae prepared in the same way as POPU, not only are a less ordered lamellar phase, but also require a longer equilibration time to achieve a monophasic structure. This longer process is certainly due to the different water uptake attitude.

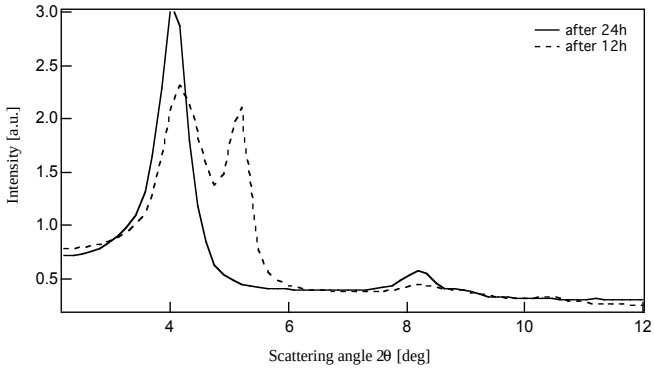

Figure2.6. Diffraction patterns of POPA bilayers 100% D_2O: 12h equilibration time (dotted line) and 24h equilibration time (line)

At least 24 hours were necessary to obtain a unique hydrated lamellar phase of POPA, whereas 12h were sufficient for POPU bilayers. After only 12h POPA samples seem to form a couple of lamellar phases, which are characterized by a different smectic period (Figure 2.6). It might reasonably indicate a different amount of water in between the lamellae. After 24h a further increase in equilibration time up to one week, does not produce any improvement of the mosaic spread or shift of the POPA lamellar peak.

On the basis of the diffraction results, we tried to investigate the local arrangement of the lipid molecules in membranes and to achieve information on the base-base interactions. In such a way, it might be easier to validate our hypothesis that, for POPA, stacking prevails over hydration energy and precludes the uptake of water, whilst for POPU it does not occur. The ideal experiment should be able to look at mesoscopic order while distinguishing different portion of the molecules, so that a connection between the arrangement on the nanoscale and information coded in the molecular subunit can be established.

Therefore, FTIR linear dichroism measurements were collected for POPC, POPA and POPU lyotropic phases of ammonium salts equilibrated at 98% as well as for neutron diffraction experiment. Figure 2.7 shows the unpolarized absorption spectra for all the three lipids in anhydrous lamellar stack. The presence of nucleic bases attached to a phospholipid skeleton affects mainly the region below 1800 cm^{-1}, as predicted by comparing the nucleolipids spectra with the nucleosides IR assignments reported in literature[8-11]. Both POPU and POPA show for instance a broad band peaked around 1700 cm^{-1}, resulting from the overlap of at least two modes. In fact, besides carboxylic and C=O ring vibrations (for uridine) also aromatic ring stretching, C=C symmetric vibration modes and NH_2 scissoring mode (for adenine) fall in this zone. As predicted by the theory, lipids as well as nucleolipids membranes do not arise any linear dichroism when their bilayer normal lies along the optical axis[12-14]. However, when the multilamellar oriented phase is rotated with respect to the incoming beam, A_p (absorbance in parallel direction) and A_s (absorbance in perpendicular direction) diverge, as depicted in Figure 2.8 by

their difference, LD signal. The lower LD effect for POPA highlights a worse long-range ordering, as expected by the neutron diffraction.

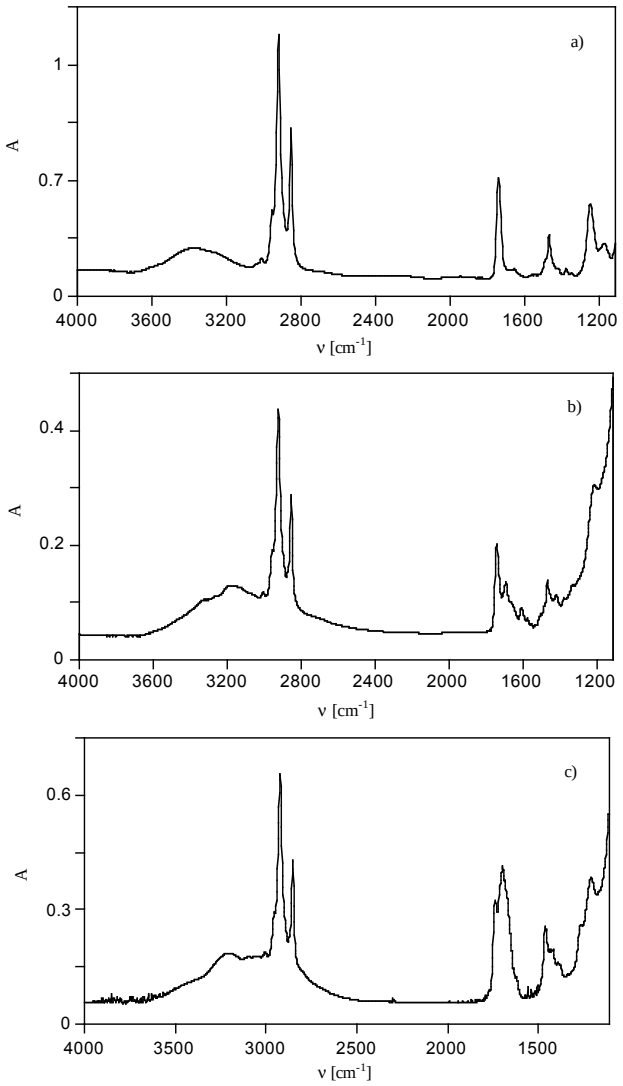

Figure2.7. Infrared Absorption Spectra of a) POPC, b) POPA and c) POPU lamellar phase.

In the 1200-1000 cm^{-1} region, the symmetric $-PO_2^-$ stretching vibrations give rise to a positive LD for both derivatives, as noted by us for POPC (data not shown) and previously obtained for other lipids[15,16]. However, some difference between the investigated nucleolipids arises; besides the phosphate vibration mode POPU shows several bands with positive LD, while in the same region POPA LD appears negative. In particular, we would like to remark on the band centered at 1175 cm^{-1}. This latter band is considered a signature of the A form - C3′-endo sugar puckering mode with an anti conformation of the base about the ribose - and it has been

attributed to sugar vibrations including mainly the C3′-O stretching in nucleic acids studies[17]. This band may be, though, attributed to C-O symmetrical stretching vibration of the ester group. A comparison with DOPC bilayers[16] and our POPC reveals that usually lipids show a negative linear dichroism of this band. As a result, the negative LD sign for POPA lamellar stack in this region could be a composition of the previous listed contributions. Nonetheless, the positive and opposite value found for POPU might indicate that a different orientation of the ribose ring could occur for the two derivatives that overcame the negative contribution of the ester group in terms of LD signals.

The negative LD at 1335cm^{-1} denotes another notable feature in describing the arrangement of the nucleolipids molecules within the membranes. This band, well visible also in the transmission spectrum of POPA bilayers, is considered the C3′ endo/anti marker band[18], which indicates the orientation of the glycosidic bond with respect to the sugar moiety. A negative LD value is a clue to the parallel orientation of this molecular group with respect to the bilayer surface in agreement with the basic definition of linear dichroism.

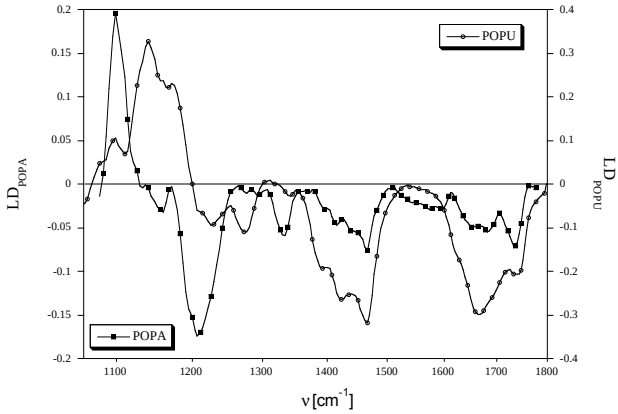

Figure2.8. LD spectrum (A_p-A_s) of POPA and POPU for an incident angle (90º-ω) equal to 40º in the region 1800-100cm^{-1}.

A comparison of the traditional absorption spectra and LD spectra allows us to distinguish several contributions that appear as a unique band in the transmission spectrum. For example, it is possible to distinguish the carboxyl stretching (~1735 cm^{-1}) from vibration mode of adenine ammonium group or uridine ring carbonyls. Moreover, LD permits to evaluate the order parameter for sub-molecular group that gives us an indication of sub-molecular group orientation and of its degree of alignment inside the bilayer. This method is very interesting for our aims, because the knowledge of the molecular group disposition in the lamellae could call attention to possible modifications induced by the molecular recognition interaction with other molecules (i.e., oligonucleotides or nucleic acid).

Table 2.2 shows the order parameter *S* for some sub-group of investigated lipids. It is clear that the values of order parameter measured for POPA membranes are truly lower than for POPU lamellae, highlighting again a worse orientation of adenosine derivatives lamellar phases as already stressed by neutron diffraction. The order parameters were also measured for POPC membranes, as a control experiment. The *S* values for this latter lipid agree with the literature value found for other phospholipids self-assembled in lamellae, highlighting well-ordered molecules within the bilayers. In general, the POPU and POPC parameters are similar except for the PO_2^-, which is considerably higher for POPU. This could be related to the slightly better mosaicity found by diffraction for this nucleolipid with respect to POPC. A comparison of POPU and POPC order parameters, though, stresses a more fluid-like phase for the first molecule, which can be expected on the basis of the higher cross sectional area per lipid molecule and the lower thickness of the apolar core of the bilayer.

Table2.2. Assignments of selected absorption bands of POPC, POPA and POPU lamellar phases.

Vibration modes	Wavenumber [cm^{-1}]	*S*
POPC		
$\nu_{as}(PO_2^-)$	1235	-0.318
ν(C=O)	1735	-0.365
$\nu(CH_2)$	2854	-0.365
POPA		
$\nu_{as}(PO_2^-)$	1208	-0.140
ν(ring)	1600	-0.189
$\delta(NH_2)$	1675	-0.180
ν(C=O)	1730	-0.200
$\nu(CH_2)$	2851	-0.197
POPU		
$\nu_{as}(PO_2^-)$	1214	-0.443
$\nu(N_1C_6)$	1275	-0.330
ν(C=O)	1738	-0.283
$\nu(CH_2)$	2853	-0.335

ν, symmetric and antisimmetric stretching vibration mode; δ, bending vibration mode

The negative sign for CH_2 symmetric stretching mode indicates that the C_2 axis of the chain is, on average, normal to the lipid bilayer surface. The wavenumber value of CH_2 confirms the liquid crystalline status of all the samples, in agreement with the DSC where the main transition temperature is at –2ºC and –7ºC for POPA and POPU ammonium salts respectively at this hydration condition.

The negative sign of the order parameter of the fatty ester C=O stretching points out that it lies parallel to the bilayer interface. This result is in close agreement with some previous studies, in which was found a planar configuration of the C-OOO-C frame[16,19]. The same observation holds for phosphate

antisymmetric stretching modes, whose negative value for all the three derivatives claims the bisector of group lies along the normal.

LD studies permit to determine γ, the mean angle between the stretching transition moments oriented along the bisector of the H-C-H angle and the surface normal, following the relation[20]:

$$S = \frac{3}{2}\cos^2\gamma - \frac{1}{2} \qquad (2.1)$$

Unfortunately because of the poor quality of the POPA membrane the value found (62º) becomes not reliable and yields hard any comparison with POPC and POPU bilayers, for which this angle was measured to be ~72º.

Despite of the tiny difference in molecular structure, POPA and POPU induce a lot of differences in terms of lyothopic equilibrium, as neutron data highlighted. LD-FTIR supports the diffraction results, indicating that these changes can be traced back to different orientations of the base moieties with respect to the bilayer normal. In particular a different orientation of the sugar-phosphate seems to validate the idea that the lower mosaicity and poor affinity for water of POPA membranes may be due to the interaction between neighbouring bases in the bilayers.

Further supporting our previous results, a simple geometrical optimization of POPA and POPU molecules has been performed with Hyperchem 5.1, using AMBER as a force field[21]. These geometrical optimizations point out that the headgroup conformations of the two nucleolipids differ (Figure 2.9 A). In particular pyrimidine ring lies, on average, perpendicular to the bilayer plane, whereas the purine ring is oriented parallel to membrane surface. According to Figure 2.9 B the connecting line of two nonesterified oxygens of the phosphate group of POPU is parallel to the bilayer plane, in agreement with FTIR results, whereas for POPA the alignment does not occur.

Running this energy minimization on a linear array of five or six molecules, as reported in Figure 2.10 A and B, POPU molecules keep the same alignment for phosphate groups, whereas POPA orientation (as far as this vector is concerned) varies for neighbouring molecules. Therefore, the geometric minimization in Figure 2.10 shows that uracyl bases are more or less oriented parallel each to other. A slight alteration of the original conformation optimized for an isolated molecule is barely detectable. POPA on the other side arranges preferentially in pair varying highly its initial orientation.

In order to gain experimental support for the indications on base arrangement inferred from calculations, we have to look at vibration modes of molecular groups located on the bases. Unfortunately, the characteristic vibrations of uracyl (C=O, C-N, C=C, N-H) fall in frequency ranges where they overlap with other vibrational modes, so that it is very hard to perform an unambiguous assignment of the marker bands. The only distinctive uracyl-band for which we can determine the order parameter (S=-0.33) is N_1-C_6 stretching (1275 cm^{-1}) whose dipolar moment results almost parallel to the bilayer surface, in agreement with the simulated structure (see Figure 2.10 B). For adenine the peak at 1675 cm^{-1}, δ(NH) of NH_2 causes a negative

linear dichroism, where the bisector of NH_2 group is, on average, parallel to the bilayer plane. This observation is strengthened by the attribution of the LD negative peak at 1335 cm^{-1} to the C3′endo/anti conformation. The accord between these measured orientations and the molecular disposition obtained by calculation is outstanding and validates the proposed geometrical minimization.

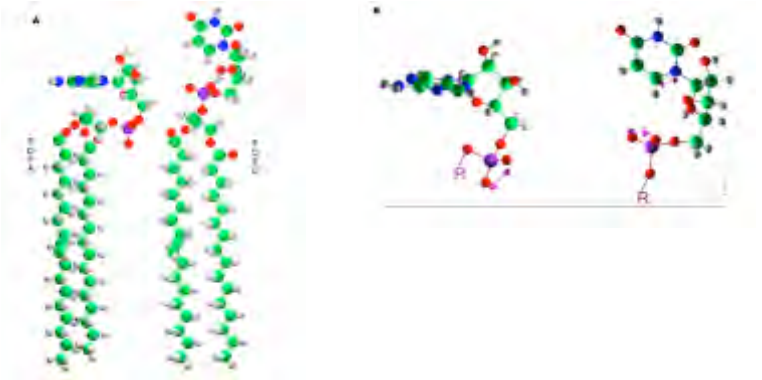

Figure2.9. (A) POPA and POPU geometrical optimizations performed with Hyperchem 5.1 using AMBER force field. (B) This particular of the headgroup stress the transition moments commented above and their orientation regarding the bilayer surface.

The different behaviour between the two nucleolipids, consequently, can be associated to stronger stacking attitudes of the purine bases with respect to pyrimidines. As a result, our previous theory can be proved by this analysis for understanding the oddness of the POPA lamellar phases in spite of being an anionic lipid.

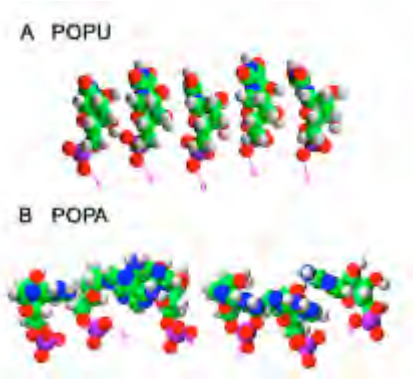

Figure2.10. Geometrical minimization for a group of POPU (A) and POPA (B) molecules performed with Hyperchem 5.1 using AMBER force field. The orientation of purinic rings is strongly altered by the interaction among bases. Pyrimidinic bases maintain more or less their original conformation.

2.2 Mixed POPA/POPU Membranes: Molecular Recognition between Base-Complementary Lipids

In the previous section, we showed the phase behaviour of POPA and POPU lamellar phases. We highlighted by experimental measurements jolly interesting alteration of nucleolipid lamellar structures with respect to neutral lipids like POPC. However, since our final goal is to investigate the interaction between nucleolipids membranes and oligonucleotides, the following step was to answer the question whether complementary bases could show molecular recognition between the patterns in lamellar phases. The answer is very important to support our study. If the molecular recognition between complementary bases was prevented when the lipids arrange in lamellar phases, it could be very difficult to imagine a possible interaction with external strand of nucleic bases.

In the past, it has already been reported that mixed vesicles made of 1,2-Oleoyl-sn-glycero-3-Adenosine (DOPA) and 1,2-Oleoyl-sn-glycero-3-Uridine (DOPU) present spectroscopic properties typical of A-U interaction. Mixture of these nucleolipids showed non-ideal behaviour, indicating that specific interactions similar to those found in nucleic acids are operating. Hypochromism and stacking excess was inferred for these lipids arranged in zero-curvature aggregates by circular dichroism and UV-absorption spectroscopy[22]. The same observations have been reported for short-chain derivative micelles by NMR studies and seem connected to the presence of the adenosine headgroup rather than to the interfacial curvature[23]. However, all these studies were performed on systems in solution, no demonstration of molecular recognition between complementary bases in lamellar phases or at this very low water content was reported so far. Consequently we decided to continue the studies of lamellar phases formed by complementary headgroup nucleolipid mixtures.

The nucleolipids investigated hereinafter were sodium salts. Sodium salts were chosen to overcome the problem of equilibration (as far as it concerns hydration) encountered with POPA ammonium salt. For the same reason we decided to use paste as preparation methods.

Two mixture were investigated: 1:2 POPA:POPU and 1:1 POPA:POPU. Full hydration and 20% w/w water contents were measured. The choice of 20% w/w water was to account for the possible difference in bilayers thickness and to address any dissimilarity to the different base arrangement induced by interaction between adenosine and uridine bases throughout the membrane mixture.

Figure 2.11 shows the neutron diffraction spectra from these two nucleolipid mixtures at full hydration. Similar results have been obtained for the analogous 80:20 lipid:water samples. The unique lamellar phase detected confirms the miscibility of the two lipids, as it should be expected from the similar chemical chains and headgroup nature.

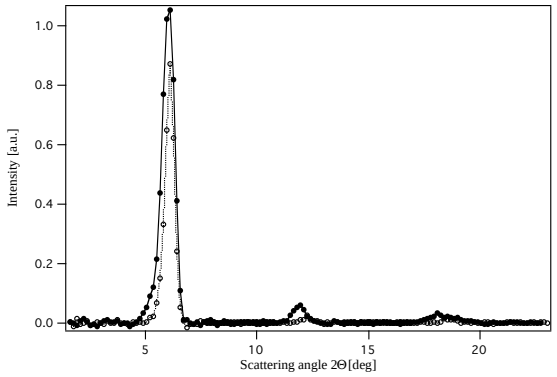

Figure2.11. Diffraction patterns of mixture at 8:92 D_2O:H_2O full hydration: (○) 1:1 POPA:POPU, (●) 1:2 POPA:POPU.

Unfortunately, for both investigated mixtures, the number of reflections is low. There are only three peaks, as many as were found for POPA pure membranes in the same hydration and preparation conditions. Therefore, POPA provides the imprinting for long-range ordering. On the contrary, the spacing of the mesophase depends on POPU molar ratio, being wider for higher POPU content.

Observing the width of the lamellar peaks in Figure 2.11, we notice that the mixture with higher POPU ratio has better sample alignment, as confirmed by rocking the samples around the Bragg position θ (data not shown). This is not a surprise. The ratio 1:2 POPA:POPU was exactly selected for improving the membrane mosaicity, being POPU by far better aligned membranes in binary systems. However, although the mosaicity was slightly improved increasing POPU content, the number of reflection remained still too low to get a well-defined scattering length density profiles. A coarse-grained SLD profile for both the mixtures is reported in Figure 2.12. Since quality is poor, it is not recommended to obtain structural information as number of water molecules, area for polar head and so on by the analysis of these profiles. Qualitatively speaking, it is only possible to figure out a thin different orientation of the polar heads inside the two mixtures. The only remarkable difference in the two profiles is, in fact, detectable in the maxima corresponding to the glycerol backbone of the lipid, representing the polar headgroups.

Together with the above-discussed information, the mixed lamellar phase shows, for both molar ratios, a lower smectic period than the pure systems. No dependence of the water content (20% w/w or full hydration) was found. This also implies a lower thickness for the nucleolipids bilayers in the mixtures.

This smaller bilayer thickness is an indication that the nucleolipids do not mix themselves ideally. In general, ideal mixture of lipid bilayers forms lamellae that have an average smectic period with respect to the pure components. Of course, there are exceptions to the former statement. But in the case that we are examining, lipids have the same chain, which should imply no changing in the space intralamella. Therefore, given that the apolar part is the same, every structural modification can be addressed only to the polar head region. So, any variation can

be explained only invoking different intermolecular interactions for the mixed systems with respect to the binary systems. As mentioned above, the low resolution of the profile does no allow us to speculate further on this point; however, we can consider the lipid cross-sectional area by Luzzati knowing the water content. At this regard, the pastes, where we added the water, should guarantee to avoid mistakes in evaluating the water imbibed within the membrane. Moreover, this calculation requires an accurate knowledge of the molecular volume, estimated to be 1349 $Å^3$ for POPU and 1383 $Å^3$ for POPA by molecular dynamic simulation. Table 2.3 reports the calculated values.

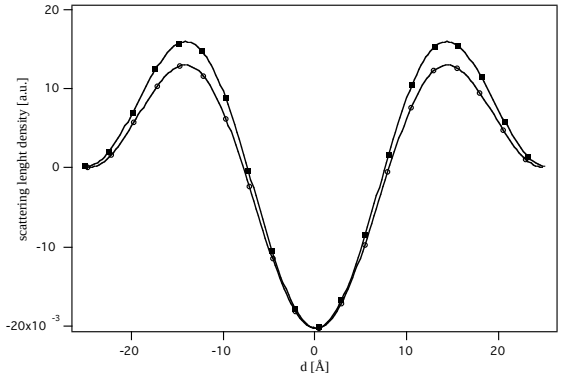

Figure2.12. Experimental scattering length density at 8:92 D_2O:H_2O: (○) 1:1 POPA:POPU, (■) 1:2 POPA:POPU.

Table 2.3. Bilayers thickness and Area for polar headgroup at 80/20 lipid/water %[w/w]

Lipid	d_L [Å]	Area [$Å^2$]
POPA	38.1±0.5	72
POPU	38.5±0.5	70
POPU:POPA 1:1	37.3±0.5	73
POPU:POPA 2:1	37.3±0.5	72

As Table 2.3 reveals, the mixed lamellar phases show no striking structural deviations from binary systems. However, it is known that area per lipid molecule can be considered as the simplest measure of the lateral organization. Therefore, in the examined samples the area is higher, although slightly, for both mixtures than for POPA and POPU separately, which implies a different orientation of the bases.

On the basis of the neutron diffraction, DSC experiments were performed to further understand and clarify whether or not ideal mixtures occurred. DSC was widely used for characterizing lipid mixtures[24-26]. When lipids form not ideal mixtures, the main transition temperatures of the mixed membranes in the thermal scan do not scale linearly with the lipid compositions. At this regard, we need to look at Figure 2.13. It shows the endothermic curves obtained for POPA and POPU binary membranes and their mixtures. The area between the experimental curve and an interpolated baseline corresponds to the heat of transition from the gel to liquid

crystalline phases. The main transition temperatures, T_m, are at -6.8°C and -9.6°C for POPA and POPU respectively. This difference, which roughly holds independently on the hydration degree, again reveals a different lateral organization for the two membranes, especially striking considering the identity of the chains and charge and the extremely similar steric hindrance[25,27]. The same trend was noticed for POPA and POPU ammonium salts organized in membranes. Therefore, POPU lamellae main phase transition temperature was observed at lower temperature than POPA beyond the amount of water imbibed and the nature of the counter-ion.

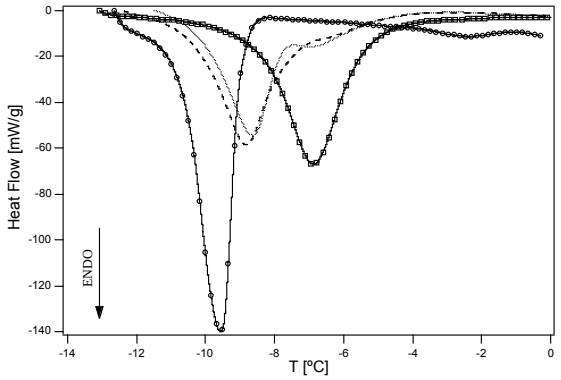

Figure2.13. Differential Scanning Calorimetry heating curves for 1:2 POPA:POPU (dashed line), 1:1 POPA:POPU (dotted line) membrane mixtures, POPA (□) and POPU (○) pure membranes at lipid/water 80/20% w/w.

As we mentioned in chapter 1, charge can influence indirectly the transition temperature changing the packing in the bilayer. The charged group can interact through inter and intramolecular hydrogen bond. This can increase the stability of the mesophase, shifting consequently the transition temperature towards higher values. That said, it is reasonable to presume that the slightly higher temperature transition always observed for POPA with respect to POPU lamellae could be due to its stronger stacking interactions between the bases. The presence of stronger intermolecular interactions for POPA than for POPU would seem to be maximized in the more ordered gel phase. The width and the shapes of DSC curves for the binary nucleolipid membranes again highlight what previously supposed. Hence, the sharpness and the intensity of POPU thermal peaks show the higher cooperativity for the L_β-L_α transition than for POPA lamellae. These observations agree with the structural information obtained by neutron diffraction for POPU, where a higher mosaicity was detected.

If we now consider the mixtures, we notice for both molar ratios one broad endothermic peak centred between the endothermic peaks of pure lipids. The T_m evaluated for 1:1 POPA:POPU membranes is –8.5ºC and that for 1:2 POPA:POPU is –8.9ºC, closer to the POPU one. Moreover, the calorimetric curves for both mixtures show a small shoulder above the main transition, more pronounced for 1:1 ratio. These shoulders clearly recall the POPA binary lamellar phase, indicating that

there are rafts in the gel phase. However, given the limited temperature range accessible for the neutron diffraction experiments, we could not verify the diffraction pattern for the mixed gels: the only evidence that we have is that the sample is monophasic in the L_α domain, but we cannot rule out any clustering of like molecules along the membrane plane.

Since the main transition temperature of the mixed membranes does not scale linearly with lipid composition, the mixtures are not ideal. Normally, DSC analysis permits to infer the non-ideality parameter[28-32] for mixed lamellar phases, whose transition temperatures are widely spaced on the T axis; however, given the width of the peaks and their small temperature difference it is not correct to apply this theory for the mixtures examined here.

After the demonstration of the non-ideality from structural and thermal point of views, FTIR measurements were carried out to get insights on the base-base interactions. IR is a powerful technique to analyse inter and intra-molecular hydrogen bonds and has been especially and extensively used to study nucleic acids or nucleotides[10,33-36]. The region between 1700 and 1550 cm^{-1} is surely the most interesting for this issue[8,12,37]. Therefore, we have recorded IR spectra on pure and mixed nucleolipid lamellar phases (Figure 2.14) to detect possible band shifts in this region. However, as already noted, a large number of vibration modes both of the lipid and of the nucleic acid occurs in this region[8,12], making a straightforward interpretation of the experimental data difficult. Figure 2.14 draws the spectra characterized by an extremely broad band, where it is difficult even to make out the contributions of the single transition. The merely exception is for POPA lamellae, where the vibrations of every single group are better separated in this region.

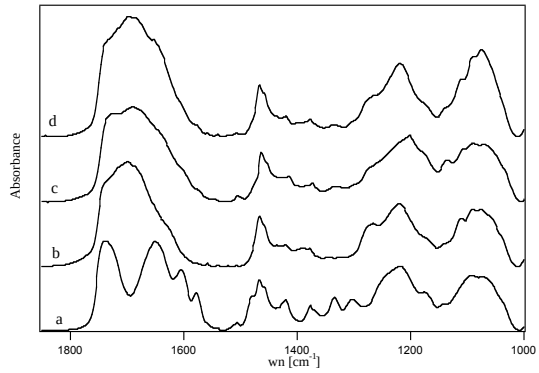

Figure2.14. Infrared absorption spectra of (a) POPA, (b) POPU, (c) mixture 1:1 POPA:POPU and (d) mixture 1:2 POPA:POPU bilayers at lipid/water 80/20% [w/w]. The curves were shifted along the left axis to enhance graphic readability.

To acquire the desired information from these spectra two different methods were used: the first was to deconvolve the bands by Gaussians functions, the second was to perform a weighted subtraction - the weight being the relative quantity of lipid in the mixture - of the spectra of the pure nucleolipids from the spectra of the mixtures.

The number of Gaussians used for fitting the spectra was chosen according to the current IR literature for nucleic acids and lipids. Table 2.4 shows the fitting results and the attribution of every single vibration mode in the region 1800-1500cm^{-1}.

Table2.4. Infrared Absorption Spectra fitting results.

POPA calculated frequency [cm^{-1}]	POPU calculated frequency [cm^{-1}]	1:1 POPA:POPU calculated frequency [cm^{-1}]	1:2 POPA:POPU calculated frequency [cm^{-1}]	Vibration modes attribution
1778	1760	1760	1760	
1745	1745	1747	1745	ν C=O carboxylic tails
1730	1730	1731	1731	ν CO-O carbonylic tails
	1705	1705	1704	ν C_2=O uri
		1690	1690	ν C_4=O uri (H-bond)
	1678	1678	1678	ν C_4=O uri (not H-bond)
1660		1662	1662	bonded δ NH_2 + ν ring ade
1640		1638	1639	free δ NH_2 + ν ring ade
	1640	1638	1639	ν C_4=O + ν ring uri
	1610	1612	1613	ν ring uri
1600		1600	1602	ν ring + δ NH_2 ade
1576		1579	1577	ν ring ade

Figure 2.15 depicts the difference spectrum where the appearance of an unique positive band at 1690 cm^{-1} for POPA:POPU 1:1 is detectable. This value is assigned to the C_4=O carboxylic stretching vibration of uridine when it forms hydrogen bond with adenosine or other complementary bases[38], highlighting that specific interaction between complementary bases in the analysed membrane mixture occurred. Beside the band at 1690 cm^{-1}, another band for 2:1 mixtures appears at 1645 cm^{-1} in the difference spectrum. This band is probably due to the adenosine NH_2 bending modes. This difference between these two ratios can be understood considering that the adenosine NH_2 could be involved in a simultaneous H-bond with uridine in 2:1 mixtures. At this regard, it is known that in 2:1 polyU:polyA mixtures (i.e., the same composition we are observing) an interaction like the latter proposed takes place to form a triple helix by both Watson-Crick and Hoogsten pairing. Therefore, we can assume that if the bases form H-bond in the membranes with the same specificity and stoichiometry as in nucleic acids, this additional feature in the difference spectrum stems from a POPU-POPA-POPU complex. This observation could explain the DSC curve for the 1:1 sample, where the formation of a POPU-rich complex seems likely.

Figure 2.16 shows the fittings for both binary and ternary mixtures. It is worth noting that an absorption band appears around 1690 cm^{-1} in the ternary mixture. This band that is missing in the pure lipid membranes spectra, was even assigned to the stretching of the uridine C_4=O. As it is visible in Figure 2.16, the purple curves in the mixtures decreases in terms of intensity with respect to the black one. They

have, instead, quite the same intensity in the pure POPU bilayers, where the carboxylic vibrations are not affected by H-bonds. This is a demonstration that the fitting procedure notwithstanding the need of a large number of Gaussians can be considered reliable. However, using this method for analysing the spectra it is impossible to observe any POPU-POPA-POPU complex or find differences between the two mixture ratios. The area under the fitting curves is indeed different between these samples, but any further speculation on this point could be misleading and uncertain.

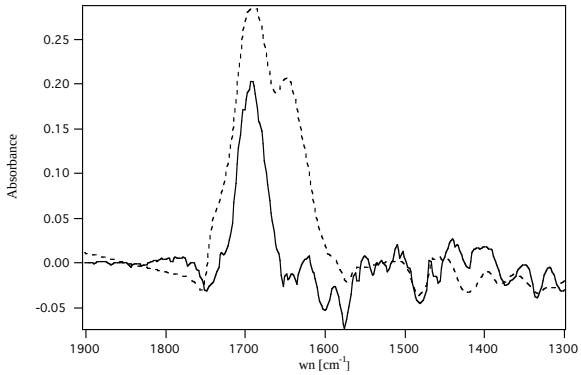

Figure2.15. Difference of infrared absorption spectra of mixture POPA:POPU 1:1 (solid line) and mixture POPA:POPU 1:2 (dashed line) bilayers at lipid/water 80/20% [w/w].

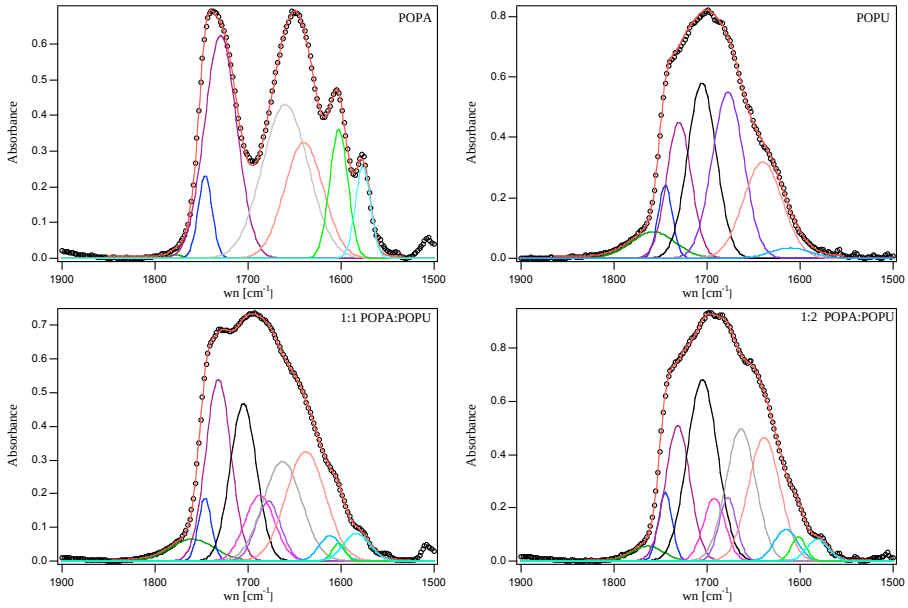

Figure2.16. FTIR absorption spectra of POPA, POPU, 1:1 POPA:POPU and 1:2 POPA:POPU membranes (circles) between 1900-1500 cm^{-1}: the fitting results are reported in red. – ν C=O, – ν CO-O, – ν C_2=O, – ν C_4=O (H-bond), – ν C_4=O (not H-bond), – bonded δ NH_2 + ν ring, – free δ NH_2 + ν ring and ν C_4=O + ν ring, – ν ring uri, – ν ring+ δ NH_2, – ν ring ade.

On the basis of these results, we used vibrational infrared linear dichroism (VLD) to study the local arrangement of the mixed membranes. Figure 2.17 depicts the collected VLD spectra for POPA, POPU and their mixed bilayers. The main difference between the dichroic spectra of binary and ternary phases is the intensity of the dichroic signal: stronger for POPU than for POPA and mixtures bilayers. This correlates very well with the different mosaicity of the lamellar samples by neutron diffraction.

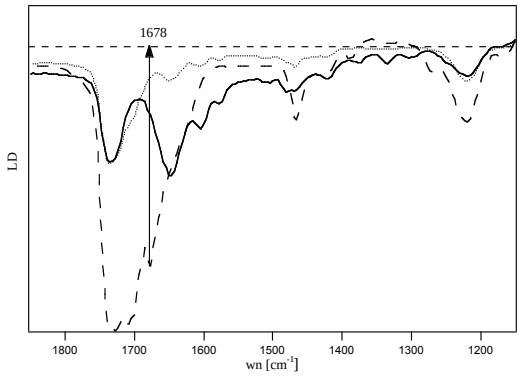

Figure2.17. Linear dichroism spectra of POPA (solid line), POPU (dashed line) and their 1:1 mixture (dotted line) for an incident angle of 40º in the region 1900-1150cm^{-1}.

VLD measurements stress another feature, this time related to the interaction between the bases rather than to the alignment of the membranes. A deeper glance at the LD spectra highlights that the LD signal of C_4=O uridine stretching mode is missing in the mixture. The lack of band at 1678 cm^{-1} might point out that C_4=O has no preferential orientation in the mixture relatively to binary POPU membrane, a consequence of the H-bond between uridine and adenosine polar headgroup. Moreover, this absence might be due to the reduced intensity. We have just stressed that growing of C_4=O H-bond band occurs in the mixture with consequent dropping of the intensity for the not H-bond modes. Being the LD signal by far less strong than the normal absorbance signal, it is logical to presume an undetectable signal for both two bonds (H-bonded and not), that is an further confirm of the interaction between the like-charged polar head.

2.3 Effect of "Helper Lipid" in Nucleolipid Membranes

In view of possible employment of nucleolipid self-assemblies as carriers of DNA or oligonucleotides, we have considered several aspects such as *in vivo*-transfection efficiency and toxicity reduction. In literature, as it will be reviewed in the next chapters, there are many examples of lipid gene delivery vehicles, in which the addition of a neutral zwitterionic lipid, called sometimes *helper*, has demonstrated to improve these issues. In the work developed here, transfection is

far to be in our plan, but in any case it is a goal that must to be consider. For this reason we thought to dilute nucleolipid lamellae with neutral lipid. Choosing POPNs as derivatives, the first zwitterionic lipid that we decided to use was POPC. This lipid has the advantage of the same hydrophobic portion than the investigated nucleolipids.

In this paragraph we will describe the variation in lamellar structures and the effect on the interaction between nucleolipid bases with this kind of molecules. The comparison with a synthetic negatively charged lipid, the same charge sign as nucleolipids, will be also taken in account to understand the bilayers modification induced by POPC dilution over POPN lamellae.

As matter of fact, there is another motivation that could support the need for using neutral lipids in the investigation of nucleolipids membranes. POPA molecules form not-well-aligned stacks of bilayers, they were always found to have a powder like-nature as consequence of a higher interaction between the polar headgroups. Therefore, our hypothesis was to mix up POPN molecules with POPC molecules to try improving the order in lamellar phase.

Furthermore, POPC was chosen because structural properties of bilayers composed of this lipid have been studied in great detail through neutron diffraction at different hydration degrees[39].

All of the spectra, collected for mixture POPN and POPC by neutron diffraction, consisted up to five diffraction orders with a mosaicity lower than 0.5°, confirming the excellent quality of the lamellar stacks obtained from the drying vesicles dispersions. Therefore, our aim to improve the lamellar order was achieved.

Figure 2.18 shows the neutron diffraction spectrum of the sample 1:1 POPA:POPC at 98% relative humidity. This molar ratio has been reasonably weighted considering helper lipid effects and molecular recognition capabilities of nucleolipids. The first lipid was thought to increase water uptake and the equilibration kinetic, whilst the latter might enable them to interact with complementary oligonucleotides.

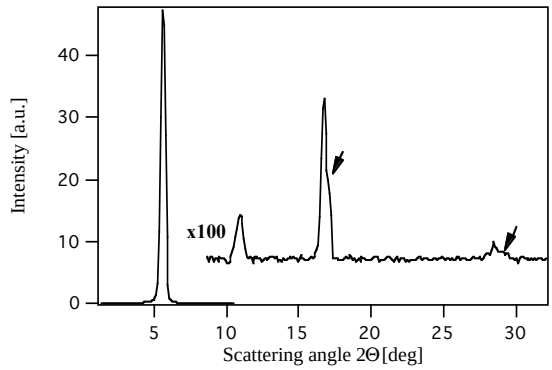

Figure2.18. Neutron Diffraction patterns of 1:1 POPA:POPC bilayers at 50:50 D_2O:H_2O.

A careful inspection of the higher diffraction orders allows detecting a slight and progressive broadening of the reflections (arrows in Figure 2.18) and eventually the appearance of a shoulder in the third and the fifth reflection. This effect might indicate the presence of a second phase in the sample, whose structural characteristics are very similar to the "main" phase. However, no evidence of chemical degradation could be detected with Thin Layer Chromatography in the sample after the neutron diffraction measurements. The smectic period of this possible second phase is smaller than the "main" phase; this difference might arise from a different hydration degree, which would contribute to the smectic period as a different thickness of the water layer in between the lamellae. Another possibility is a different or uneven bilayer thickness along the bilayer plane, due to partial de-mixing of POPC and POPA, with the presence of POPA-enriched microdomains. We can label these two effects as "vertical" and "in plane" phase separation. "In plane" phase separation could also be coupled with a different degree of hydration, utterly complicating the scenario.

If complete mixing were indeed occurring, the observed phase separation should be eliminated by longer equilibration times, which was not the case, at least up to six days, well beyond the normally used equilibration times for unsaturated lipids. Moreover, repeated temperature cycles, which should speed up equilibration, were attempted without any detectable improvement in the spectrum.

None of the observed spacings (52.3Å and 53.0Å, respectively), which it is possible to infer from the highest collected Bragg order, can be traced back to the spacings of the pure components (54 Å for POPC and 50.5Å for POPA in the same experimental conditions). This rules out phase separation of pure POPA (or POPC) from the admixed lipids.

The previous observations prompted us to hypothesize the occurrence of POPA-enriched-domains. This lipid, as already mentioned, displays peculiar behavior in self-assemblies due to the high stacking constant of the polar head. Microdomains, in fact, are not a novelty for this class of lipid; the previous paragraph showed by DSC scans that mixture of POPA and POPU lamellae might favour separation of one component enriched cluster in gel-like phases. So it is worth presuming that the formation of these clusters might have been shifted towards higher temperature by the addition of a lipid, which should not have any kind of affinity with nucleolipids.

However, these POPA microdomains should correlate both "in-plane" and in the direction normal to the lamellae for causing appearance of a second lamellar progression in the neutron diffraction spectra. This would imply 3D-cluster presence in the mixture. A working hypothesis is that the stacking among the bases promotes no a real separation, but a sort of epitaxial growth.

Therefore, the conclusion that we draw is: 1:1 POPC:POPA mixture results in lamellar phase with non-perfect mixing; together with a bulk zone - which cannot be traced back to none of the pure components and therefore it is a truly mixture - there are a few regions enriched in POPA content. Likely, they form 3D-clusters.

In spite of the many questions still open regarding the exact nature of this separation, which is beyond the aim of this thesis, we have attempted a

reconstruction of the bilayer scattering length density (SLD) profile considering either a monophasic mixture or a two-phase mixture. A separation of the two contributions to the scattering intensities is possible including an additional Gaussian component for the second phase, whose theta position was fixed, to reproduce the experimental structure factors. This second approach to reconstruct the SLD profile does not yield consistent results; thus, it suggests that only one phase mixture profile has to be considered.

Figure 2.19 reports the scattering length density profiles obtained for the "main" phase along the normal to the membrane plane obtained via Fourier synthesis from the structure factors for the three isotopic compositions of the hydrating atmosphere. The reported pattern reproduces well the typical features expected for a lipid lamellar structure. The profile represent the elementary cell of the oriented samples, that is one lipid bilayer with its hydration shell; the centre of the elementary cell, which also corresponds to a global minimum of the scattering length density, is located in the middle of the bilayer profile, constituted by the terminal methyl group of the acyl groups of the phospholipids (ρ=-0.859·10^{10}cm^{-2} for $-CH_3$ versus ρ=-0.083·10^{10}cm^{-2} for each $-CH_2$ group). The two maxima, peaked at z=-17Å and z=17Å correspond to the phospholipids headgroup/glycerol backbones of the lipid. The two shoulders at the middle of the graphic represent the alkyl chain regions, with the inflection points representing the localization of the double bond.

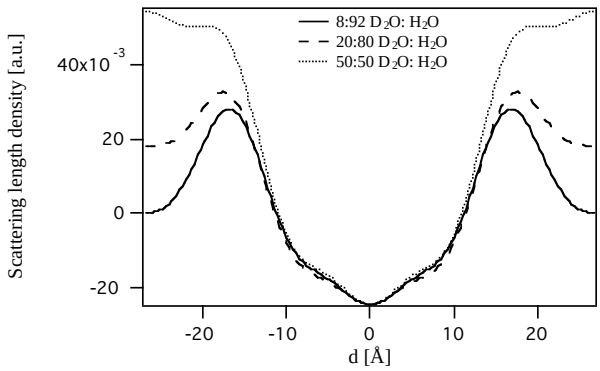

Figure2.19. Experimental scattering length density profiles from diffraction data of 1:1 POPA:POPC mixtures at all the three measured contrasts.

Figure 2.19 shows that contrast variation does not produce alterations in the scattering profile except for the edges of the diagram (z=-26.8Å and z=26.8Å), where the water penetration within the bilayers is located. This feature permits to infer the water distribution profile directly from the experimental neutron diffraction data, subtracting the profile obtained at 8% D_2O from the 50% D_2O one (Figure 2.20).

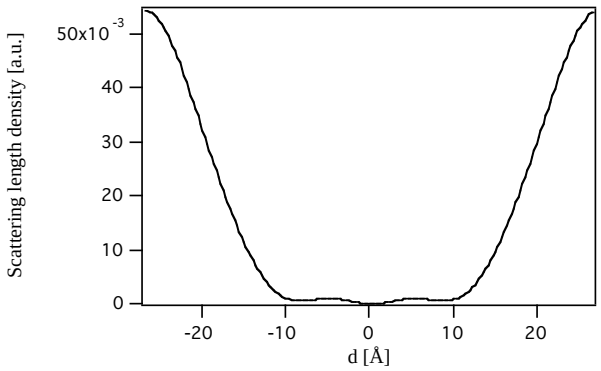

Figure2.20. Experimental water profile from diffraction data of 1:1 POPA:POPC mixtures.

To overcome the cluster formation, we tried to further dilute POPA following the hypothesis that a higher POPC content should guarantee faster equilibration and better smectic ordering of the bilayers. Therefore, 2:3 POPA:POPC mixtures were studied, too.

Unexpectedly, 2:3 POPA:POPC mixture showed a higher separation degree, in terms of relative intensity of the diffraction peaks (see arrows in Fig. 2.21) notwithstanding the larger amount of POPC. Since POPA is here in lower amount than in the 1:1 mixture, we may state that the peak shoulders were not due to the POPA powder like nature, but rather to the supra-molecular properties of its headgroup.

Elaboration of the data by Gaussian linear fit of each scattering peak allowed us to trace a nice SLD profile (not shown) for the "main" phase.

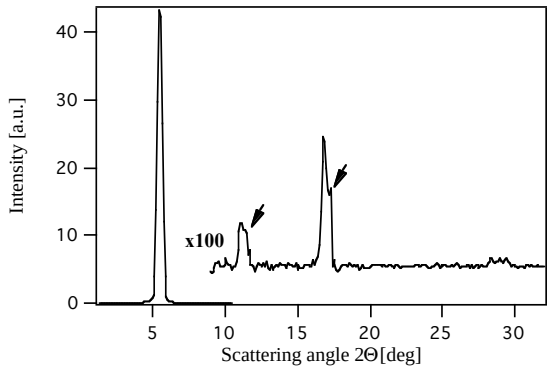

Figure2.21. Neutron Diffraction patterns of 2:3 POPA:POPC bilayers at 50:50 D_2O:H_2O.

Given the quality of the data, experimental scattering profiles have been modelled in order to get structural insights of POPA/POPC bilayers. The spatial distribution of each molecular group (headgroup plus the glycerol backbone, acyl tails and terminal CH_3) was considered to have a Gaussian profile. A combination of five Gaussian curves was used to represent the profile:

$$\rho(z) = \rho_0 + a_H \cdot \exp\left(-\left(\frac{z - z_H}{b_H}\right)^2\right) + a_C \cdot \exp\left(-\left(\frac{z - z_C}{b_C}\right)^2\right) + a_{CH_3} \cdot \exp\left(-\left(\frac{z}{b_{CH_3}}\right)^2\right) + a_H \cdot \exp\left(-\left(\frac{z + z_H}{b_H}\right)^2\right) + a_C \cdot \exp\left(-\left(\frac{z + z_C}{b_C}\right)^2\right) \quad (2.2)$$

where a_H, a_C, a_{CH_3}, b_H, b_C and b_{CH_3} are the amplitudes and the width of the Gaussian functions, which represent sub-molecular-groups in the scattering length density profile. To maintain the ratio among the peaks in the profiles, the ratios between the areas subtended by the Gaussian profiles were kept constant, according to the ratios between the known scattering length densities of the individual subgroups of the molecules. Therefore, a_H and a_{CH_3} were not variable parameters, but rather a function of the other parameters, as below outlined:

$$a_H = k \cdot \frac{a_C b_C}{b_H}$$

$$a_{CH_3} = k' \cdot \frac{a_C b_C}{b_{CH_3}}$$

where k and k' are the ratios between the known scattering length densities of the headgroup and the tail and the methyl terminal and the tail, respectively. These SLD were evaluated knowing the molecular composition and lipid volumes.

The solid line (Figure 2.22) represents the global fit result for one of the measured mixtures. Table 2.6 shows the relevant parameters evaluated from the width and length of each Gaussian.

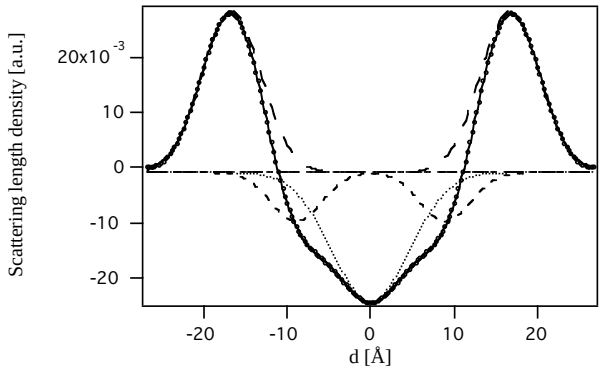

Figure2.22. Experimental scattering length density profile from diffraction data of 1:1 POPA:POPC mixtures at 8% D_2O contrast (circles) and Gaussian model of the profile (solid line). The other lines represent the contributions of each sub-molecular group: methyl group (dots), chain (dashes), headgroup (long dashes).

From these values the charge density on the bilayer plane can be calculated and results to be $1e^-/137Å^2$ for 1:1 POPA:POPC and $1e^-/170Å^2$ for 2:3 POPA:POPC in the main phase.

Within the experimental uncertainty, the refinement procedure yields very similar parameters. The bilayer spacing is quite similar and the evaluated number of water molecules associated with each lipid headgroup is about 17 for both ratio mixtures. Actually, the amount of imbibed water, gravimetrically determined, was quite the same for these two samples (~20% [w/w]).

Table2.6. Structural parameters of 1:1 POPA:POPC mixtures

	1:1	POPA:POPC	2:3	POPA:POPC
	Experimental	Model	Experimental	Model
Bilayers spacing, d	53.6 ± 0.5 Å		54 ± 0.5 Å	
thickness, d_b	~40 Å	38.4 ± 0.1 Å	~40 Å	38.7 ± 0.1 Å
Headgroup Area		~68.5 Å^2		~68 Å^2
Molecular length		19.2 ± 0.1 Å		19.3 ± 0.1 Å
Chain length, d_c		14.2 ± 0.1Å		14.2 ± 0.1Å
n_w [a]		17.0 ± 1		17.0 ± 1
$\tilde{n}_w$ [b]		5.8 ± 1		5.8 ± 1

a: n_w, water molecules per phospholipids molecule; b: $\tilde{n}_w$, water molecules *within* the bilayer

As further confirmation that this peculiar and ambiguous phase separation was due to inter-polar head couplings that eventually lead to POPA clustering, control experiments have been performed on analogously charged POPG:POPC mixed membranes. POPG is a commercial anionic phospholipids whose mixed lamellar phases with POPC in a 1:3 (POPG:POPC) mole ratio, have been studied in some details by Neutron Diffraction[40].

The hydrated lamellar stacks, obtained by drying 1:1 POPG:POPC vesicles dispersion and by rehydrating their film at 98% R.H. as for POPA:POPC, point out an excellent smectic order. The Bragg lamellar progression, reported in Figure 2.23a, shows very sharp peaks, with no sign of shouldering or broadening up to the fifth order. No higher reflections were collected, due to the tight experimental schedule, but the detectability of higher orders is probably feasible with a sample of such quality. At this regard, the rocking curve shows a narrow signal with a FWHM of about 0.2º (Figure 2.23b), which is among the best obtainable with this experimental technique.

Any phase separation can be safely ruled out for this mixture; actually, several studies employ this anionic/zwitterionic lipid mixture to simulate typical model membranes for studying behaviour of bacteria or interaction with protein[41-43].

A Gaussian deconvolution of the scattering length density profile (Figure 2.24) was applied to this sample and compared to the available neutron diffraction data in the literature for 1:3 POPG:POPC mixture[40]. As expected, we found an increased hydration degree (n_w=20 ± 2 water molecules) with respect to the literature (n_w=17± 2), ascribable to the higher content of POPG, which has, being an anionic lipid, a higher water affinity than the zwitterionic component. This behaviour properly agrees with the theory and again it underlines the odd water uptake of POPA lamellae.

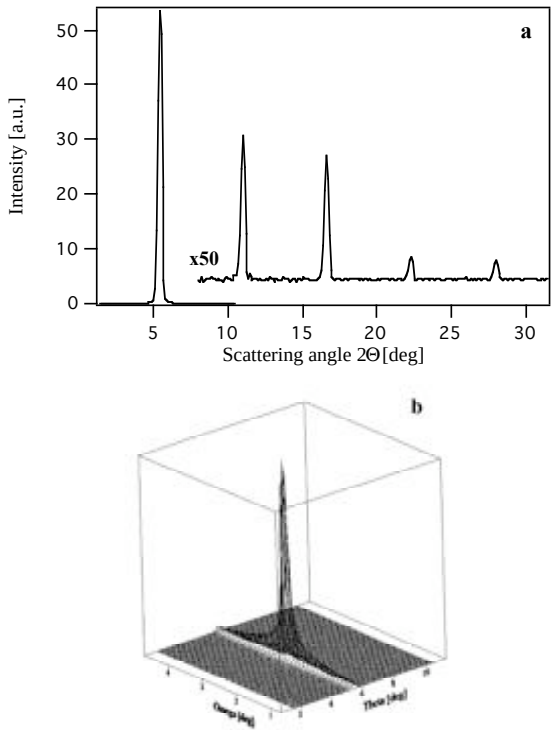

Figure2.23. a) Neutron diffraction patterns and b) Rocking curves obtained by rotating the sample around the 1st Bragg peak of 1:1 POPG:POPC bilayers at 50:50 D_2O:H_2O.

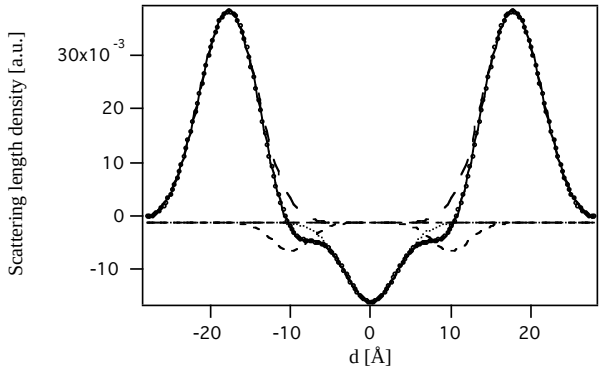

Figure2.24. Experimental scattering length density profile from diffraction data of 1:1 POPG:POPC mixtures at 8% D_2O contrast (circles) and Gaussian model of the profile (solid line). The other lines represent different the submolecular groups as obtained from the fitting: methyl group (dots), chain (dashes), headgroup (long dashes).

The structural information deduced for 1:1 POPG:POPC lamellar phase is shown in Table 2.7. A comparison with 1:1 POPA:POPC mixture reveals that the area for lipid evaluated for the nucleolipid membrane at the same anionic lipid ratio,

has a considerable smaller value in agreement with the smaller glycerol headgroup than the adenosine one.

Table2.7. Structural parameters of 1:1 POPG:POPC mixtures

	Experimental	Gaussian model
Bilayers spacing, d	56 ± 0.2 Å	
thickness, d_b	~42 Å	40.9 ± 0.1 Å
Headgroup Area		~60 Å^2
Molecular length		20.4 ± 0.1 Å
Chain length, d_c		15.2 ± 0.1Å
n_w [a]		15 ± 1
$\tilde{n}_w$ [b]		5.2 ± 1

a: n_w, water molecules per phospholipids molecule; b: $\tilde{n}_w$, water molecules *within* the bilayer

To complete our investigation we have measured the ternary lipid mixture 1:1:2 POPA:POPU:POPC. This system was chosen for several reasons: i) to get knowledge of the molecular recognition between two different bases self-assembled in bilayers, ii) to study interaction between nucleolipid with oligonucleotides having different bases, which is the further development of this study, and iii) to improve the membrane mosaicity. The last motivation is prompted from well-structured membranes of POPU molecules (see paragraph 2.1). Therefore, the idea would be to add POPU and improve the mosaicity without decreasing the molecular recognition capabilities of the membrane. However, the behaviour of nucleolipid molecules, particularly when complementary bases that might molecular recognize each other are present, is not easily predictable. In fact, POPA:POPU:POPC were not better organized than POPA:POPC (Figure 2.25a). We found shoulders in the diffraction patterns as well as for POPA mixtures (Figure 2.25b). However, the measured bilayers spacing was in agreement with our previous investigation on 1:1 POPA:POPU in the same experimental conditions (see paragraph 2.2); that is, due to interacting headgroups of the complementary nucleolipids, a slight smaller bilayers spacing, ~53 Å, occurs.

Figure 2.26 shows the scattering length density profile of this last sample. The profile shape is appreciably different with respect to the POPA:POPC mixture, shown in Figure 2.19. We do need to taken in account this difference. If the lipids mixed ideally throughout the membrane it would be logic to presume that no difference should appear in the profile. Therefore, the observed difference in membrane profile should be ascribed to not-ideal arrangement of the lipid, probably due to molecular recognition interactions between the complementary nucleic bases polar heads.

Moreover, considering the very similar scattering length densities of POPA and POPU molecules, it is worth assuming that POPA and POPU might have changed their orientation within the bilayer with respect to POPA:POPC mixture, thus determining the development of an unexpected SLD profile.

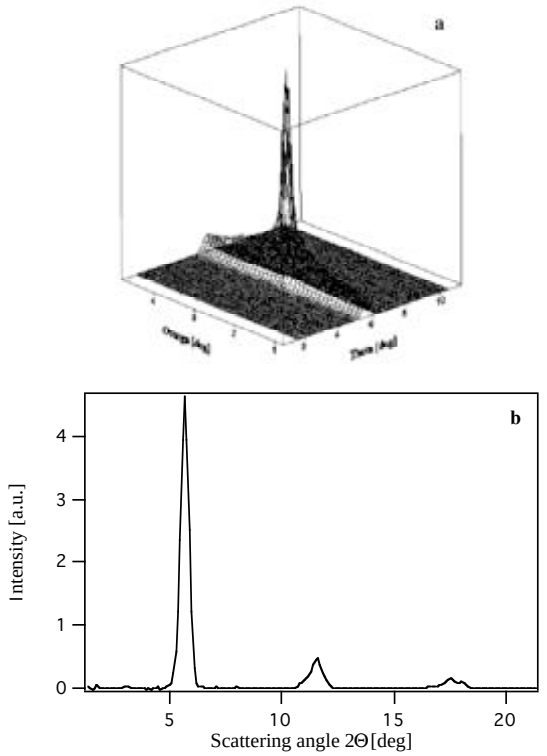

Figure2.25. a) Rocking curves obtained by rotating the sample around the 1st Bragg peak of 1:1:2 POPA:POPU:POPC bilayers at 50:50 D_2O:H_2O and b) Neutron diffraction patterns of 1:1:2 POPA:POPU:POPC bilayers at 8:92 D_2O:H_2O.

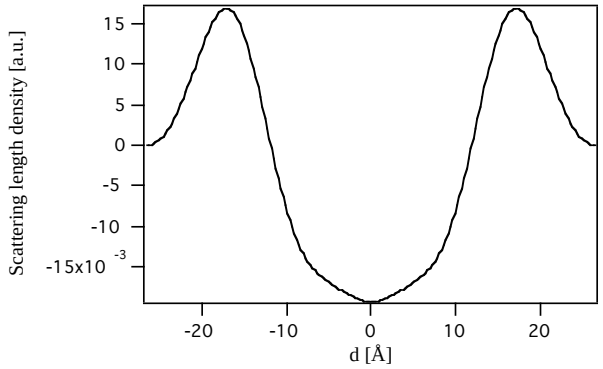

Figure2.26. Experimental scattering length density profile from diffraction data of 1:1:2 POPA:POPU:POPC mixture membrane at 8% D_2O contrast.

Bibliography

(1) Rosemeyer, H. *Chemistry and Biodiversity* **2005**, *2*, 977-1063.
(2) Berti, D.; Franchi, L.; Baglioni, P.; Luisi, P. L. *Langmuir* **1997**, *13*, 3438-3444.
(3) Berti, D.; Keiderling, U.; Baglioni, P. *Progr. Colloid Polym. Sci.* **2002**, *120*, 64-73.
(4) Mitchell, P. R.; Sigel, H. *Eur. J. Biochem.* **1978**, *88*, 149.
(5) Solie, T. N.; Schellman, J. A. *J. Mol. Biol.* **1968**, *33*, 61.
(6) Dante, S.; Hauss, T.; Norbert, A. D. **2002**, *Biophys. J.*, 2610-2616.
(7) Armen, R. S.; Uitto, O. D.; Feller, S. E. *Biophys. J.* **1998**, *75*, 734-744.
(8) Banyay, M.; Sarkar, M.; Graslund, A. *Biophys. Chem.* **2003**, *104*, 477-488.
(9) Bellamy, L. J. *The Infrared Spectra of Complex Molecules*: London, 1958.
(10) Ivanov, A. Y.; Krasnokutski, S. A.; Sheina, G.; Blagoi, Y. P. *Spectochimica Acta Part A* **2003**, *59*, 1959-1973.
(11) Yohimasa, K.; Lord, R. C.; Rich, A. *J. Am. Chem. Soc.* **1967**, *89*, 496-504.
(12) Fringeli, U. P.; Gunthard, H. H. In *Membrane Spectrosocpy*; Grell, E., Ed.; Springer-Verlag: Berlin, 1981.
(13) Johansson, L. B. Å.; Lindblom, G. *Quarterly Reviews of Biophysics* **1980**, *13*, 63.
(14) Nillson, A.; Holmgren, A.; Lindblom, G. *Chem. Phys. Lipids* **1994**, *71*, 119.
(15) Akutsu, H.; Nakahara, Y. K. H.; Fukuda, K. *Chem. Phys. Lipids* **1975**, *15*, 222-242.
(16) Holmgren, A.; Johansson, L. B. Å.; Lindblom, G. *J. Phys. Chem.* **1987**, *91*, 5298-5301.
(17) Pohle, W.; Fritzsche, H. *Nucl. Acid Res.* **1980**, *8*, 2527-2535.
(18) Liquier, J.; Akherbat, A.; Taillandier, E.; Coelin, F.; Huynh Dinh, T.; Igolen, J. *Spectochimica Acta* **1991**, *47A*, 177-186.
(19) Fringeli, U. P. *Z. Natureforsch.* **1977**, *32c*, 20-45.
(20) Saupe, A. *Z. Naturforsch.* **1964**, *19A*, 161-171.
(21) Weiner, S. J.; Kollman, P. A.; Nguyen, D. T.; Case, D. A. *J. Compt. Chem.* **1986**, *7*, 230-252.
(22) Berti, D.; Bonaccio, S.; Barsacchi-Bo, G.; Luisi, P. L.; Baglioni, P. *J. Phys. Chem. B* **1998**, *102*, 303-308.
(23) Berti, D.; Barbaro, P. L.; Bucci, I.; Baglioni, P. *J.Phys.Chem B* **1999**, *103*, 4916-4922.
(24) McElhaney, R. N. *Chemistry and Physics of Lipids* **1982**, *30*, 229-259.
(25) Blume, A. *Thermochimica Acta* **1991**, *193*, 299-347.

(26) Cheng, W. H. *BBA* **1980**, *600*, 358-366.
(27) Lewis, R. N. A. H.; McElhaney, R. N. In *The Structure of Biological Membranes*; press, C. R. C., Ed., 1992; pp 74-155.
(28) Mabrey, S.; Sturtevant, M. J. *Pric. Natl. Acad. Sci.* **1976**, *73*, 3862-3866.
(29) Findlay, E. J.; Barton, G. *Biochemistry* **2400**, *17*, 2400-2405.
(30) Garidel, P.; Johansson, L. B. Å.; Blume, A. *Biophys. J.* **1997**, *72*, 2196-2210.
(31) Nibu, Y.; Inoue, T.; Motoda, I. *Biophysical Chemistry* **1995**, *56*, 273-280.
(32) Nibu, Y.; Inoue, T. *Chemistry and Physics of Lipids* **1995**, *76*, 181-191.
(33) Lindqvist, M.; Sarkar, M.; Winqvist, a.; Rozners, E.; Stromberg, R.; Graslund, A. *Biochemistry* **2000**, *39*, 1693-1701.
(34) Kyogoku, Y.; Lord, R. C.; Rich, A. *J. Am. Chem. Soc.* **1967**, *89*, 496-504.
(35) Liquier, J.; Akherbat, A.; Taillandier, E. *Spectochimica Acta* **1991**, *47A*, 177-186.
(36) Saenger, W. *Principle of Nucleic Acid Structure*; Springer Verlag: New York, 1984.
(37) Miles, H. T.; Frazier, J. *Biochemistry* **1978**, *17*, 2920-2927.
(38) Miles, H. T. *Pric. Natl. Acad. Sci.* **1964**, *51*, 1104-1109.
(39) Dante, S.; Hauss, T.; Dencher, N. A. *Biochemistry* **2003**, *42*, 13667-13672.
(40) Bringezu, F.; Wen, S.; Dante, S.; Hauss, T.; Majeroicz, M.; Waring, A. *Biochemistry* **2007**, *46*, 5678-5686.
(41) Beschiaschvili, G.; Seelig, J. *Biochemistry* **1990**, *29*, 52-58.
(42) Jing, W.; Demcoe, R. A.; Vogel, J. H. *J. Bacteriology* **2003**, *185*.
(43) Seelig, J. *Biochem. Biophys. Acta* **1997**, *1331*, 103-116.

Chapter 3

A new paradigm: Nucleolipoplexes

In the previous chapter we have shown the properties of nucleolipids assembled in lamellar phases. We have demonstrated that their phase behaviour is understandable neither considering the bare hydrophilic/hydrophobic energies nor merely the nucleic acids capabilities of H-bond and stacking between bases. However, the ability for molecular recognition between complementary bases seems to be guaranteed when nucleolipid molecules are arranged in any mesophases, displaying typical biological functionalities. These features let envisage possible applications, such as, for instance, the engineering of biocompatible vectors of single or double strand nucleic acids, with an important difference with respect to the state-of-the-art lipid-based approaches. The vast majority of synthetic non-viral vectors consists of cationic lipid assemblies, called lipoplexes, where nucleic acids are bound to liposomes thanks to charge interactions between the negative polyelectrolyte and the cationic headgroup of the lipid (see for more details part II)[1-3]. The main drawback of this approach, though, is the cytotoxicity, the immunogenic effects associated with some formulations and the possible binding to serum proteins, mostly negatively charged at physiological pH. Therefore, our strategy, directly inspired by nature, was to verify if anionic self-assemblies, less cytotoxic and enzymatically cleaved by phospholipases[4], could complex or at least encapsulate nucleic acid preserving their functionalities. This route is indeed a challenge and requires completely different strategies for bounding nucleic acid.

Our strategy relies on molecular recognition: in DNA or RNA, two like-charged strands pair thanks to chemical selectivity that overcomes electrostatic repulsion. In the following paragraphs, we will show that negatively charged nucleolipids can interact with negatively charged single strand nucleic acids, as well as nucleic acids double strands, thanks to their polar headgroup, whose molecular recognition capability is maintained or better promoted from the self-assembly.

Owing to the mild interaction we are taking into account, it was thought to avoid introducing, at the beginning, further parameters, such as buffer and ionic effects that could affect both lipids and nucleic acids, especially when dealing with

long polymer strands. The first system that has been taken into account consists in liquid bilayers at low water content. Diffraction techniques in the past have been used to highlight meaningful changes in bilayer profile and to observe lipid membranes structural modification by addition of proteins in-between lipid lamellae[5-7].

3.1 Nucleolipids Bilayers-Nucleic Acids Interactions

As a first step towards the engineering of nucleic acid/nucleolipid complexes, polynucleic acids (polyUridilic, polyU and polyAdenylic, polyA) were added to POPN membranes. These long-strands RNA polymers (sketched in Figure 3.1) were chosen due to their relatively low cost. They are prepared by the catalytic action of the enzyme, polynucleotide phosphorylase, and the appropriate, ribonucleoside diphosphate as substrate. They are thus real polymer. In general, polymers have the disadvantage of being molecules at high polymerization degree. And having a relatively high polydispersity, it is difficult to determine exactly a single molecular weight a priori. Packages of these products report an average indication of the number of bases or an average molecular weight, determined by electrophoresis normally in the range of 800kDalton-1000kDalton. Polynucleotides can have, depending on their stacking tendency, different conformations, like DNA. In particular, it is thought that a secondary structure could exist for polyA, whereas polyU should arrange in random-coil conformation[8-10]. This different conformation and not-uniform distribution of the molecular weights, represents a complication in understanding the interaction with nucleolipids.

The investigation of such polymers, embedded within nucleolipid assemblies, can provide useful indications concerning new strategies for delivering nucleic acid-based therapies into cells, without using carriers potentially dangerous as viruses or often cytotoxic as cationic lipid assemblies. Therefore, these systems seem to have all needed properties to become a new paradigm in lipids bilayer-nucleic acids interaction.

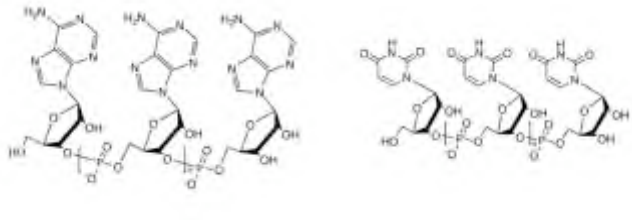

Figure3.1. Chemical Structures of polyA, polyAdenylic acid, on the left and polyU, polyUridilic acid, on the right.

Keeping in mind this scenario, we started an investigation on POPN/polyN in lamellar phases. The first step was to decide the strategy for sample preparation. It is, in fact, clear that it is hard to solve polyN in an organic solvent, without modifying its function, and then to prepare lipid films that contain these molecules.

Therefore, the *modus operandi* could be either starting from hydrated powder (pastes) or starting from aqueous liposomes dispersions. The first set of experiments was performed on pastes. This method allows knowing the exact amount of water added, which could aid to identify changes in the lamellar structures due to the polynucleotides. However, how much water is necessary to sufficiently hydrate nucleolipid membranes, considering, furthermore, that incorporated polyN molecules can subtract water from the lipid environment? To go beyond this question we proposed to work in large excess of water, to always guarantee full hydration conditions and liquid crystalline phases. This value was set at 50% w/w for all the investigated lipid membranes. To promote through mixing, both nucleolipid powder and polynucleotidic acid salts were dissolved in pure water; they were further lyophilized and re-hydrated to obtain the desired hydration. A recent investigation has reported diC_8P-Adenosine (1,2 dioctanoyl-phosphatidyl-adenosine) globular micelles interact with ss-polyUridylic acid in TRIS buffer to form superstructures that eventually evolve into an hexagonal mesophase where the biopolymer is confined between cylindrical micelles[11]. In the hypothesis that TRIS buffer might have a role in promoting the formation of this adduct, we decided to add also some TRIS salt in the sample, taking into account the symmetrically different POPA/TRIS molar ratio.

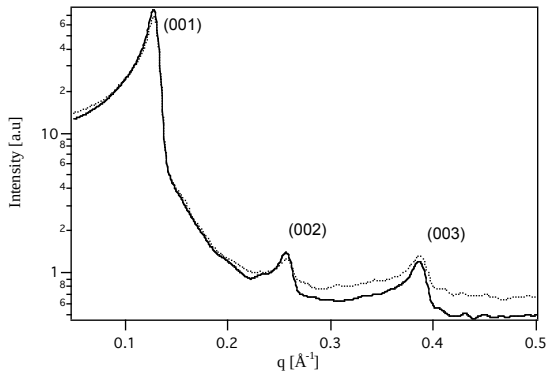

Figure3.2. Small Angle X-Ray Diffraction Spectra of pure POPA/Na^+ membranes at 50% w/w water and room temperature: after preparation (solid line) and after annealing at 50ºC (dotted line).

Figure 3.2 shows the SAXD pattern of POPA bilayers swollen with TRIS buffer (0.1M pH 7.5) to reach 50% w/w, corresponding to 47% v/v. The membrane is fully hydrated at this water content, as previously reported. If heated at 50ºC for one hour and then cooled down to RT, the smectic period (48Å) and line shape are fully recovered from the usual lamellar shrinkage due to the temperature increase. From the known lipid volume fraction a membrane thickness, δ_m, of 22.5 Å can be evaluated. However, we need to take into account the unusual low water uptake of POPA membranes (reported in the former paragraphs) and its powder-like nature. These features could point out that not all the water molecules added to POPA bilayers are in the interlamellar space, but rather phase separate. This separation has

an effect on the final bilayers spacing value, determining a not correct estimation of the bilayers thickness value.

The addition of TRIS salt does not affect appreciably the bilayers behaviour with respect to water. The number of reflections is low, as usual with this derivative. Moreover, the found spacing value resembles reasonably the value obtained in pure water (49 Å). It is possible that the slight increase in salt concentration exposes the POPA lamellae to a small osmotic stress, causing a negligible decrease of the bilayer thickness.

Interestingly, the addition of polyU, dissolved in the hydrating buffer in a 1:2 ratio (on a monomer basis) with respect to the lipid, produces, upon the same thermal treatment as for pure POPA membranes, a novel lamellar phase (Figure 3.3) with a smectic period of 57 Å, higher than that found for POPA bilayers (48Å).

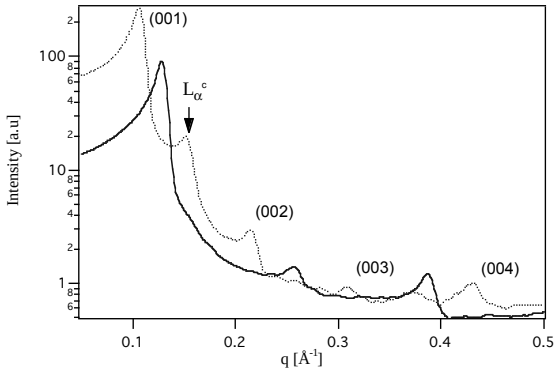

Figure3.3. Small Angle X-Ray Diffraction Spectra of POPA/polyU 2:1 complex at 50% w/w water and room temperature: after preparation (solid line) and after annealing at 50ºC (dotted line).

The most remarkable feature of this spectrum is the appearance of a broad peak between the first and the second lamellar Bragg reflections. This behaviour has first been observed for DOTAP/DOPC/DNA systems and has been attributed to spontaneous ordering of DNA in between the lamellae[12,13]. Following the same logic, the additional peak was attributed to an ordered lamellar phase of the type L_α^c, as the 1D lattice of DNA is called in lipoplexes[14-16]. The results obtained for lower polyU/lipid ratios confirmed our hypothesis. In fact, as it is depicted in Figure 3.4, varying the lipid/polynucleotide molar ratio, the broad peak, which it is impossible to assign to any different phase of POPA nucleolipid (e.g., cubic or hexagonal phases), shifts in the SAXD spectrum. The correlation distance decreases as the polynucleotide mole ratio is increased supporting that the reflection can be attributed to the ordering of single strands in between nucleolipid membranes, similarly to the "classical lipoplexes"[12,17-19]. The 1D lattice of polynucleotide chains corresponds to characteristic spacing of 38Å for POPA/polyU 2:1 ratio. The space available for the polymer in this membrane can be evaluated considering that the lipid bilayer thickness (d_L=26.7 Å) remains almost constant while encapsulating polynucleotides. Therefore, an estimate of the polyU thickness could be obtained by subtracting the bilayers spacing of pure nucleolipid membrane from the bilayers

spacing measured after annealing. This value results in about 5 Å that is, amazingly, in agreement with the average dimension of a nucleic acid base[20].

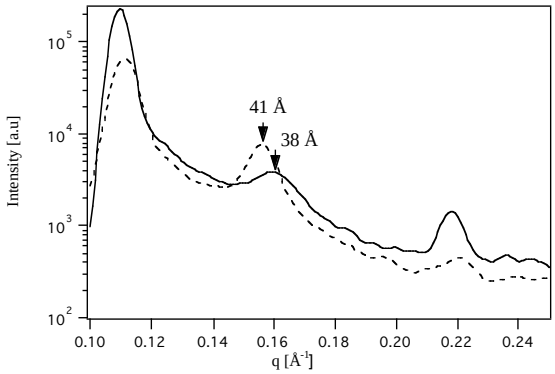

Figure3.4. Comparison of SAXS spectra of POPA/polyU complexes at different molar ratios: POPA/polyU 2:1 (solid line), POPA/polyU 10:1 (dashed line). The arrows indicate the broad peak assigned to polynucleotide ordering between the bilayers.

As already mentioned, our system substantially differs from conventional lipoplexes, where the driving force leading to the polynucleotide/membrane interaction is mainly of electrostatic nature. In our case the presence of like charges on membranes and on the polyelectrolyte, excludes the aspecific charge contribution. Considering that adenosine and uridine are complementary bases in RNA, a possible working hypothesis is the presence of molecular recognition between the bases decorating the anionic bilayer and the complementary bases on the strand that contribute to the formation of a novel mesostructure. This is strengthened by the fact that the addition of the non-complementary polyA to POPA bilayers does not produce either structural evolution upon annealing or formation of any new peak due to the ordering of polynucleotide within the lamellae. Figure 3.5 reports the SAXD spectrum for the former system.

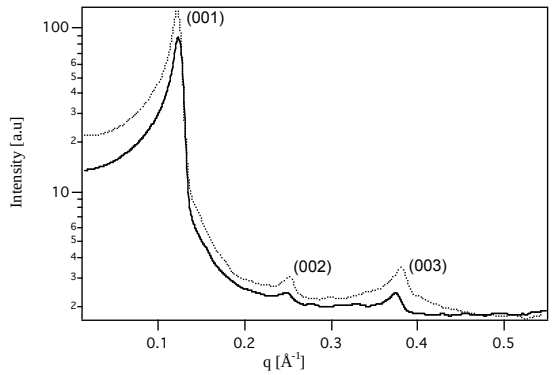

Figure3.5. Small Angle X-Ray Diffraction Spectra of POPA/polyA membranes at 50% w/w water and room temperature: after preparation (solid line) and after annealing at 50ºC (dotted line).

Unfortunately, the low number of reflection prevents us from obtaining a scattering electron density for these complexes. This profile would allow us to achieve details on the effect of the polynucleotides on nucleolipids polar head.

The same investigation was performed also on POPU/polyA systems. Figure 3.6 reports the SAXD pattern of POPU bilayers swollen with TRIS buffer (0.1M pH 7.5) to reach about 47% v/v. This spectrum shows that POPU lamellae are in a situation of water excess and again it highlights different behaviour in water uptake for POPA and POPU membranes. The shape of the scattering curve depicts that beside the diffraction of the lamellae there is also a diffuse scattering, indicating indirectly that there are a number of water molecules free within the bilayers; they take apart neighbour bilayers and hence they hinder the observation of higher diffraction order. Therefore, POPU membranes give rise only two broad peaks in the SAXD spectrum not because they have low mosaicity, but because there is a hindrance in detecting the lamellar order. The measured bilayer spacing results ~ 66 Å. This value is slightly smaller than the value found in pure water (69 Å), as for POPA the salt presence shrinks the lamellae.

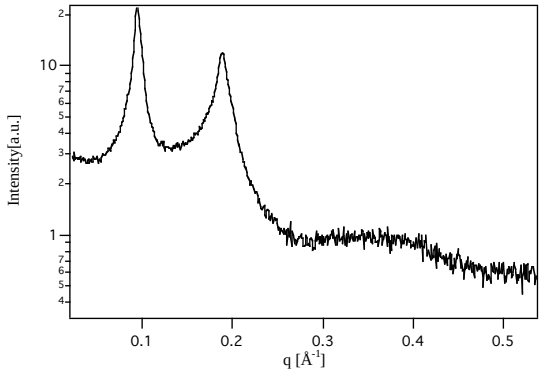

Figure3.6. Small Angle X-Ray Diffraction Spectrum of pure POPU/Na^+ membranes at 50% w/w water and room temperature after preparation.

Figure 3.7 shows spectrum obtained upon swelling with polyA solutions inside POPU membranes. Unexpectedly, three Bragg peaks emerge. Moreover, there is a decrease in the lamellar spacing of the sample measured just after preparation. The spacing drops from 66 Å to 51 Å. This decrease indicates that shrinkage of the bilayer due to osmotic stress is occurring. However, this value is very similar to thickness of POPU lamellae at ~26% w/w, which corresponds at the spontaneous water sorption. As if some water in excess was squeezed out of the bilayer to favour the interaction with polyA molecules. After annealing the lamellar phase swell and eventually evolve in two different lamellar phases with different spacing. The larger is located at ~0.11 Å^{-1} (~57 Å) and the smaller is at ~ 0.125 Å^{-1} (~50 Å). Owing to the overlap of the patterns, it is difficult to detect a peak of a possible 1D phase. As-matter-of-fact no extra peaks were observed within three weeks of repeated monitoring.

Remarkably, the investigated ternary systems (POPA/polyU/TRIS and POPU/polyA/TRIS) reach the same spacing after the annealing treatment. A

possible explanation of the appearance of a second phase and the fact that the 1D ordering of polyA does not show up, as for polyU, in the last system, could be attributed to the water excess. But it could be also due to the polyA conformation that should be destroyed in H-bonding with the uridine polar heads of POPU membranes.

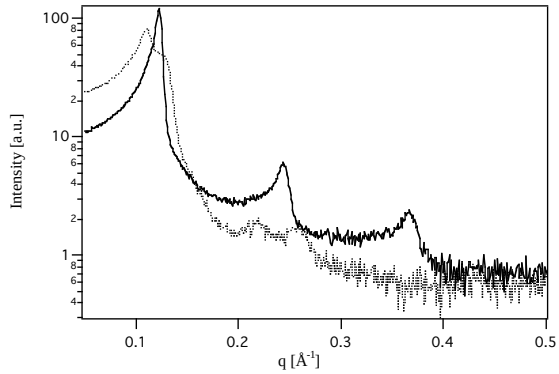

Figure3.7. Small Angle X-Ray Diffraction Spectra of POPU/polyA 2:1 at 50% w/w water and room temperature: after preparation (solid line) and after annealing at 50ºC (dotted line).

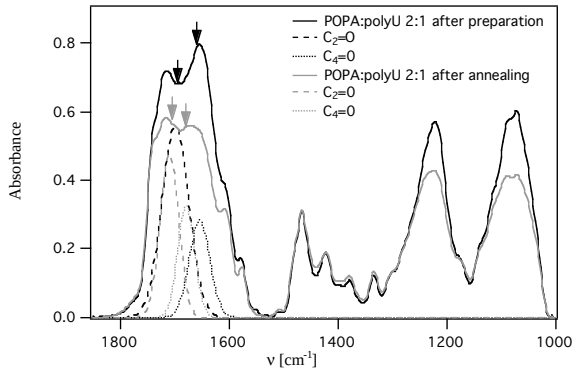

Figure3.8. FTIR spectra of POPA/polyU/TRIS buffer (50% w/w) after preparation (black line) and POPA/polyU/TRIS buffer (50% w/w) after annealing (grey line). C_4=O and C_2=O carbonyl stretching bands (sketched lines) are the de-convolved bands by Gaussians.

However, these structural modifications could be due to the molecular recognition between complementary bases. To infer direct evidence of the interactions, we have performed FTIR spectroscopy on the lamellar phase hosting the polynucleotide. Figure 3.8 shows the IR spectra of POPA/polyU systems freshly prepared and after the annealing procedure. From the literature[21-23] of the lipids and nucleotides the bands accounting for the specific bonds between adenosine and uridine bases are in the region 1600-1800 cm^{-1}. However, the broad band occurring in this region does not allow observing any shifts, at once. This region absorption bands were thus de-convolved using Gaussians contributions (Table 3.1). Assignments have been obtained by comparison with classical nucleic acid

literature. Nine functions were used to de-convolve these spectra; five functions allow for the POPA contributions (see more in paragraph 2.2 Part I) and four functions are due to polyU molecules.

The evolution of the ternary system during the annealing procedure, which yields the structural transformation observed with SAXD, can be illuminating. In the freshly prepared sample, characteristic bands, due to C_4=O and C_2=O stretching of the uridine moiety, can be noticed at about 1660 cm^{-1} and 1690 cm^{-1} respectively (black arrows Figure 3.8); after the annealing, these bands, that are diagnostic for H-bonding with adenosine, shift to 1675 cm^{-1} and 1712 cm^{-1}, i.e. in the direction expected for the formation of a Watson-Crick pair (grey arrows in Figure 3.8). Evidence of excess base stacking, due to insertion of polyU in the bilayer, has been also obtained through UV spectroscopy. Since the samples are highly concentrated, the measurements have been performed sandwiching the sample between two quartz slides, using retinol as internal standard[24]. This standard was used to compare the spectra obtained on the same sample at different temperatures and after the annealing treatment. Retinol is a hydrophobic molecule and therefore it is embedded into the membrane. The advantage in using it, is mainly related to the absorbance peak between 300 and 400 nm that does not strongly affect the main absorbance peak at 260 nm of the nucleolipid and the polynucleotide. To take into account possible modifications of the spectra due to scattering or environment differences, we have compared against the retinol absorption peaks. However, to reduce possible artefacts, we have performed UV measurements on the same sample. Figure 3.9 represents the UV spectra for the sample POPA/polyU 2:1. It shows the characteristic 260-centered band and a shoulder centred at 330 nm due to the absorption of retinol. This picture shows that the characteristic base peak at 260 nm decreases upon formation of the nucleolipoplex. The hyperchromic effect observed upon heating to 50ºC is related to a known de-stacking effect between neighbouring adenosine bases on the membrane induced by growing the temperature.

Table3.1. POPA/polyU 2:1 IR absorption fitting results.

After preparation	ν [cm^{-1}]		After annealing	ν [cm^{-1}]	
	1772 ±1			1773 ±1	
	1745 ±1	C=O		1745 ±1	C=O
	1728 ±1	C=O		1729 ±1	C=O
	1691 ±1	ν C_2=O polyU		1712 ±1	ν C2=O polyU
	1660 ±1	ν C_4=O polyU		1675 ±1	ν C4=O polyU
	1651 ±1	δ NH_2+ν ring		1655 ±1	δ NH_2+ν ring
	1617 ±1	ν ring polyU		1617 ±1	ν ring polyU

It is noteworthy that sample annealing is associated to a meaningful hypochromism, i.e., the signature for base stacking. These observations support that inclusion of polynucleotide single strands between anionic POPA membranes, observed through SAXD, occurs via molecular recognition between complementary base pairs and overcomes electrostatic repulsion.

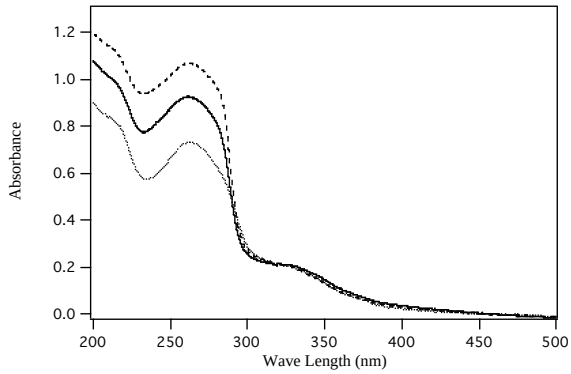

Figure3.9. UV spectra for POPA/polyU (2:1) bilayers with retinol sandwiched between sealed quartz slides. Solid line freshly prepared sample at RT, dashed line sample heated at 50°C, dotted line after annealing sample at RT.

To support the previous observations UV measurements have been also performed on POPA membranes. Figure 3.10 highlights the heating-induced hyperchromism as expected. However, the UV absorbance does not return to the starting value after the annealing treatment (dotted curve). This could indicate that nucleic base polar head changes its conformation upon heating and it does not recover the initial configuration after annealing. In our opinion, this change in conformation may be responsible for the interaction between POPA and polyU molecules after annealing at 50ºC. POPA behaviour over thermal annealing consolidates the observed hypochromism for POPA/polyU system.

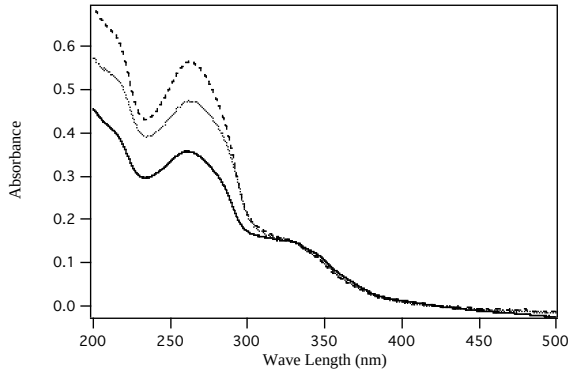

Figure3.10. UV spectra for POPA bilayers with retinol sandwiched between sealed quartz slides. Solid line freshly prepared sample at RT, dashed line sample heated at 50°C, dotted line after annealing sample at RT.

Even if POPU/polyA membranes do not form a unique phase, phase separation can occur in response to specific interactions between complementary A-U bases. The reasons why all of the systems do not evolve as POPA/polyU complexes, are currently not completely understood.

To gain further insights, FTIR absorption spectra for POPU/polyA have been collected. In fact, if there were some interactions, even partial, IR spectroscopy is able to stress it. Figure 3.11 shows that carboxylic uridine bands shift towards higher frequencies with annealing. This change matches the bands shifts observed for the same transition in the formation of polyA:polyU double helix.

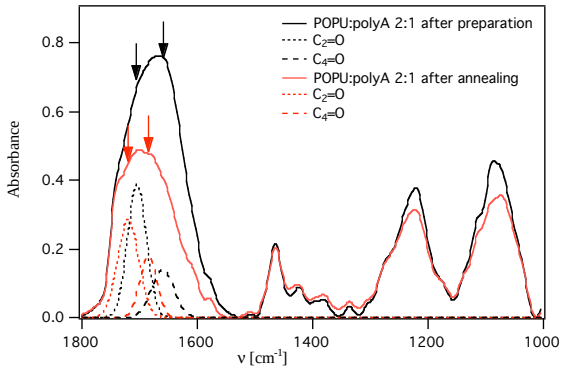

Figure3.11. FTIR spectra of POPU/polyA/TRIS buffer (50% w/w) after preparation (black line) and POPU/polyA/TRIS buffer (50% w/w) after annealing (red line). C_4=O and C_2=O carbonyl stretching bands (sketched lines) are the de-convolved bands by Gaussians.

To complete our investigation, we have performed an analysis on anionic POPG membrane with and without polynucleotides. If none of the observed effects were detected for identically charged membranes formed by POPG, any unspecific effect due to the biopolymer presence within nucleolipid membranes would be ruled out. Figure 3.12 illustrates SAXD spectra for POPG lamellae and for POPG/polyU lamellae swollen with TRIS buffer (0.1M pH 7.5) at 50% w/w. As it is visible, the addition of polyU, dissolved in the hydrating buffer in a 1:2 ratio with respect to the lipid, as for POPA and POPU lamellae, does not produce, upon the same thermal treatment as for POPN, any modification in POPG membranes. The only remarkable difference is a reduction of the bilayers spacing due to osmotic stress that sometimes may occur in agreement with the theory[25-27].

Finally, to support these data we have performed a thermal analysis on all the former investigated systems. DSC endothermic scans were collected avoiding freezing water in order to observe melting of the real gel-liquid crystalline transition[28]. The lipids studied in this work have a main transition temperature below zero degrees. If one wants to observe the transition in the melting direction, let water freeze, can represent a hurdle. In literature there are many examples where this is avoided by adding some addictives to water in order to decreasing its freezing temperature. However, we decided to not introduce further variables to our systems, taking advantage that the ice crystal formation is observed, by DSC, below zero when water is bound to other molecules. It is, in fact, known that there are at least three types of water molecules, which freeze at different temperatures[29-32]: the first kind, “supercooled”, is usually bulk water and it is observed to freeze at about -20ºC, the second one is an intermediate type water observed at ~ -50ºC and the third

is named unfreezable water. If these different kinds of water are frozen, they melt all together at 0ºC or near 0ºC if they occupy the interlamellar space[33,34].

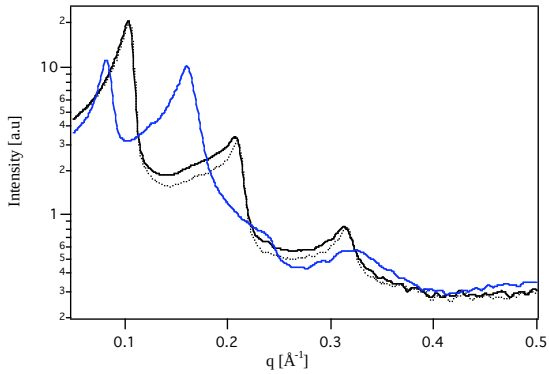

Figure3.12. Small Angle X-Ray Diffraction Spectra of POPG bilayers (blue line) and POPG/polyU 2:1 at 50% w/w water and room temperature: after preparation (solid line) and after annealing at 50ºC (dotted line).

Figure 3.13 reports the thermal scans for POPA and POPA/polyU mixtures. The peaks represent the melting of nucleolipids chains in the lamellar phase. It is our bare opinion that if interactions between the complementary bases of uridine and the adenosine headgroup of POPA occurred, the chain should be affected and they should change the gel-liquid crystalline phase transition. It is in fact known that small molecules, as ions, or large, as proteins affect the temperature transition, even if they interact with the polar part of the membrane [35].

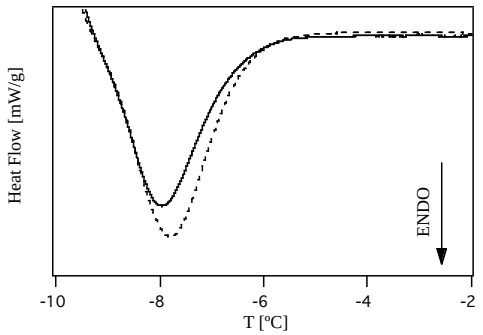

Figure 3.13. Differential Scanning Calorimetry heating curves for POPA (solid line), POPA/polyU 2:1 (dashed line) membranes at lipid/water 50/50% w/w.

As it is shown, when polyU is added, the main transition temperature shifts towards slightly higher values than for pure POPA membranes. The same shift was also detected for POPU/polyA adduct, where, however, was impossible to avoid freezing of water because of the lower transition temperature of POPU lamellae in water excess (Figure 3.14). Interestingly, the water-melting curve also changes its shape when the polynucleotides are present. A couple of effects influence the shape of the thermal peak, reflecting the presence of two lamellar phases, as SAXD

highlighted. Moreover, the heat of transition, which corresponds to the area between the experimental curve and an interpolated baseline, indicates the occurrence of interactions among nucleolipid lamellae and polyN. The enhanced enthalpy values prove a stabilization of the membranes when the polymers are incorporated, as reported in Table 3.2. Furthermore, it was reported that neutral lipid intercalating DNA strands within their lamellae by cation-bridges increases the chain melting temperature transition[36], as it happens in our case.

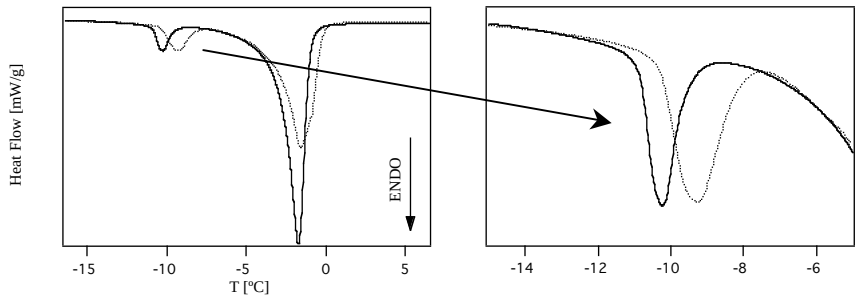

Figure 3.14. Differential Scanning Calorimetry heating curves for POPU (solid line), POPU/polyA 2:1 (dashed line) membranes at lipid/water 50/50% w/w. On the left a zoom of the lipid chain transition.

Table3.2. Main transition temperature and enthalpy of POPN and POPG lamellae with and without polyN

POPA	POPA /polyU	POPU	POPU /polyA	POPG	POPG /polyU
-8 ºC 13 [J/g]	-7.5 ºC 16 [J/g]	-10 ºC 15 [J/g]	-9 ºC 25 [J/g]	-6 ºC 16 [J/g]	-8 ºC 5 [J/g]

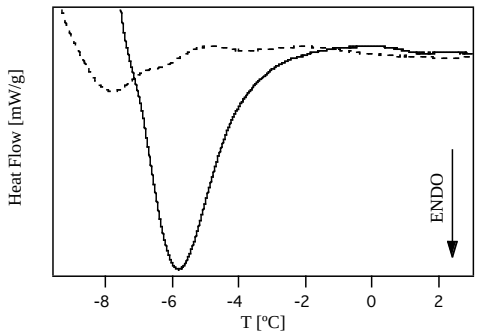

Figure 3.15. Differential Scanning Calorimetry heating curves for POPG (solid line), POPG/polyU 2:1 (dashed line) membranes at lipid/water 50/50% w/w.

Similar experiments, carried out for POPG/polyN systems, show (Figure 3.15) a decreasing of cooperativity throughout the membrane chain, as expected because of the increased osmotic stress, already observed through SAXD. To confirm this result, a polymer (PEG) notoriously used to produce membrane osmotic stress was

added to POPG lamellae. As it is possible to see in Figure 3.16, PEG decreases the tails cooperativity in POPG membranes, as well as polyN.

Amazingly, despite the same charge of the lipids, DSC scans, performed on POPG and nucleolipids membranes, show an opposite behaviour with the addition of polynucleotides.

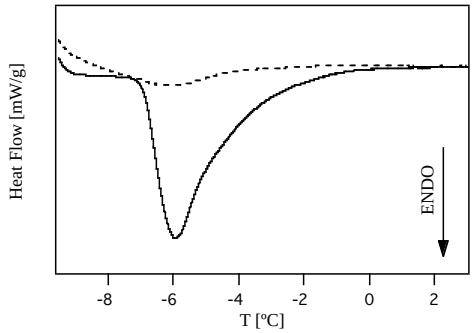

Figure 3.16. Differential Scanning Calorimetry heating curves for POPG (solid line), POPG/PEG (dashed line) membranes at lipid/water 50/50% w/w.

Concluding, all the experimental evidence support that inclusion of polynucleotide single strands between anionic POPN membranes, namely polyU L_{α}^{c} arrangement within POPA membranes observed through SAXD, occurs via molecular recognition between complementary base pairs and overcomes electrostatic repulsion. Figure 3.17 reports a descriptive model for the possible suprastructure.

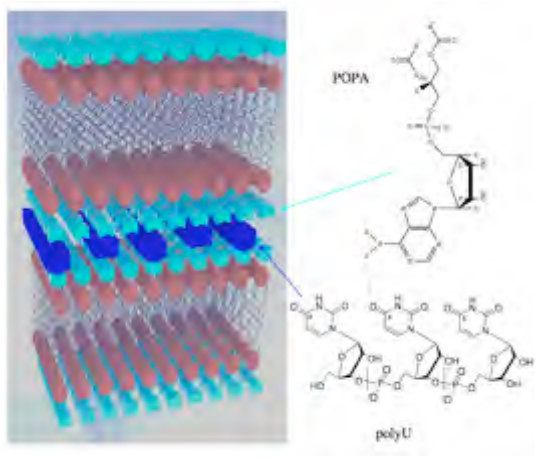

Figure3.17. Illustrative cartoon for a possible polyU arrangement in a nucleolipoplex. For the sake of clarity PolyU is here represented as a rigid rod.

3.1.1. Single strand DNA interaction with Nucleolipids Membranes

In this sub-section, we will show how 50-base oligonucleotides can be encapsulated between nucleolipid lamellae, in the same way as polynucleotides. This further investigation is not, so to say, a mere speculative test. We need to demonstrate that also single strand DNA can be encapsulated. In fact, we need to verify that also small strand of nucleic acids can interact with our nucleolipids, because short oligonucleotides are, as it will be accurately described in the next section, very interesting in views of future applications. For these reasons, a SAXD investigation has been performed on POPN/50-mers in the same environments previously studied. The only difference with respect to the systems with polynucleotides, is the different molar ratio between oligonucleotides and nucleolipid polar head. As reported in the caption of Figure 3.18, we have increased the amount of nucleolipid in the mixture. The reason of this choice is the very high cost of oligonucleotide products. In the systems, analyzed below, we used 50 thymine oligos, 50dT, and 50 adenosine oligos, 50dA (Figure 3.19).

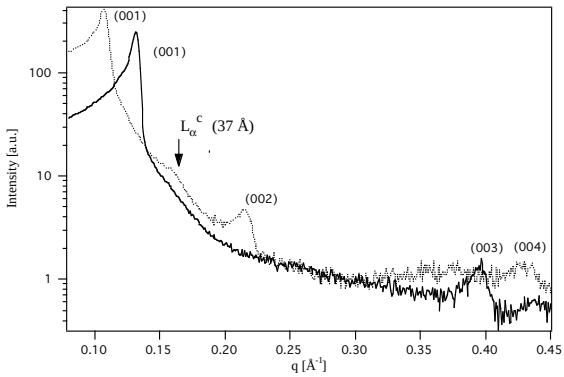

Figure3.18. Small Angle X-Ray Diffraction Spectra of POPA/50dT 3:1 complex at 50% w/w water and room temperature: after preparation (solid line) and after annealing at 50ºC (dotted line).

Aside from the varied ratio, the Figure 3.18 reproduces quite the same trend found previously when mixing polyU. However, it is worth highlighting some differences. At first glance, this shorter polymer seems carrying stronger modification within POPA bilayers. In fact, SAXD spectrum of the freshly prepared sample is very different with respect to POPA binary system (see Figure 3.2). Curiously, the second reflection disappears from the diffraction patterns. This is not due to a decrease in mosaicity, because the third reflection is still visible, but rather it is an indication that something is changed in the lamellae, affecting the form factor of the lipid. Any other speculation on this point is unfeasible due to the low number of reflections for both binary and ternary systems. However, it might be a signal of molecular recognition between complementary bases. On the base of this scenario, we could think that the 50dT 1D lattice might form more easily than for polyU. On the contrary, the experimental datum displays a different result after annealing process. The ordered lamellar phase of the type L_α^c is quite detectable and it appears less sharp than for polyU. The final lamellar spacing is, instead, slightly

larger turning out 58.5 Å. The characteristic distances between two close ordered chains is 37Å, fairly equal to the polyU one.

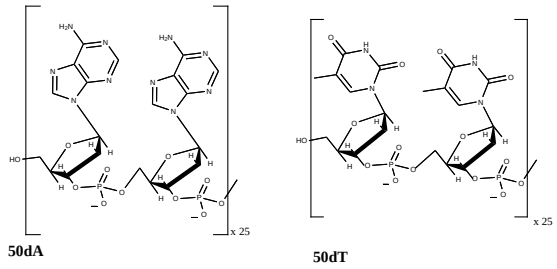

Figure3.19. Chemical Structures of 50-mer Thymine, 50dT, and 50-mer Adenosine, 50dA.

Why 50dT orders less easily within POPA lamellae is still under investigation. We guess, however, that shorter strands having fewer constraints could arrange more randomly in between the lamellae than long polymer chain.

Astonishing is what was found for POPU/50dA systems by SAXD (Figure 3.20). Once again, we cannot obtain a single lamellar phase. However, we obtained a confirmation that it is the excess of water inter-lamellae that hamper the complete swelling of the POPU bilayers when complementary base oligos are interacting with its special polar head, and it is not the polyA secondary structure that prevents the complete enlargement. As well as for POPA/50dT adduct, the freshly prepared sample has a different trend of diffraction patterns with respect to POPU binary systems. We have, though, to specify that a reduction of the bilayer spacing is still observed (51Å) because of the water squeezing, that in principle does not allow us to compare these two systems. However, observing the behaviour of POPA/50dT with respect to POPA and observing the SAXD spectrum of the freshly prepared POPU/polyA in Figure 3.7, it is possible to imagine that the reduced intensity of the second diffraction order for POPU/50dA may be due to the same cause affecting the SAXD spectrum of POPA/50dT; that is, bases pair between complementary bases.

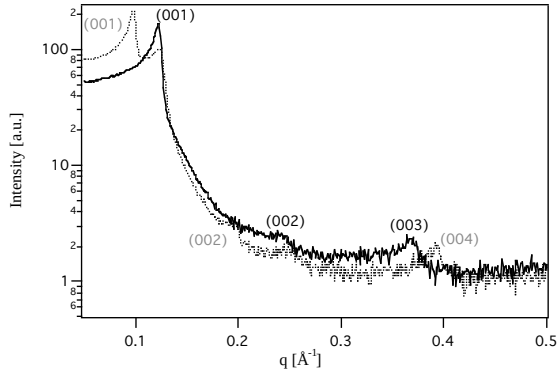

Figure3.20. Small Angle X-Ray Diffraction Spectra of POPU/50dA 3:1 complex at 50% w/w water and room temperature: after preparation (solid line) and after annealing at 50ºC (dotted line).

Outstanding is the larger lamellar phase dimension, about 65Å. This value is by far larger than the value found in the polyA case. Moreover, the appearance of the fourth order for the annealed sample (see Figure 3.20) - demonstration of increased order in the membrane organization - might induce the thought that missing the smaller lamellar phase the peak of the 1D lattice could be detectable.

3.2 Intercalation of Single Strand Oligonucleotides in-between POPN:POPC membranes

The previous paragraphs have demonstrated that it is possible to encapsulate single strand RNA or DNA inside nucleolipids membrane, taking advantage of specific hydrogen bonding between adenosine/uridine lipid headgroup and complementary oligonucleotide (Thymidine or Uridine) bases. As already said, these studies could represent a new approach in gene-delivery. However, there are many points that need our attention, as for example improving the lamellar mosaicity in order to obtain key information on the polymer ordination. This issue requires particular attention because it might permit to understand better mechanisms of encapsulation, in such a way to make easier designing more robust carrier for gene material. On this basis, we need to improve the number of collected reflection in order to work out a scattering profile of the lamellae. Chapter 2 showed that diluting POPA in nucleolipid lamellar could be an easy way to increase nucleolipid membrane mosaicity. Furthermore, we have already hinted at the important role of the helper lipid for transfection. So, we resumed in this section the results obtained for mixtures POPN:POPC and oligonucleotides, obtained dehydrating mixed lipidic vesicles and oligonucleotides, by neutron diffraction.

Three different systems, nucleolipid membrane/oligos, were taken into account: 1:1:1 POPA:POPC:50dT (on a monomer mole basis), 2:3:2 POPA:POPC:50dT and 1:1:2:2 POPA:POPU:POPC:50dAT. To assess again that likely any modification in the profile it driven only by molecular recognition between complementary bases, 1:1 POPG:POPC mixtures and oligonucleotides have been studied. A sketch of the molecular formula of all the molecules used in this analysis is reported in Figure 3.21.

The diffraction spectra of 1:1:1 POPA:POPC:50dT are depicted in Figure 3.22. This membrane seems to be at least biphasic, even if the presence of a possible third phase cannot be ruled out. The first peak is at 5.75 degrees, which corresponds to ~52Å; the second one is located at 5.20 degrees, which is ~58Å.

A first comparison with the system without oligonucleotides (see Chapter 2 Figure 2.18) highlights the presence of an extra phase with higher spacing than the binary system. As shown in Figure 3.22, the number of Bragg reflections decreases from five for the lipid mixture to three and the mosaicity obviously results worse.

The occurrence of this novel 58Å-spaced membrane cannot be observed in mixed lipid membranes without the oligos. Amazingly, this novel smectic period closely matches the SAXS spacings observed for POPA membranes with Polyuridylic acid or 50dT strands confined in the inter-lamellar space. However, the

presence of two phases in the present case complicates data interpretation. Besides the increased spacing, we observed for POPA/polyU the occurrence of an extra peak observed after annealing process, due to polyU ordering in-between the lamellae. Unfortunately, the limited available beam time for the neutron diffraction experiments precluded such analysis. Moreover, the phase separation does not permit to obtain any membrane profile that was one of our targets. However, some considerations have to be done for explaining such behaviour. First of all, phase separation is not connected to the presence of the helper lipid (because it had not been observed with POPA membranes): a reasonable hypothesis is that the presence of complementary oligonucloeotides in the fluid interlamellar space drives further the separation from POPC, favouring segregation into POPA/oligonucleotide rich domains. Secondly, the increase of thickness can be explained only invoking a possible variation of the base orientation with respect to the bilayer normal while including oligonucleotides.

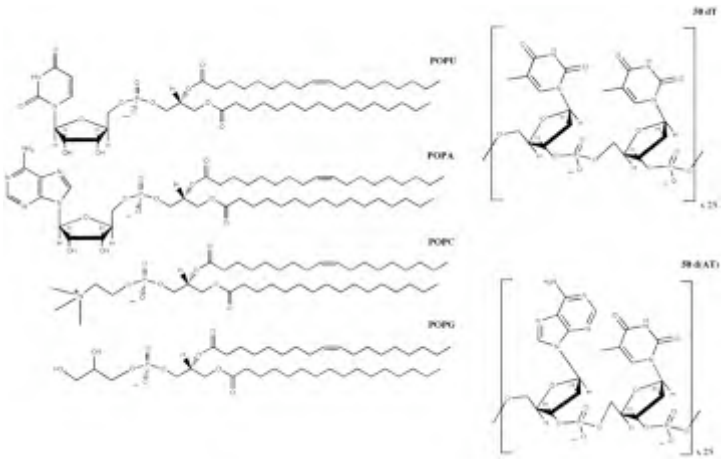

Figure3.21 Chemical structures of lipids (on the left) and oligonucleotides (on the right).

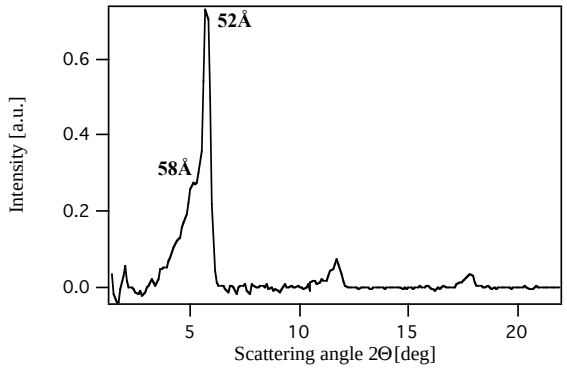

Figure3.22. Neutron diffraction patterns of 1:1:1 POPA:POPC:50dT bilayers at 8:92 D_2O:H_2O content.

A comparison with POPG:POPC:50dT system could help this interpretation. In fact, the presence of oligonucleotides produces no changing in the Bragg periodicity of the hydrated lamellar stacks, as shown in Figure 3.23a, with respect to the pure mixture (see paragraph 2.3). However, some dissimilarity with POPG:POPC can be found in the mosaicity (0.25º instead of 0.20º), see Figure 3.23b. Interestingly the *total* number of water molecules, as determined with gravimetric methods, does not vary with respect to the POPG:POPC case (~20% w/w). This would indicate *prima facie* no structural variation at all. A finer level of analysis, consisting in the SLD profile obtained from the same experimental data, shows however that the position of maximum contrast, corresponding to the headgroups for pure membranes, is shifted to higher values from the bilayer centre (i.e., the CH_3 terminal groups, profile not shown). Many factors might have caused this shift, which would indicate a higher bilayer thickness or a varied contrast profile.

From the literature on phospholipid bilayers, it is expected that the presence of polymers does not affect or at least it decreases the bilayer spacing and thickness because of the increased osmotic stress. Such a decrease has been for instance observed by us in previous SAXS experiments on POPG membranes swollen with polyUridylic aqueous solutions.

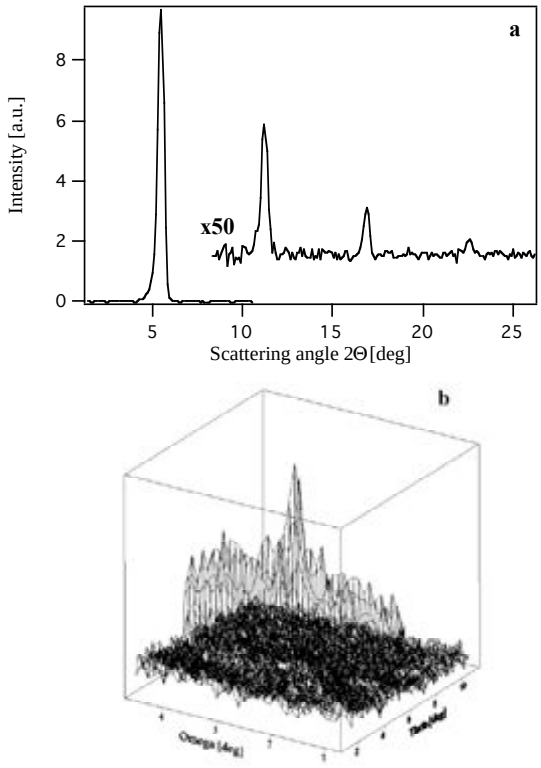

Figure3.23. a) Neutron diffraction patterns of 1:1:1 POPG:POPC:50dT bilayers at 50:50 D_2O:H_2O content, b) Rocking curves obtained by rotating the sample around the 1st Bragg peak of 1:1 POPG:POPC:50dT bilayers at 50:50 D_2O:H_2O.

A working hypothesis is that in the present case the oligonucleotide competes for water molecules with phospholipid headgroups, which result less hydrated, consistent with a higher bilayers thickness. However, to draw decisive conclusions on this aspect, experiments with varying concentrations or polymerization degree of the oligonucleotide should be performed, which is beyond the aim of this work.

A comparison between 1:1:1 POPA:POPC:50dT with the identically charged POPC:POPG, therefore, highlights that the effect of POPA interaction with 50dT is two-fold: it favours phase separation and increases the lamellar period.

A sketched model of the POPA:POPC:50dT structure is reported below (Figure 3.24). It is important to emphasize that, at this stage, we have no indications about the composition of the two lamellar phases; the more likely situation is that the higher smectic period phase is rich in POPA, whereas the second phase is down on nucleolipid ratio.

One key point that should be addressed is whether this lipid-lipid separation originates in the lamellar stacks or it is instead already present in the liposomal solution used for preparing these samples, a Cryo-TEM investigation will be performed to answer to this questions (see Chapter 5 pag.108).

However, it is worth noting that these mixtures prepared from liposomal suspensions seem to favour the interaction. A comparison with POPA/50dT prepared as pastes indicates that without annealing process a higher lamellar phase, due to the H-bond between adenosine headgroup in the bilayers surface and the oligonucleotides thymidine base, is occurred thanks to the liposomal preparation method and addition of helper lipids.

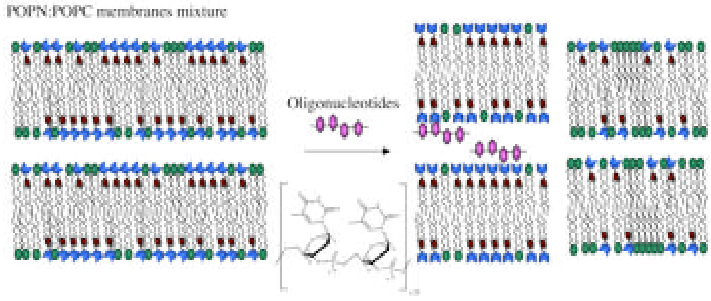

Figure3.24. Sketched of POPN:POPC mixed membrane without and with oligonucleotides, with a possible model for phase separation.

2:3 POPA:POPC mixed membranes, swollen with aqueous solution of 50dT looks more or less like the 1:1:1 POPA:POPC:50dT system. In this case we can still observe the occurrence of two new phases, whose bilayer spacings are the same as in the 1:1 mixture. However, it is worthwhile to note that the relative intensity of the peak for the predominant and large-spaced phase is, on a relative scale, higher in this mixture (Figure 3.25). In our opinion this effect can be correlated with the occurrence, as for pure membranes, of a phase separation, more pronounced for this latter composition. It is reasonable to hypothesize that the presence of POPA domains facilitates the interaction and reorganization of bilayers in the presence of oligonucleotides.

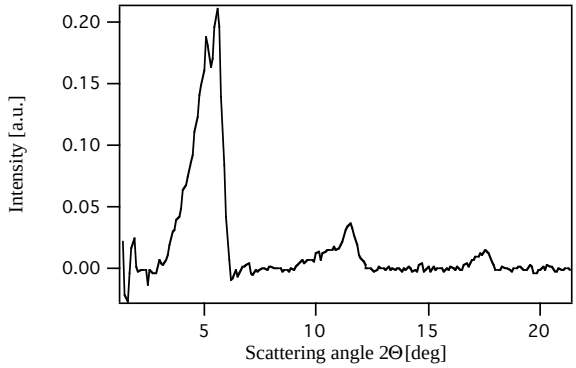

Figure3.25. Neutron diffraction patterns of 2:3:2 POPA:POPC:50dT bilayers at 8:92 D_2O:H_2O content.

Eventually, POPA:POPU:POPC samples swollen with 50d(AT) solutions behave in the same way as POPA:POPC oligos mixtures. Novel phases, whose spacings are ~53.5Å and ~62.5Å, can be observed in the neutron diffraction spectrum, as shown in Figure 3.26. Again the higher-spacing phase is predominant in this sample, further strengthening our hypothesis. The higher effects upon interaction with oligonucleotides can be observed for those lipidic compositions that already displayed phase separation. Therefore, phase separation and selective interactions with oligonucleotides can be traced back to the same driving force: H-bonding between complementary bases located on nucleolipid polar head and nucleic acid strands; that is molecular recognition. If we observe molecular recognition in pure lipid mixtures, then the system will exhibit selective interaction with complementary nucleic acids. This is an important guiding principle for the design and preparation of hybrid nucleolipid/oligonucleotides.

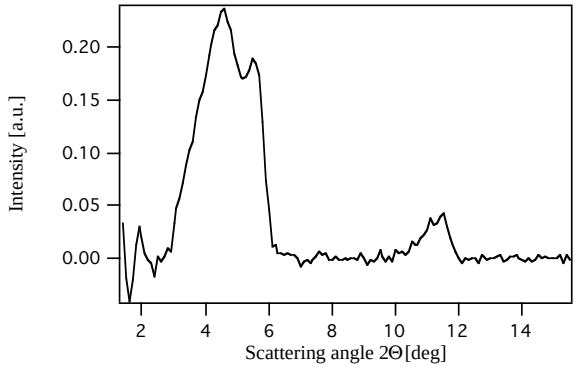

Figure3.26. Neutron diffraction patterns of 1:1:2:2 POPA:POPU:POPC:50d(AT) bilayers at 8:92 D_2O:H_2O content.

Moreover, before concluding, we would like to consider that phase separation in lipid-DNA systems is not a novelty. In particular, it was observed that natural lipid and DNA bound by divalent cations, can arise two lamellar phases[37-39]. This

system surely less difficult to modulate, thanks to the electrostatic interaction between ions bound to the membrane surface and negatively charged nucleic acid strands, allowed the researchers to address the composition of these two phases. Their conclusion was that one lamellar phase would be constituted by DNA within the lamellae. In this phase DNA would result condensed and strongly attached to lipid bilayers by means of divalent cations. The second lamellar phase, on the contrary, should be deprived in DNA and constituted only by pure lipid, which however would be less hydrated. Beside the different composition and driving force of nucleic acid embedding, this last consideration seems to adapt very well to our systems, as before suggested.

Bibliography

(1) Smyth-Templeton, N.; Lasic, D. D. *Therapeutic Mechanisms and Strategies*; Marcel Dekker Inc.: New York, 2000.

(2) Mahato, R. I.; Kim, S. W. *Pharmaceutical Perspectives of Nucleic Acid-Based Therapeutics*; Taylor and Francis: London and New York, 2002.

(3) Felgner, P. L.; Gadek, T. R.; Holm, M.; Roman, R.; Chan, H. W.; Wenz, M.; Northrop, J. P.; Ringold, G. M.; Danielsen, M. *Proc. Natl. Acad. Sci.* **1987**, *84*, 7413-7417.

(4) Shuto, S.; Ito, H.; Ueda, S.; Imamura, S.; Fukukawa, K.; Matsuda, A.; Ueda, T. *Chem. Pharm. Bull.* **1988**, *36*, 209.

(5) Bradshaw, J.; Davies, S. M. A.; Hauss, T. *Biophys. J.* **1998**, *75*, 889-895.

(6) Bringezu, F.; Wen, S.; Dante, S.; Hauss, T.; Majeroicz, M.; Waring, A. *Biochemistry* **2007**, *46*, 5678-5686.

(7) Dante, S.; Hauss, T.; Dencher, N. A. *Biophys. J.* **2002**, *83*, 2610-2616.

(8) Richards, E. G.; Flessel, C. P.; Fresco, J. R. *Biopolymers* **1963**, *1*, 431-446.

(9) Rich, A.; Davies, D. R.; Crick, F. H. C.; Watson, J. D. *J. Mol. Biol.* **1961**, *3*, 71.

(10) Sarkar, P. K.; Yang, J. T. *J. Biol. Chem,* **1965**, *240*, 2088-2093.

(11) Banchelli, M.; Berti, D.; Baglioni, P. *Angew. Chem.* **2007**, *47*, 3070 –3073.

(12) Salditt, T.; Koltover, I.; Radler, O. J.; Safinya, C. R. *Phys. Rev. Lett* **1997**, *79*, 2582-2585.

(13) Radler, O. J.; Koltover, I.; Salditt, T.; Safinya, C. R. *Science* **1997**, *275*, 810-813.

(14) Radler, O. J.; Koltover, I.; Jamieson, A.; Salditt, T.; Safinya, C. R. *Langmuir* **1998**, *14*, 4272-4283.

(15) Caracciolo, G.; Pozzi, D.; Amenitsch, H.; Caminiti, R. *Langmuir* **2005**, *21*, 11582-11587.

(16) McManus, J. J.; Radler, O. J.; Kenneth, A.; Dawson, K. A. *J. Am. Chem. Soc.* **2004**, *126*, 15966-15967.

(17) Koltover, I.; Salditt, T.; Safinya, C. R. *Biophys. J.* **1999**, *77*, 915-924.

(18) Safinya, C. R. *Curr. Opin. Struc. Biol.* **2001**, *11*, 440-448.

(19) Pott, T.; Roux, D. *FERBS letters* **2002**, *511*, 150-154.

(20) Saenger, W. *Principles of Nucleic Acid Structure*; Springer-Verlag: New York, 1984.

(21) Miles, H. T.; Frazier, J. *Biochemistry* **1978**, *17*, 2920-2927.

(22) Banyay, M.; Sarkar, M.; Graslund, A. *Biophys. Chem.* **2003**, *104*, 477-488.

(23) Liquier, J.; Taillanddier, E. In *Infrared spectroscopy of Biomolecules*; Chapman, D., Ed.; Wiley-Liss Inc.: New York, 1996; pp 131-158.

(24) Rajendra, J.; Damianoglou, A.; M.;, H.; Booth, P.; Marck Rodger, P.; Rodger., A. *Chem. Phys.* **2006**, *326*, 210-220.

(25) McIntosh, T. J.; Simon, S. A. *Biochemistry* **1986**, *25*, 4058-4066.
(26) Seelig, J. *J. Biochem.Biophys.Acta* **1997**, *1331*, 103-116.
(27) Burgess, S. W.; McIntosh, T. J.; Lentz, B. R. *Biochemistry* **1992**, *31*, 2653-2661.
(28) Koster, K.; Webb, M. S.; Bryant, G.; Lynch, D. V. *Biochimica et Biophysica Acta* **1994**, *1193*, 143-150.
(29) Ladbrooke, B. D.; Chapman, D. *Chem. Phys. Lipids* **1969**, *3*, 304-367.
(30) Ter-Minassian-Saraga, L.; Madelmont, G. *Journal of Colloid and Interface Science* **1981**, *81*, 369.
(31) Ter-Minassian-Saraga, L.; Madelmont, G. *Journal of Colloid and Interface Science* **1982**, *85*, 375.
(32) Lee, H. B.; Jhon, M. S.; Andrade, J. D. *Journal of Colloid and Interface Science* **1975**, *51*, 225.
(33) Aoki, H.; Kodama, M. *Thermochimica Acta* **1998**, *308*, 77-83.
(34) Kodama, M.; Kawasaki, Y.; Aoki, H.; Furukawa, Y. *Biochimica et Biophysica Acta* **2004**, *1667*, 56-66.
(35) Papahadjopoulos, D.; Moscarello, M.; Eylar, H. E.; Isac, T. *Biochimica et Biophysica Acta* **1975**, *401*, 317-335.
(36) Tarahovsky, Y. S.; Khusainova, R. S.; Gorelov, A. V.; Nicolaeva, T. I.; Deev, A. A.; Dawson, K. A.; Ivanitsky, G. R. *FEBS letters* **1996**, *390*, 133.
(37) Uhrikova, D.; Hanulova, M.; Funari, S. S.; Khusainova, R. S.; Sersen, F.; Balgavy, P. *Biochimica et Biophysica Acta* **2005**, *1713*, 15-28.
(38) McManus, J. J.; Radler, O. J.; Dawson, K. A. *Langmuir* **2003**, *19*, 9630-9637.
(39) McManus, J. J.; Radler, O. J.; Dawson, K. A. *J. Phys. Chem. B* **2003**, *107*, 9869-9875.

PART II

Chapter 4

Liposomes as Therapeutic delivery Vehicles

Liposomes are colloidal particles consisting of one or more lipid bilayers arranged around an aqueous core. Since the discovery of their structure, liposomes were recognized as a very useful model of biological membranes and they were applied as synthetic carrier for delivering drugs. The advantage of liposomes as drug-delivery systems is based on their colloidal structure. These aggregates, made typically of natural, biodegradable, non-toxic and nonimmunogenic lipid molecules, either can dissolve hydrophilic molecules inside their aqueous core or they can intercalate hydrophobic particles within their apolar chain. Moreover, owing to the numerable kinds of lipid polar heads, liposomes can bind other molecules, from small ionic particles up to large macromolecules, on their surface.

The development of their potential, though, required techniques for the generation of unilamellar liposomes and the design of processes for encapsulating drugs or macromolecules within them. It is known that there are many methods to prepare liposomes, but many of them are time consuming and not efficient in preparing liposomes of optimal size and polydispersity. Likewise, the methods of encapsulation need to be tailored to the drug's nature rather than to follow standard procedures. To this scenario we should add that the optimal size for delivering is an ambiguous concept. It seems in fact that only liposomes of small dimensions, around 100 nm, can vehicle drug without resulting toxic for cell membrane. Unilamellar vesicles of such size were found to be large and stable enough to carry sufficient amount of encapsulated material, but they were small enough to circulate for a sufficient time to reach the site of disease. On the other hand, larger liposomes were in several cases found working without increasing toxicity level with respect to the smaller one.

Furthermore, it is worth saying that use of liposomes as drug delivery carriers is even more confused as it comes to gene-therapy. Since the end of eighties, when Felgner *et al.*[1] discovered that cationic liposomes when mixed with DNA were able to transfect (i.e. the transport of DNA into cell followed by expression) nucleic acid

material within the cell, the number of liposomes-DNA complexes has grown enormously, mainly because of the need for enhancing their low *in-vivo transfection* efficiency in comparison with their competitors, viral vectors. The kind of encapsulation agents and the reported strategies for DNA embedding are as large as the number of proposed complexes, revealing often different and not in accord results.

The next paragraphs will resume liposomes classification and they will focus on liposomes-DNA complexes looking at the effect of preparation, structure and in vivo activity.

4.1 Classification and Preparation of liposomes

There are several classes of liposomes. Liposomes are classified either by their method of preparation or by the number of bilayers present in the vesicle, or by their size. When liposomes are described on the bases of the number of bilayers they are described as unilamellar vesicles (ULV) or multilamellar vesicles (MLV). Reverse-phase evaporation (REV), French press vesicles (FPV) and ether injection vesicles (EIV) are the descriptions based on method of preparation, while when liposomes are described based on their size, they are named LUV, large unilamellar vesicles, and SUV, small unilamellar vesicles. Three different nomenclatures could be confusing; however, the description based on lamellarity and size are more common than by methods of preparation[2].

In order to produce liposomes of whatever kind, lipid molecules must be introduces into an aqueous environment. However, dry lipid films do not form multilamellar vesicles spontaneously, if hydrated. They need additional mechanical energy (i.e. shaking, swirling, pipetting or vortexing) to expose hydrophobic edges resulting in formation of liposomes. This is connected with the theory of self-assembly[3]. It is known that spherical vesicles are thermodynamically favoured over planar bilayers due to their lower aggregation number, N, which indicates number of molecules necessary to form an aggregate. It seems that as soon as phospholipids are placed in aqueous solution the lipids initially form “neat mesomorphic phase” (bilayers or myelin figures) since as the lipids diffuse out of the bulk into water the local lipid concentration is initially very high. Once formed, bilayers cannot reform into vesicles without first having to break up. Initial stages of the formation of a spherical bulge from a infinite membrane is energetically favourable, but then the separation involves both adhesion and fusion at the neck of the bulge as the vesicle comes away from bilayers. For this to occur, a certain activation energy must be overcome, and it is this energy that is given by the mechanical agitation process. But even then the total concentration must be sufficiently low to be diluted enough not to interact significantly with each other. Thus, it is true that spherical vesicles are thermodynamically favoured over infinite bilayers, but they do not form spontaneously from bilayers.

To obtain MLV, it is sufficient to re-hydrate and then to shake the lipid films in an excess of aqueous buffer. However, the lamellarity can be modulated for

example increasing ability of drug encapsulation, by adding lipids with charged polar heads, such as negatively charged phosphatidyl serine PS, phosphatidyl inositol PI or phophatidyl glycerol PG or positively stearyl amine. Therefore, drug encapsulation may be favoured because of the increased interlamellar distance.

Sonication of this MLV dispersion is, historically, among the first mechanical treatments[4]. There are two sonication techniques: either the tip of a sonicator is immersed into the dispersion or a sample in a glass vials is placed into a bath sonicator. The first method is more common and largely used to produce SUV. However, a problem associated with the sonicator probe is its metal particle shedding. Conversion of MLV to SUV can be also achieved by passing trough a narrow orifice under high pressure[5]. This method is affected by many preparation variables. So, liposomes of different size were obtained by changing those parameters rather than sample composition. It was reported that multiple passes through the device are needed to obtain uniform vesicle size and the pressure is another parameter to be taken into account to obtain homogeneous particles. SUV can also be prepared by solvent injection methods such as ether injection or ethanol injection. In the former method, lipids dissolved in diethyl ether are slowly injected into warm water by a syringe. Subsequently the ether is removed from the preparation by applying vacuum. The resulting product are single layer vesicles[6].

Large unilamellar vesicles LUV are capable of holding larger volumes of solution in their cavity and thus have high encapsulation efficiency. An advantage of LUV is economy of lipids that can result from large quantity of drug inclusion in a smaller quantity of lipid. Large, speaking of liposomes, means larger than 100 nm. LUV are produced by REV or detergent dialysis technique[7]. However, LUV can be obtained from MLV by sequential extrusion through small size polycarbonate membranes under high pressure[8].

This latter method, so-called high-pressure extrusion technique, is very often used to prepared ULV. This technique is efficient because it is possible to obtain particles of controlled dimension and polydispersity. After swelling organic lipid film by aqueous buffer thanks to mechanical agitation, MLV are forced by means of a pressure (i.e. air or nitrogen) to pass through polycarbonate membranes of different pore sizes, according to the desired final size of the vesicles. It appears that when MLV are forced through the small hole of polycarbonate membrane, layers of bilayers are removed from liposome structure, as the layers of onionskin are separated when it is peeled. The homogeneity in size is guaranteed by several repetitions of this passage. Therefore, the morphology of liposomes sized by extrusion technique matches the size of the polycarbonate membrane as assessed by several characterizations performed by electron microscopy and photocorrelation spectroscopy. This method and/or this kind of liposomes were chosen to investigate nucleolipid/oligonucleotides systems in this work.

The procedure for preparation of REV liposomes was introduced by Szoka and Papahadjopoulos in 1978[7]. This method is comprised of two steps. The 1st one consists in preparing a water-in-oil emulsion of lipid and water buffer in excess of organic phase; in the 2nd step the organic solvent is removed under reduced pressure. Removal of the organic solvent under vacuum causes the lipid coated

water droplets to come together to form a gel like matrix. Further organic solvent subtraction brings the gel-matrix into a paste of smooth consistency. The pastes result a suspension of LUV particles. This method was used to encapsulate both small and large molecules. However, the main drawback of this method is the exposure of drugs to organic solvents, which may lead drugs, usually organic compounds, to denaturation or to damage. Biologically active molecules such as enzymes, protein, pharmaceutical products, and nucleic acid molecules may undergo conformational changes, protein denaturation, or breakage of DNA strands due to the harsh conditions of organic solvent. REV procedure gives mainly unilamellar liposomes, even though some multilamellar vesicles could form.

It exists another methods to obtain liposomes, which is called Freeze-dried rehydration vesicles (FRVs)[8]. This method is not used only to prepare pure liposomes, but even to encapsulate drug within liposomes. FRVs are formed from preformed vesicles. Starting from these vesicles very high entrapment efficiencies, even for macromolecules, can be achieved. Preformed liposomes are attached to a lyophilizer so to eliminate all water under vacuum. Then rehydration of the lipid is performed adding slowly very small portions of water solution. The total volume used for swelling must be smaller than the starting volume of liposome dispersion. The drying process brings the lipid bilayers and material to be encapsulated into close contact. Therefore, upon further swelling the chances for entrapment of adhered molecules are large.

4.2 Cationic Liposomes-DNA Complexes

Cationic liposomes are widely used to complex DNA. The reason is that positively charged polar headgroup of cationic lipids can bind through charge-charge interactions the negatively charged phosphate of nucleic acids strands. The formation process of these complexes, typically called lipoplexes, is spontaneous because of electrostatic interaction. Upon binding, DNA is compacted or condensed. In the condensed state, the helical segments are locally aligned and only one or two layers of water may separate DNA helices[9]. Cationic lipids providing this compaction protect DNA from nuclease degradation, as positively charged proteins do in nature[10]. This represents a key factor for DNA delivery vehicles research. In fact, it is known that naked-DNA has a low efficiency in reaching the target cell and often it cannot express the interested protein; in spite of these shortcomings the direct transport of naked-DNA inside cells found some useful applications[11]. Wolff and colleagues[12] showed, in fact, that genes could be expressed by means of direct injection into skeletal muscle, generating antiviral immune response. These immune responses are sufficient to protect animals from a wide variety of live infectious agents, leading to a new class of therapeutic modality called ‘DNA vaccines’[13]. Aside from this interesting field, though, the non-condensation of DNA is one of the most troublesome aspect of direct pure naked-DNA injection.

Moreover, the research in this sector is triggered by the need to find less dangerous DNA-vehicles for gene-therapy. In fact, non-pathogenic attenuated viruses are usually employed as delivery systems for DNA molecules[14]. These systems can efficiently transfer DNA molecules into cells due to millions of years of evolution as infective agents. For therapeutic purposes, the gene of interest is assembled in the viral genome and the virus uses its innate mechanism of infection to enter the cell and release the piece of DNA. Gene then enters the nucleus, is integrated into the host gene pool, and is eventually expressed. Retrovirus, parvovirus, adenovirus, lentivirus and herpes simplex virus were the most famous non-pathogenic attenuated viruses investigated for employing them in gene-therapy, because of their ability to transfer DNA within the cell[15]. Of course, gene therapy use viral delivery systems has made considerable progress for treatment of a wide range of diseases. In fact, one significant advantage of viral DNA vectors is their extremely high transfection efficiency in a variety of human tissues. Despite such improvements for gene transfer, there are several concerns over viruses to delivery DNA therapeutics in human beings. The key concern is the toxicity of the viruses and the potential for generating a strong immune response owing to their *proteinaceous capsid.* This is the main stimulus in researching other routes for DNA transfer, while shielding.

Although, numerous studies have demonstrated that cationic liposomal formulations[16,17] are able to delivery different DNA plasmids, better than injecting naked-DNA - in a wide range of cells[18], both *in vivo* and *in vitro* - there are several problems in transfection efficiency[11] of these complexes with respect to viruses. At this regard, one of the problems is that mechanisms of DNA transfer via cationic lipid still remain poorly understood[19]. However, to enhance efficiency there is a strong need to comprehend the supramolecular structures of lipoplexes and their interaction with cell membranes and eventually the mechanism by means of which DNA is released within the nucleus. As a consequence, low transfection efficiency has been attributed to heterogeneity in morphology and instability of lipoplexes. One of the more common structures, which form spontaneously when DNA is complexed with cationic liposomes, is a multilayer assembly of DNA sandwiched between bilayer membranes[20-24]. It seems that through DNA-lipid condensation, the cationic lipid tends to fully neutralize the phosphate groups on the DNA, releasing the originally condensed counterions in solution and determining high-order self-assemblies[19]. Following the same logic, other morphologies can be obtained varying the lipid mixture or the total charge on the lipid surface. It was found that CL-DNA mixture where DOPE (1,2-Dioleoyl-sn-Glycero-3-Phosphoethanolamine) was used instead of DOPC as helper lipid may give rise to a columnar inverted hexagonal liquid-crystalline structure, H_{II}^{C}[25,26]. In this structure DNA is coated with a lipid monolayer arranged on a hexagonal lattice. These different structures are reported to have a different stability and a diverse activity in gene-transfer. It was found out, for example, that transfection is more efficient in liposomes and DNA made of cationic lipid DOTAP and neutral DOPE than in mixture of the same cationic lipid and a similar quantity of helper lipid DOPC. What makes the H_{II}^{C} structure more functional than L_{α}^{C}, it is not yet understood. A hypothesis would be, as highlighted

in studying mouse fibroblast L-cells, that, in contrast with L_{α}^{C}, which remains stable inside the cells, the H_{II}^{C} complex shows fusion of its lipids with the mouse cell membranes, determining a consequent DNA release[27]. Clearly to comprehend all mechanisms of lipoplexes transfection efficiency, it is necessary to elucidate the effect of helper-lipid in modifying the structure and the ability of cationic lipid to complex DNA. Currently, zwitterionic lipids are believed to help the fusion due to perturbation of the cell membrane and increase the lamellarity[28-33]. Another explanation could be found in modulation of the $DNA^{-}/lipid^{+}$ ratio that could grow up lipid packing defects due to lipid separation between regions of DNA/surface interaction and regions where complex is not formed. These packing defects would destabilize the lipid/DNA complex and they would have an effect on transfection.

Hence, in addition to electrostatic attraction, hydrophobic interactions are believed to aid beyond complex formation between lipids and nucleic acids, also the mechanism of inter-change with the cell membrane[34]. Depending on the positive to negative charge ratio, in fact, lipoplexes enter cells through electrostatic interaction with charged residues at the cell surface, or by hydrophobic interaction with hydrophobic regions of plasma membrane.

As mentioned, lipoplexes provide the condensation of DNA. This means that the DNA conformation changes into the complex, leading to modify the chirooptical features of DNA. Some authors suggested that this change affect the biological properties of lipoplexes, as far as it concerns transfection efficiency[35,36]. They demonstrated that the secondary structure could be modulated by means of the gemini surfactant stereochemistry, which is used for binding.

Moreover, the transfection ability of lipoplexes depends on many other parameters, such as the type of target cell, the incubation condition and lipoplexes' preparation methods. An example of how preparation can affect the lipoplexes dimension was proposed by Rakhmanova *et al.*[37]; they showed that simply changing the addition order of DNA (vortexed or extruded liposomes added to DNA and vice versa) or the speed in adding (drop by drop or at constant rate) it possible to obtain many lipoplexes of different size. And it is important to note that the size of the complex is crucial in order to have an good lipofection efficiency[38]. At this regard, it was stressed that when negative complexes are formed, adding liposomes to an excess of DNA, smaller aggregated can be obtained, whereas large aggregation results in reverse the addition. This latter complex is reported to have a lower ability of transport DNA.

In conclusion, concentration of lipid and DNA, at time of mixing, cationic lipid/DNA ratio, order of addition, mixing rate, vesicle size, ionic strength of buffer used for swelling liposomes are some of parameters that might affect the lipoplexes "shape" and delivery-skill.

4.3 Cytotoxicity issues applicable to lipoplexes in gene-therapy

The previous paragraph highlights that nonviral transfection systems such as cationic liposomes are generally preferred over viruses because they are nonimmunogenic, are relatively easy to assemble, and are amenable to scale-up for industrial production. In addition, liposomal delivery vehicles offer versatility with a diverse range of morphologies, size, and release characteristics; they can be used for tissue targeting and provide protection of the plasmid DNA from attack by degradative nucleases. Since their introduction lipoplexes, have been used in numerous research protocols for DNA delivery in a range of cell types and are currently being investigated in several gene therapy clinical trials.

However, cationic liposomes can be inactivated in the presence of serum, and they are reported of being unstable upon storage, even though they are relatively efficient in delivering DNA into cells. Therefore, beside the problem in poor transfection efficiency, lipoplexes are affected by other concerns.

At this regard, citotoxicity of cationic liposomes is a key topic[39]. Cationic lipids have, in fact, showed toxicity level in several in vivo and in vitro studies, since long. In one of the earliest in-vivo investigation, Adams and Hamilton[40] demonstrated that when cationic liposomes were administered via intraocular instillation, an inflammation of the eyes occurred. Moreover, positively charged liposomes have also been noted to cause inflammatory response when administered intraarticularly into knees or they have induced acute systemic inflammatory reaction into mice lungs. As well as cationic liposomes, positively charged lipoplexes either have caused the formation of emboli in mice circulation after intravenous injection or were found to be highly toxic when administered orally, provoking a dramatic hypothermia resulting eventually in the death of some mice[15]. The most famous commercially available cationic lipid-nucleic acid base transfection agent, Lipofectamine, has been again reported to induce toxicity in various tissues, such as pulmonary cells both in vivo and in vitro.

The major reasons of this large citotoxicity are mainly two. The first is represented by the positive charge of cationic lipids. These molecules, when in contact with cell membranes, mainly made of negatively charged lipids, suffer from electrostatic repulsion that eventually injures the cell rather than provoking a benefit. Therefore, the mechanism of toxicity of lipoplexes would depend on the alteration of the net charge of the cell membranes. This would affect the activity of ion channels, membrane receptors and enzymes. The second is represented by the size of these self-assemblies, often too large, resulting noxious for cells.

However, it was observed that in some carriers replacing DOPE by DPPC, a reduction of the toxicity occurs[41]. This introduces another effect of the helper lipid in researching for the optimal formulation for in vivo gene transfer, further complicating this scenario.

Despite the appreciable success of these vehicles as novel promises of gene therapy, it is evident that there is a need for efficient and well-tolerable delivery systems to exploit the benefit of gene medicine.

4.4 Other Liposomes Delivery Systems for DNA transfer

Anionic Liposomes:

As an alternative to cationic lipids, anionic lipids for DNA delivery represent a more challenging task and need to make up different strategies for complexing the similarly charged DNA. A few studies were, though, reported where furthermore the safety of anionic lipids was highlighted when these adducts were administered to epithelial lung tissue[42]. Anionic lipoplexes were achieved by the formation of a ternary complex between plasmid DNA and anionic liposomes using Ca^{2+} ion bridges[43,44]. During formation of the anionic lipid/DNA complex, it was shown that DNA conformation is dramatically different from that of the binary complex of plasmid DNA and Ca^{2+} alone. In these systems, DNA undergoes to a conformational transition from native B-DNA to condensed Z-DNA. Ca^{2+} alone without anionic lipid is not able to favour this transition.

Another example describes entrapment of DNA in anionic DPPC/DMPG liposomes prepared with Freeze-dried rehydration vesicles method in presence of bivalent cations[45]. In this work it seems that DNA was practically only within the liposomes, indicating a complete different way of protecting DNA with respect to lipoplexes where the DNA is external. Moreover, these authors point out that anionic liposomes releases easily DNA from the complexes when interacting with cell membranes. This is a very important topic given the low DNA release of lipoplexes that prevents them from a high gene expression. However, it further highlights that absence of calcium or other ions DNA has no effect on negatively charged liposomes because electrostatic repulsion does not allow them to interact with these molecules. This result is extremely interesting, in view of the work that will be described in this thesis. The structure of DNA/anionic liposomes mediated by divalent cations were described as a lamellar structure with alternating layers of like-charged DNA and anionic membrane bound together with these ions[46]. As the membrane charge density is increased, a new phase with no analogue in CL-DNA was found. This phase is composed from anionic lipid lamellar stacks where the attraction is ruled by divalent cations without DNA. In contrast to lipoplexes structures, no in-plane correlation was observed with these systems. Authors hypothesize that the DNA peak loss may be caused by weak in-plane ordering, which in fact can be easily broken by strengthening the anionic lipids concentration.

Similarly, anionic liposomes were capable of delivering oligonucleotides into bacterial cell. In this case, the encapsulation of single strands was facilitated by Na^+ and K^+ ions[45].

Zwitterionic Liposomes:

This approach is likely the same of cationic liposomes. The driving force of complexation is in fact electrostatic interaction. The surface positively charged of

cationic lipid vesicles can be obtained by addition of metal bivalent cations to neutral lipids[47].

Two structures were found for this kind of DNA carriers: the first, as already mentioned in previous chapter, almost similar to lipoplexes resemble a sandwich of DNA in between lipid bilayers. However as reported by Francescangeli *et al.*[48] two coexisting lamellar phases were found: one with DNA strand intercalated in the water lipid bilayer and another formed only by pure lipid bilayers. The second kind of structure showed a rectangular organization of DNA within neutral lipid bilayers[49].

However, Pott *et al.*[50] proved the complexation of DNA in neutral lipid membrane without mediation by divalent cations. They formed DNA-NL as complex by preparing soy bean diacylphosphatidylcholine membranes mixed with a small amount of monoolein to facilitate MLV formation. Nevertheless, in the absence of electrostatic interactions the DNA is connected into the interstitial space rather than condensed by counterion mechanism as in lipoplexes. The structure that they proposed is outstandingly similar to lipoplexes, however they suggested that in this case L_{α}^{C} should be indicated as confined instead of as condensed. Moreover, DNA in such structure does not interact strongly with membrane surface, promising an easier release.

Unfortunately, even if very promising, by our knowledge all these systems have not yet been tested either in vitro or in vivo.

Stabilized plasmid-lipid particles (SPLP):

Owing to their size and positive charge characteristics, as said, lipoplexes showed low circulation lifetime in serum and tendency to be cleared rapidly from circulation. For this reason, recently it was developed a different approach for preparing more stable particles. These particles were called stabilized plasmid-lipid particles SPLP[51]. They are made of monodisperse DNA encapsulated in a unilamellar lipid vesicles composed of DOPE and a cationic lipid DODAC, which drives the complexation, and PEG-ceramide. SPLP are formed by detergent dialysis procedure thanks to the stability and solubility of cationic lipid-DNA in organic solvent. These particles are small enough, around 70 nm, which, we remind, is basic to guarantee low toxicity and to exhibit extended circulation lifetime. They satisfy the demands of plasmid encapsulation and serum stability as well. Moreover, it seems that PEG coating might module the transfection properties.

Bibliography

(1) Felgner, P. L.; Gadek, T. R.; Holm, M.; Roman, R.; Chan, H. W.; Wenz, M.; Norhrop, J. P.; Ringold, G. M.; Danielsen, M. *Proc Natl Acad Sci* **1987**, *84*, 7413-7417.

(2) Vemuri, S.; Rhodes, C. T. *Pharm. Acta. Helv.* **1995**, *70*, 95-111.

(3) Isrealachvili, j.; Mitchell, D. J.; Ninham, B. W. *J. Chem. Soc. Faraday Trans.* **1976**, *72*, 1525.

(4) Papahadjopoulos, D.; Watkins, J. C. *Biochim. Biophys. Acta.* **1967**, *135*, 639.

(5) Hamilton, R. L.; Goerke, J.; Guo, L. *J. Lipid Res.* **1980**, *21*, 981-992.

(6) Deamer, D.; Bangham, A. D. *Biochim. Biophys. Acta.*, *443*, 629-634.

(7) Szoka, F.; Papahadjopoulos, D. *Proc Natl Acad Sci* **1978**, *75*, 4194-4198.

(8) Lasch, J.; Weissig, V.; Brandl, M. In *Liposomes*; Torchilin, V. P.; Weissig, V., Eds.; Oxford University Press, 2003; pp 3-29.

(9) Bloomfield, V. A. *Curr. Opin. Struc. Biol.* **1996**, *6*, 334-341.

(10) Gelderblom, H. R. In *Medical Microbiology*; Baron, S., Ed.; Univ of Texas Medical Branch; 4th edition, 1996.

(11) Li, S.; Haung, L. *Gene Therapy* **2000**, *7*, 31-34.

(12) Wolff, J. A.; Malone, R. W.; Williams, P.; Chong, W.; Acsadi, G.; Jani, A.; Felgner, P. L. *Science* **1990**, *247*, 1465-1468.

(13) Ulmer, J. B.; Donnelly, J. J.; Parker, S. E.; Rhodes, G. H.; Felgner, P. L.; Dwarki, V. J.; Gromkowski, S. H.; Deck, R. R.; Dewitt, C. M.; Friedman, A.; Hawe, L. A.; Leander, K. R.; Martinez, D.; Perry, H. C.; Shiver, J. W.; Montgomery, D. L.; Liu, M. A. *Science* **1993**, *259*, 1745-1749.

(14) Kamiya, H.; Tsuchiya, H.; Yamazaki, J.; Harashima, H. *Adv. Drug Deliv. Rev.* **2001**, *52*, 153-164.

(15) Patil, S. D.; Rhodes, D. G.; Burgess, D. J. *Aaps Journal* **2005**, *7*, E61-E77.

(16) Cotten, M.; Wagner, E. *Curr. Opin. Biotech.* **1993**, *4*, 705-710.

(17) Felgner, P. L. *Adv. Drug Deliv. Rev.* **1990**, *5*, 163-187.

(18) Marshall, J.; Yew, N. S.; Eastmann, S. J.; Jiang, C.; Scheule, R. K.; Cheng, S. H. In *Nonviral Vectors for Gene Therapy*; Wagner, E., Ed.; Academic Press: San Diego, 1999.

(19) Safinya, C. R. *Curr. Opin. Struc. Biol.* **2001**, *11*, 440-448.

(20) Radler, J. O.; Koltover, I.; Salditt, T.; Safinya, C. R. *Science* **1997**, *275*, 810-813.

(21) Salditt, T.; Koltover, I.; Radler, J. O.; Safinya, C. R. *Phys. Rev. Lett* **1997**, *79*, 2582-2585.

(22) Koltover, I.; Salditt, T.; Safinya, C. R. *Biophys. J.* **1999**, *77*, 915-924.

(23) Salditt, T.; Koltover, I.; Radler, J. O.; Safinya, C. R. *Phys. Rev. E* **1998**, *58*, 889-904.
(24) Lasic, D. D.; Strey, H.; Stuart, M. C. A.; Podgornik, R.; Frederik, P. M. *J. Am. Chem. Soc.* **1997**, *119*, 832-833.
(25) Farhood, H.; Serbina, N.; Huang, L. *Biochim. Biophys. Acta-Biomembr.* **1995**, *1235*, 289-295.
(26) Koltover, I.; Salditt, T.; Radler, J. O.; Safinya, C. R. *Science* **1998**, *281*, 78-81.
(27) Lin, A. J.; Slack, N. L.; Ahmad, A.; Koltover, I.; George, C. X.; Samuel, C. E.; Safinya, C. R. *J. Drug Target.* **2000**, *8*, 13-27.
(28) Zuhorn, I.; Oberle, V.; Visser, W. H.; Engberts, J. B. F. N.; Bakosky, U. *Biophys. J.* **2002**, *83*, 2096-2108.
(29) Crook, K.; Stevenson, B.; Dubouchet, M.; Porteous, D. *Gene Therapy* **1998**, *5*, 137-143.
(30) Hui, W. S.; Langer, M.; Zhao, Y. L.; Ross, P.; Hurley, E.; Chan, K. *Biophys. J.* **1996**, *71*, 590-599.
(31) Sakurai, F.; Nishioka, T.; Saito, H.; Baba, T.; Okuda, A.; Matsumoto, O.; Taga, T.; Yamashita, F.; Takakura, Y.; Hashida, M. *Gene Therapy* **2001**, 677-685.
(32) Ma, B.; Zhang, S.; Jiang, H.; Zhao, B.; Lv, H. *J. Control Release* **2007**, *123*, 184-194.
(33) Rakhmanova, A. V.; McIntosh, J. T.; MacDonald, C. R. *Cell. Mol. Biol. Lett.* **1995**, *5*, 51-65.
(34) Wong, F. M. P.; Reimer, D. L.; Bally, M. B. *Biochemistry* **1996**, *35*, 5756-5763.
(35) Bombelli, C.; Borocci, S.; Diociaiuti, M.; Faggioli, F.; alantini, L.; Luciani, P.; Mancini, G.; Sacco, M. G. *Langmuir* **2005**, *21*, 10271-10274.
(36) Bombelli, C.; Faggioli, F.; Luciani, P.; Mancini, G.; Sacco, M. G. *J. Med. Chem.* **2005**, *48*, 5378-5382.
(37) Rakhmanova, V. A.; Pozharski, E. V.; MacDonald, R. C. *J. Membr. Biol.* **2004**, *200*, 35-45.
(38) Ross, C. P.; Hui, W. S. *Gene Therapy* **1999**, *6*, 651-659.
(39) Dass, C. R. *J. Pharm. Pharmacol.* **2001**, *54*, 593-601.
(40) Adams, D. O.; Hamilton, T. A. *Ann. Rev. Immunol.* **1977**, *2*, 283-318.
(41) Filion, M. C.; Philips, N. C. *Biochim. Biophys. Acta.* **1997**, *1329*, 345-356.
(42) Dokka, S.; Toledo, D.; Shi, X. G.; Castranova, V.; Rojanasakul, Y. *Pharm. Res.* **2000**, *17*, 521-525.
(43) Patil, S. D.; Rhodes, D. G.; Burgess, D. J. *Aaps Journal* **2004**, *6*, 1-10.
(44) Patil, S. D.; Rhodes, D. G.; Burgess, D. J. *Biochim. Biophys. Acta.* **2005**, *1711*, 1-11.
(45) Fillion, P.; Desjardins, A.; Sayasuth, K.; Lagace, J. *Biochim. Biophys. Acta.* **2001**, *1515*, 44-54.
(46) Liang, H.; Harries, D.; Wong, G. C. L. *Proc Natl Acad Sci* **2005**, *102*, 11173-11178.

(47) Uhrikova, D.; Hanulova, M.; Funari, S. S.; Khusainova, R. S.; Sersen, F.; Balgavy, P. *Biochimica et Biophysica Acta* **2005**, *1713*, 15-28.
(48) Francescangeli, O.; Stanic, V.; Gobbi, L. *Phys. Rev. E* **2003**, *67*, 011904.
(49) McManus, J. J.; Radler, J. O.; Dawson, K. A. *J. Am. Chem. Soc.* **2004**, *126*, 15966-15967.
(50) Pott, T.; Roux, D. *FEBS letter* **2002**, *511*, 150-154.
(51) Wheeler, J. J.; Palmer, L.; Ossanlou, M.; MacLachlan, I.; Graham, R. W.; Zhang, Y. P.; Hope, M. J.; Scherrer, P.; Cullis, P. R. *Gene Therapy* **1999**, *6*, 271-281.

Chapter 5

Hybrid Structures between Nucleolipid liposomes and Oligonucleotides

In the previous chapter we have summarized all the reported approaches of lipid non-viral vectors for gene therapy. These carriers for DNA became the subject of intense research in the last decades in order to find drug delivery systems that can be less dangerous for human health and less cytotoxic for cells. In the first part of this thesis, we have highlighted that our strategy is to mimic Nature in designing these new less toxic vectors for nucleic acids. We showed that it is possible to drive interaction between complementary bases if it exists a structure (e.g., lipid lamellar phase) that strengthens the molecular recognition capability of the nucleolipid polar heads. However, lamellar phases in the low water content regimes, that demonstrate and describe this nucleolipids ability, are far from being drugs' carrier, requiring other approaches and further studies for achieving our aims. As widely discussed in the previous chapter, liposomes are utilized in a great deal of formulations due to their ability either to encapsulate or to transport or to release drugs. Moreover, liposomes form, thanks to the lipid organization, bilayers. Therefore, in principle, we should not find dissimilarity with respect to our previous data, despite working with liposomes instead of infinite membranes. Nevertheless, the concentration of nucleolipids and nucleic acids we will use to prepare liposomes are by far lower than for membrane systems, thereby we need to verify that these interactions can occur following the same mechanisms.

In the further sections, the buffer, the need for annealing, the oligonucleotides encapsulation techniques and the kinetic of possible processes will be taken into account, discussing the obtained results for POPN liposomes and oligonucleotides systems.

5.1 Effect of Buffer on Nucleolipids/Polynucleotides interaction

The interaction of polynucleotides (ss-RNA) with POPA, POPU and POPG liposomes were investigated. Three different buffers solutions were chosen to study these self-assemblies: TRIS 0.1M buffer, Phosphate 0.1M buffer and TRIS 0.1M/KCl 0.1M buffer. Buffers were set at pH 7.5 in this investigation. This value was chosen in relation to future test in vitro due to its biological relevance. Another reason is related to POPA molecules, which having an amino group on the adenosine base can be charged at acidic pH, affecting comparison with the other lipids.

Polynucleotides were added to the lipid aggregates following two preparation methods. In the first one, after swelling the lipidic film with buffer, liposomes were usually sized down by extrusion. After liposome preparation, a given amount of polynucleotides dissolved in the same buffer was added. In the second approach, the polynucleotide solution itself was used to swell the lipidic film and then the mixture was co-extruded. As reported in chapter 4, both preparations are generally used in liposomes/drugs formulation and in particular in liposome/DNA vehicles due to different formulation approaches and diverse strategies for complexation. We would like to remind the mild character of interactions that can arise between nucleolipids and polynucleotides, being molecules of the same charged. Therefore, the second procedure, where the polyN are co-extruded with the lipid vesicles, might increase the interaction between the nucleolipid headgroup and polynucleotides bases, including the polyN molecules also inside the liposomes. So selective interactions, if any, might occur both inside and outside liposomes. Favouring the encapsulation, this second preparation, as for stabilized plasmid-lipid particles, should guarantee a larger DNA transfer in future applications. Moreover, in this second method of preparation, polynucleotides solutions in different buffers were heated at about 50ºC before swelling the nucleolipids films.

After preliminary tests on liposomes of different sizes, we investigated only 100 nm liposomes (ULV or LUV). This choice arises from the fact that for smaller liposomes (extruded through 50nm pore size) the obtained size was affected by the nature of the lipid. In fact, nucleolipids being stiffer due to stacking interaction between the headgroup on the liposomes surfaces, as highlighted in part I of this thesis, show larger diameters with respect to the polycarbonate membranes' pore size and larger than POPG liposomes, which are taken as reference. This can preclude us to observe other differences, as condensation by molecular recognition. On the other hand, dimension larger than 200 nm might be too high in view of pharmaceutical delivery use, allowing for the accredited cytitoxicity of lipoplexes' size. Likewise, they are not suited for light scattering measurements because the higher polydispersity can shadow growth effects and make the results ambiguous. All of the lipids used are anionic, so they form unilamellar vesicles spontaneously upon swelling, and indeed diameters smaller than 200 nm could occur also before extrusion.

Remarkably, POPA and POPU molecules show different self-assembly patterns, depending on the nature of the buffer solution used for preparation. For a given lipid concentration, undergone through the same extrusion steps, very different light scattering intensities are observed.

TRIS Buffer:

In TRIS buffer, light scattering measurements performed typically at an angle of 90º, given the expected structures (liposomes), show different features. POPU gives rise to a lower light scattering intensity than POPA. These observations lead to conclude that POPU molecules rarely form vesicles in TRIS buffer; generally other structures having lower scattering cross section should be present to account for this intensity loss. To explain this odd behaviour despite the similar molecular structure and identical chains, Small Angle X-ray Scattering (SAXS) measurements have been carried out on those dispersions. Owing to the low electron density of these molecules and low contrast, though, concentration needs to be increased from 0.5 mM, normally used for light scattering and spectroscopy experiments, to at least 10 mM. SAXS spectra of POPU in TRIS buffer, show the typical bump for vesicles due to form factor oscillations, but no q^{-2} scaling law was found at low q (Figure 5.1). Consequently, the coexistence of more structures is likely. Although a fitting of SAXS spectra could be theoretically done using a set of form factors to separate different components and to trace back the final morphology composition of the dispersion, the results could be misleading or erroneous without having any other information on the system, since this is not our final goal. Different ratio compositions are possible considering the different concentration used in X-ray and light scattering experiments of this study, therefore we have not investigated further this behaviour for concentred samples.

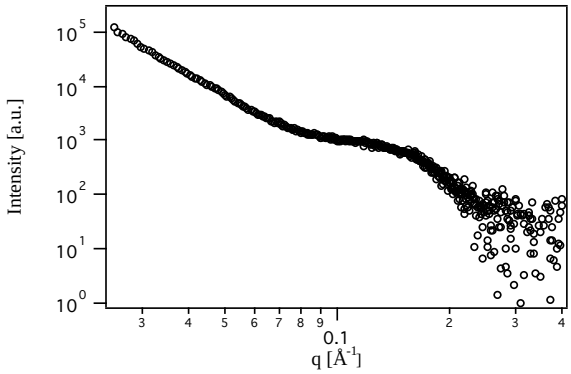

Figure5.1. SAXS spectrum of POPU 10mg/ml in TRIS buffer pH 7.5.

However, the knowledge of the structures properties of the samples used for complexation of polyN is necessary. Therefore, to clarify the structure of the self-assemblies, Cryo-TEM microscopy experiments have been performed using the same concentrations as for light scattering experiments. Amazingly, having only one chemical component aside from the buffer solution, the images display mixed self-assemblies. Three different structures, at least, can be detected (see arrows in Figure 5.2): very small vesicles, liposomes around 100 nm, which is the size we expected after extrusion, and "perforated vesicles". Owing to the well-ordered lamellar phases, which we found at low water content, we can attribute to the salt

presence an explanation why POPU membranes should not be formed or why bilayers should be favoured in solution. Perforated vesicle structures were found previously when cationic surfactants were used to dissolve sonicated lecithin vesicles in presence of NaCl salt[1]. With salt present, the vesicles grow slowly and form perforated membranes. These structures were observed elsewhere in phase diagrams, between micelles and lamellar phase structures[2,3]. Such vesicles scatter much less light since the volume of the pieces which acts as the effective scattering particle, is by far smaller than the volume of the vesicles.

Except common liposomes, every other structure is unexpected considering the long chain of POPU molecules, particularly vesicles of around 15 nm (see Figure 5.2 arrow A). However, these so small particles have different diffusion coefficients with respect to 100 nm vesicles, and contribute with modest scattering intensities; this is consistent with light scattering results for POPU dispersions in TRIS buffer.

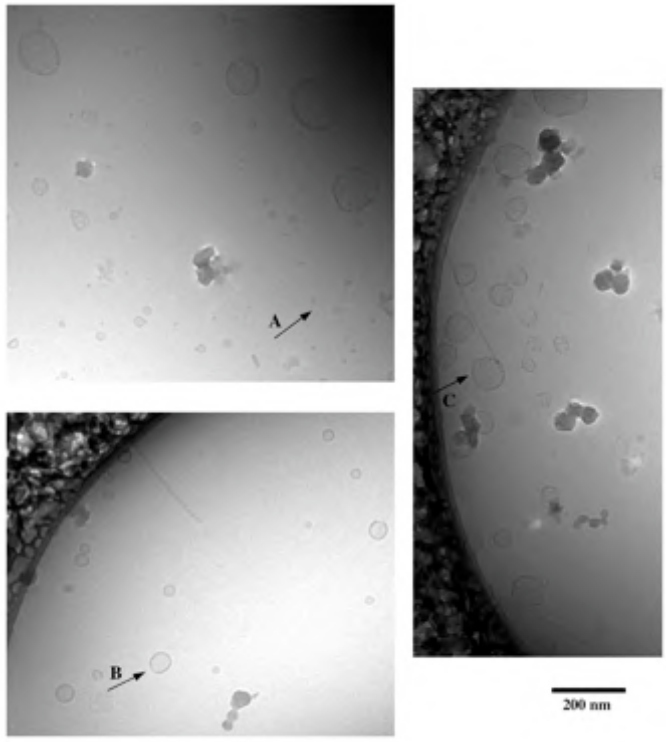

Figure5.2. Cryo-TEM micrographs of POPU dispersions 1 mM in TRIS buffer pH 7.5. (A) small unilamellar vesicles, (B) liposomes size around 80-100nm and (C) "perforated vesicles" size around 100-150nm.

While POPU vesicles cannot be obtained homogenously hydrating from TRIS buffer, POPA, undergone through the same treatment, yields regular liposomes. SAXS measurements, performed at the same concentration as for POPU dispersions, record a typical marker bump of bilayers and the low q range has a

typical scaling law q^{-2} (Figure 5.3). A fitting of the spectrum was performed using the form factor reported below:

$$F(q) = (2\pi)^{1/2}[2\sigma_H \exp(-\sigma_H{}^2 q^2/2)\cos(qz_H) - \sigma_C \rho_r \exp(-\sigma_C{}^2 q^2/2)] \quad (5.1)$$

This model considers the scattering electron density profile of a multibilayers structure as represented by Gaussians, where the electro-dense region corresponds to two Gaussians and the electron region of the methyl terminus of the hydrocarbon chains by another Gaussian with negative amplitude. In this model the electron density of the membrane accounts for the contrast variation between the lipidic assembled molecules and the aqueous core solution. This ratio is defined:

$$\rho_r = (\rho_c - \rho_a)/(\rho_H - \rho_a) \quad (5.2)$$

where ρ_c is the scattering electron density of the lipid chain, ρ_H is the scattering electron density of headgroup and ρ_a is the scattering electron density of the aqueous core, which is considered zero in case of pure aqueous solution. The Fourier transformation of such modelled electron density profile produces the form factor reported in equation 5.1, which has been widely used to obtain information of phospholipids vesicles in L_α phase[4,5]. The fitting of POPA SAXS spectrum by this form factor yields a value of bilayer thickness around 40Å, which matches our previous data obtained for pure POPA lamellae in low water content regime, and the minima observed in the scattering pattern point out that only one kind of assembly is present in this dispersion.

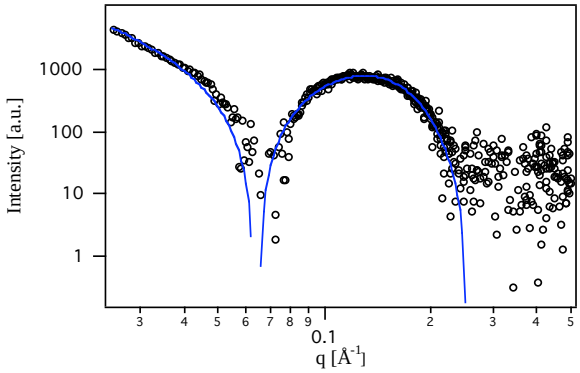

Figure5.3. SAXS spectrum of POPA 10mg/ml in TRIS buffer pH 7.5. Blue line indicates fitting result.

Notwithstanding these clear results, Cryo-TEM microscopy has been performed, using 1mM concentration, to confirm the structure in view of the peculiarity of POPU dispersion in TRIS buffer. Figure 5.4 shows indicative micrographs of POPA molecules in TRIS buffer. As it is possible to see the particles are mainly liposomes of size around 60 nm. There is only a particular that should be stressed: small patches of lamellae or small not defined particles are embedded within the liposomes.

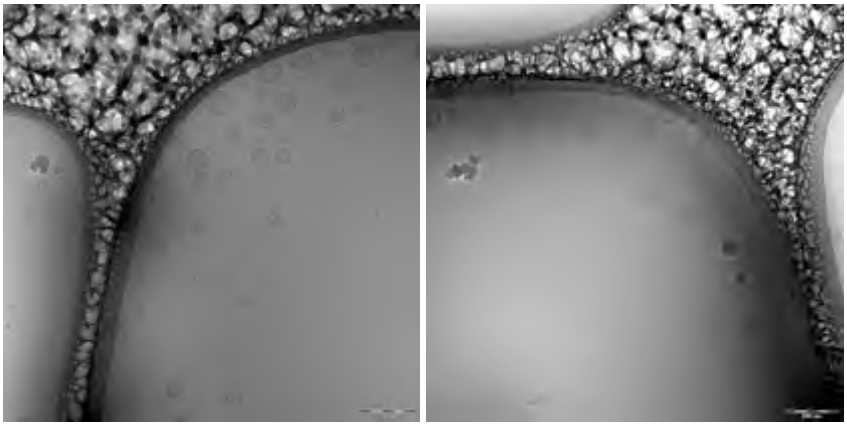

Figure5.4. Cryo-TEM micrographs of POPA dispersions 1 mM in TRIS buffer pH 7.5.

It is interesting to monitor the behaviour of these dispersions when polynucleotides are added.

Before going on further, it is worth saying that thanks to the relatively low scattering of polynucleotides in this buffer, the scattering of liposomes results unaffected in light scattering measurements if polyN is not bound to the liposomes themselves. To validate this statement, we performed a light scattering investigation on polynucleotides in this environment. Dynamic light scattering shows that the intensities of polyN at the same concentration, buffer and experimental setup, are about two orders of magnitude below POPN liposomes, fairly similar for both polynucleotides. Both polynucleotides show a high polydispersity. Interestingly, the R_H is smaller for polyA than polyU, confirming a more globular structure of the former polymer. We found out an average R_H value of 159 nm for polyU and of 90 nm for polyA by CONTIN inversion. A static light scattering investigation has been also performed to determine the other structural parameters of this polymer that possibly can influence the interaction with nucleolipids. Since the structure factor is constant for dilute systems such as the one considered in this study, we used the partial Zimm plot (equation 5.3) to assess R_g (gyration radius) of these polymers in the limit of $qR_g < 1$.

$$\frac{1}{I_{ex}(q)} = C\left(1 + \frac{R_g^2 \cdot q^2}{3}\right) \tag{5.3}$$

The results of the fitting are reported in Figure 5.5 (a,b).

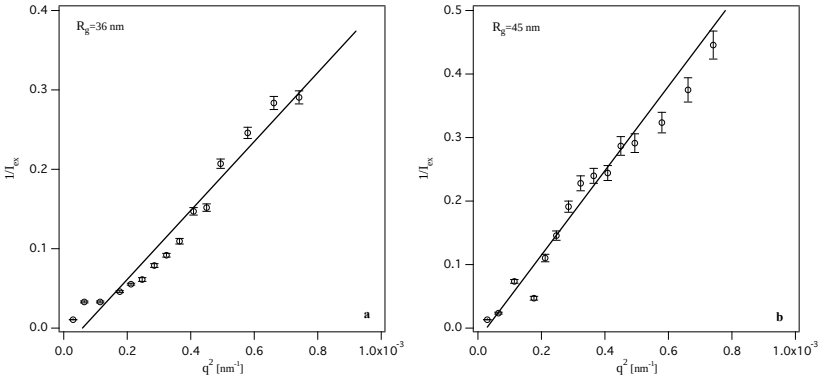

Figure5.5. Partial Zimm Plot of polyU (a) and polyA (b).

Dynamic Light scattering measurements of POPU/polyN systems show an increase of the z-weighted average size when polynucleotides are added. These results occur in spite of the previously mentioned POPU relatively low intensity and polydispersity, which is obviously higher than expected for extruded liposomes due to the coexistence of more assemblies. On the other hand, when polynucleotide solutions are used to swell the lipid film, the final dispersions have considerable smaller sizes than pure POPU (Figure 5.6). Some differences arise when different polynucleotides are used.

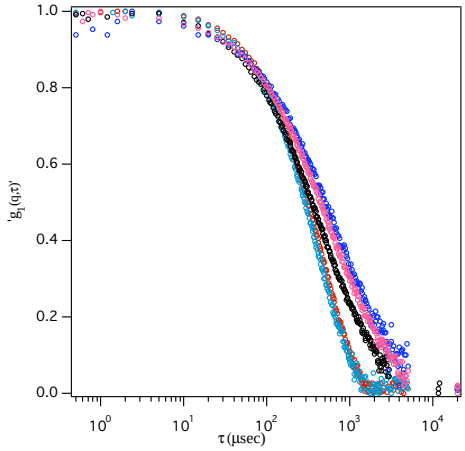

Figure5.6. Autocorrelation functions of POPU liposomes and polyN after one day from preparation. The autocorrelation functions were normalized to assess the difference among the pure lipid dispersion (black circles) and the dispersion in which the polyA or polyU were added to the dispersion (blue and pink circles) or used to hydrated the dispersion (azure or red circles).

Addition of polyN to POPA liposomes does not produce any relevant change in size although a slight reduction in the diameter is observed when polyU solution is utilized for swelling the lipidic film (Figure 5.7). Furthermore, as already found for POPU samples, it seems that polyA affects the size of the nucleolipid liposomes more than polyU, yielding smaller liposomes.

Even if, at the first glance, the observed effects are small and the results obtained for POPA/polyA mixtures might indicate that complementary patterns do not drive possible interaction, bases are influenced from each other in such a way. This observation is strengthened by the differences between systems with polyA or polyU. Moreover, no interaction, no differences between polyA and polyU exist for POPG liposomes. Light scattering measurements on POPG liposomes record size reduction when polyN are added during the swelling process, as observed for nucleolipids. However no difference between polyA and polyU was found (Table 5.1).

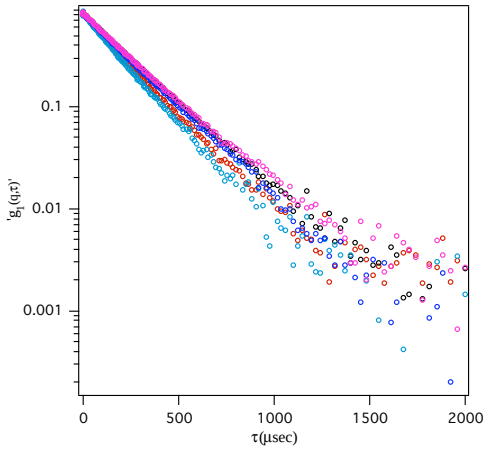

Figure5.7. Autocorrelation functions of POPA liposomes and polyN after one day from preparation. The autocorrelation functions were normalized to assess the difference among the pure lipid dispersion (black circles) and the dispersion in which the polyA or polyU were added to the dispersion (blue and pink circles) or used to hydrated the dispersion (azure or red circles).

Table5.1. LS results for POPA and POPG liposomes with and without polyN

sample	d [nm]	poly	I [Kcps]
POPA	100	0.083	19
POPA + polyU	101	0.101	19.3
POPA + polyA	97	0.094	20.4
POPA + polyU co-extruded	84	0.133	15.9
POPA + polyA co-extruded	78	0.145	10.5
POPG	100	0.1	23
POPG + polyU	100	0.105	22.9
POPG + polyA	100	0.09	23.1
POPG + polyU co-extruded	89	0.08	14.8
POPG + polyA co-extruded	90	0.075	15.2

poly=polydispersity; parameters obtained by cumulat analysis.

The scattering intensity trend shows again some differences between polyA and polyU with POPA and none with POPG.

Analysing light scattering measurements, though, some remarks are in order about the osmotic shock for the samples, where the polynucleotide was added to liposomes already formed. Usually when a solution with diverse ionic strength is added, liposomes change their size because the bilayer acts like a semipermeable

membrane[6,7]. Here, polynucleotides solutions have a higher ionic strength than the bare buffer, so the water inside liposomes should be squeezed out to re-establish the equilibrium, causing size decrease in the assemblies. Furthermore, polynucleotides, should subtract hydration water from the membrane headgroup; again, the removal of water from the hydration shell should diminish the effective area of the headgroup, creating compression of the liposomes[8,9].

Interestingly, in the samples studied, this shrinkage did not appear at all. An explanation is the too low polyN concentration with respect to buffer one. Therefore, any osmotic shock occurred neither to nucleolipids nor to POPG liposomes.

Light scattering measurements indicate that there are specific interactions between nucleolipids liposomes and polynucleotides, and also that they may affect each other modifying the base orientation with respect to bilayer plane or changing their conformations. To gain further insights on these interactions, spectroscopic measurements have been performed. However, one of the most important problems in UV (ultraviolet spectroscopy) and CD (circular dichroism spectroscopy) measurements is the scattering of the analyzed samples. In our cases, since CD and UV spectra of POPG liposomes with polynucleotides have identical shapes with respect to pure polynucleotides spectra in solution (data not shown), we have used POPG UV and CD spectra (also affected by scattering) to decouple possible genuine recognition effects from unspecific scattering artefacts.

UV curves point out that uridine bases on POPU headgroup interact with polyA adenosine bases. It is possible to observe hypocromism and a blue shift, which do not occur when polyA is simply added to the dispersion (Figure 5.8 a). To further confirm previous results, sodium dodecyl sulfate, SDS, (final concentration 0.01M) was added to the solution to break down liposomes and likely the interactions between lipid and polymer. As it is visible in Figure 5.8 b, the blue shift disappears and the absorbance for every sample is about the same with respect to the “simulation curve”, which was obtained adding POPU/SDS spectrum to polyA/SDS one.

POPA liposomes and POPA/polyN systems investigated by CD spectroscopy are reported in Figure 5.9 a,b. As observed by light scattering, the larger structural differences are mainly observed when the polynucleotides are both inside and outside the liposomes; it is thus reasonable that the most significant variations on circular dichroic spectra are recorded for these samples. However, it is worth saying that polyU has a large effect upon POPA liposomes, see Figure 5.9 a. A comparison with the sum of single spectra outlines a blue shift of the maximum of the positive CD band located at ~ 270nm, and even the development of a positive band at 290 nm. This effect is more stressed for POPA and polyU systems where the polymer was co-extruded with POPA liposomes. All these issues indicate a more stabilized structure likely by staking of the bases and formation of H-bond pair[10]. Moreover, the increase of the negative peak at 210 nm for the sample where the polyuridine is also encapsulated inside POPA liposomes, resembles CD signal of condensed DNA.

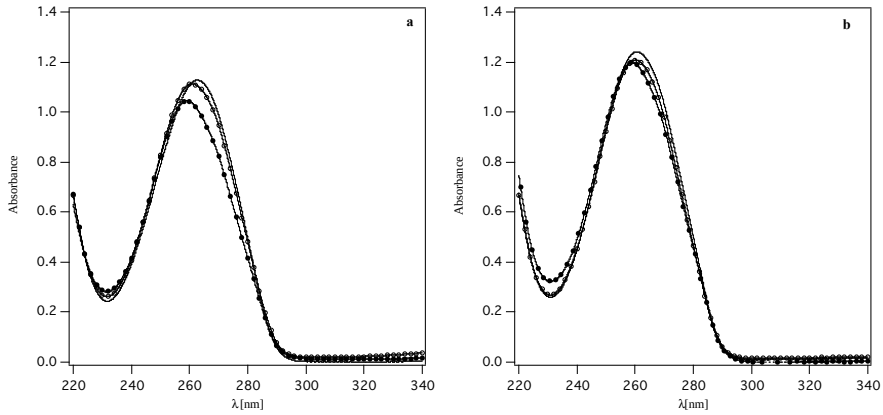

Figure5.8. a) Absorbance spectra of POPU and polyA hybrid structures in TRIS buffer. b) Absorbance spectra of POPU and polyA hybrid structures in TRIS buffer plus SDS 0.01M: experimental spectrum of POPU/polyA circles, experimental spectrum of POPU/polyA co-extruded full circles and solid line computed spectrum POPU + polyA single spectra.

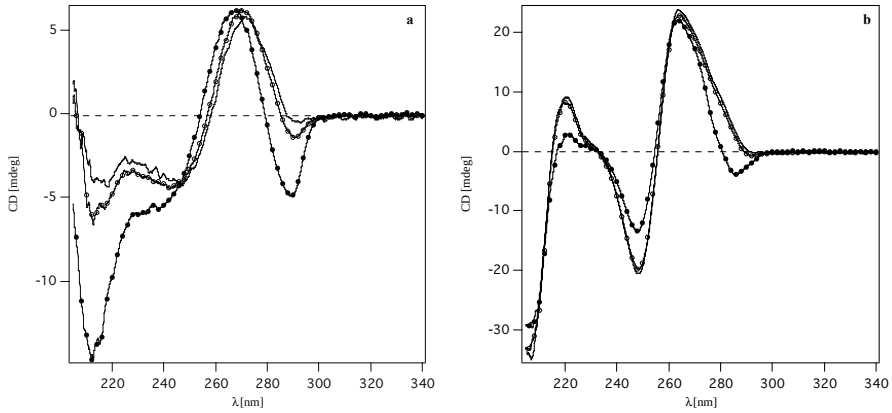

Figure5.9. a) Circular dichroism spectra of POPA and polyU hybrid structures in TRIS buffer. b) Circular dichroism spectra of POPA and polyA hybrid structures in TRIS buffer. Experimental spectrum of POPA/polyN circles, experimental spectrum of POPA/polyN co-extruded full circles and solid line computed spectrum POPA + polyN single spectra.

When SDS 0.01M was added to these systems, all these differences were erased in the dichroic spectra, so the solid curve of the simulated spectra is utterly overlapped to the spectra of "POPA and SDS" with polynucleotides (Figure 5.10). This behaviour explains that all the structures formed among liposomes and polynucleotides were destroyed.

It is worth noting that POPA itself having high stacking attitude shows a remarkable different dichroic spectrum and higher molar absorbance, that is hyperchromism, when SDS is added to the liposomes. The dichroic spectrum of the former sample (open circles) looks like the spectrum of adenosine (data not shown) and it appears different with respect to mere POPA liposomes (full circles) highlighting bases de-stacking (Figure 5.11).

Remarkably, it is the aggregation of the hydrophobic residues that build up the interaction, energetically disfavoured also between nucleotides in solution, among the nucleic bases of the nucleolipids. As for DNA, cooperative effects are necessary for base-base interaction.

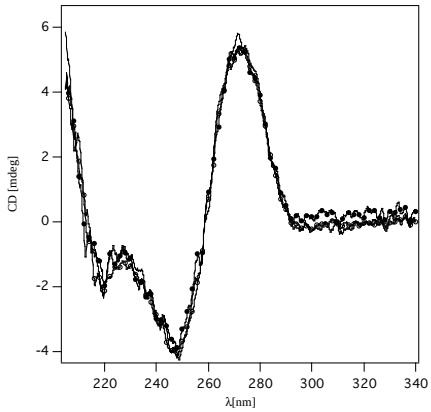

Figure5.10. Circular dichroism spectra of POPA and polyU hybrid structures in TRIS buffer plus SDS 0.01M: experimental spectrum of POPA/polyU/SDS circles, experimental spectrum of POPA/polyU/SDS co-extruded full circles and solid line computed spectrum POPA/SDS + polyU/SDS single spectra.

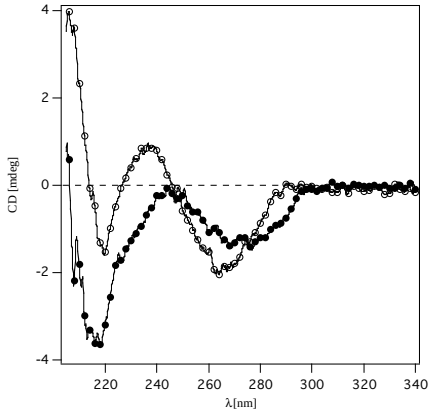

Figure5.11. Circular dichroism spectra of POPA liposomes (full circles) and POPA/SDS (open circles) in TRIS buffer.

To understand the modification in liposomes structures assessed by circular dichroism and to check that specific interactions between complementary bases have occurred, a Cryo-TEM investigation has been performed on these hybrid systems nucleolipid/polynucleotides in TRIS buffer.

Figure 5.12 illustrates some images of POPA where polyU solution was added to the prepared liposomes. Interestingly, the uncanny objects inside POPA liposomes disappear almost completely from liposome nuclei because of the addition of complementary RNA base strands.

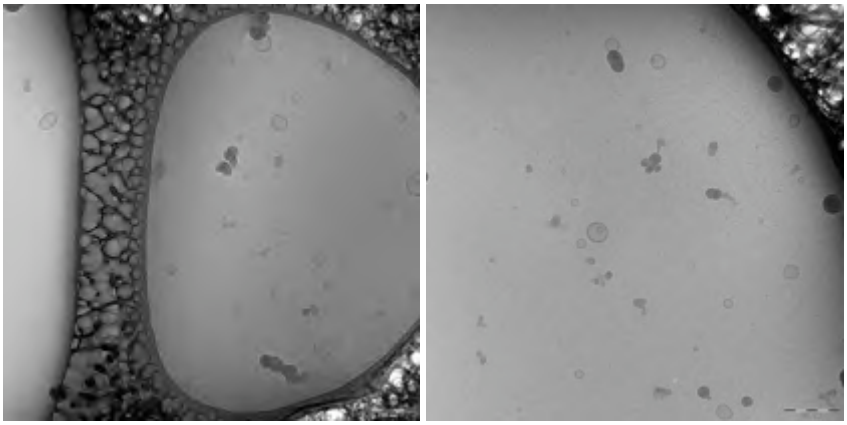

Figure5.12. Cryo-TEM micrographs of POPA/polyU dispersions in TRIS buffer pH 7.5.

The dispersion appears more polydisperse by mixing polyU and also smaller vesicles are present in the system. The increase in polydispersity is perfectly in agreement with light scattering measurements (see Table 5.1); however, scattering experiments indicate slightly larger particles, considering furthermore the higher polydispersity that possibly drops the calculated dimension values. To explain this difference, we need to take into account that polynucleotides are not visible by Cryo-TEM. If polynucleotides are attached to the lipid membranes, but they do not cover all the liposomes, they could increase the size of the scattering particles without being visible in the micrographs. It is worthwhile to remind that scattering particles volume affects tremendously light scattering measurements. The structural modifications, found by means of CD and Cryo-TEM investigations, can account for the inconsistency between the two techniques (scattering and microscopy).

Remarkably, the biggest vesicles become ellipsoidal and have trimmed or not regular edges, as shown in POPA/polyU micrographs.

POPA and polyU co-extruded liposomes do not show any material within their aqueous pool in Cryo-TEM images, as well as POPA liposomes where polyU was added after vesicles preparation. There are some regions where are present large aggregate of material (see arrows in Figure 5.13) without a definite structure. These assemblies can justify the larger polydispersity value with respect to pure POPA liposomes. Moreover, the strong CD spectra changes may also be due to these not defined structures. As in the previous case, where polyU was added to already prepared liposomes, it is possible to observe ellipsoidal particles. Many of these ellipsoidal particles seem to be formed by the union of two vesicles.

These conformational transformations, which do not appear for POPG/polyN liposomes, can be explained only imaging that polynucleotides affect the polar heads of nucleolipids in the bilayer inducing structural changes.

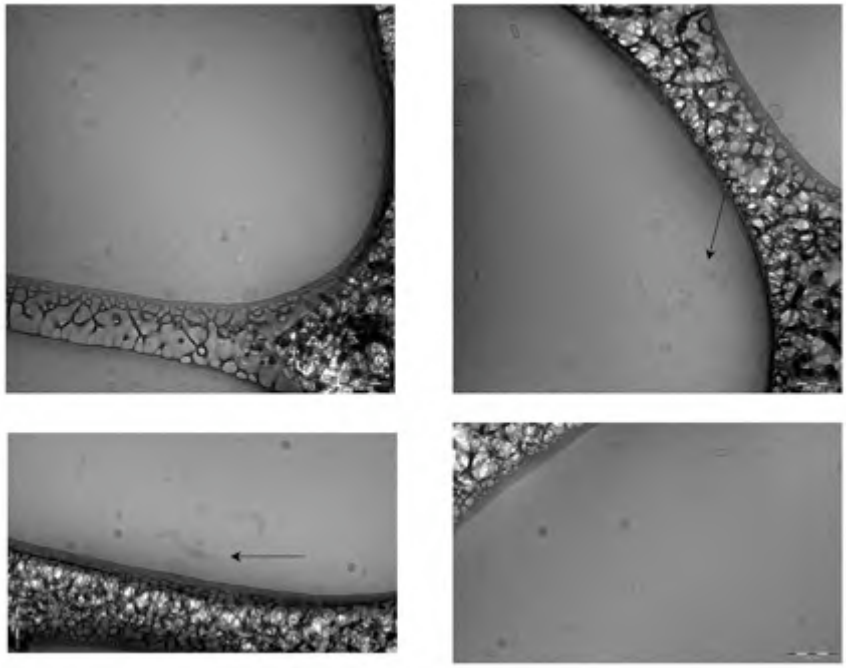

Figure5.13. Cryo-TEM micrographs of POPA/polyU co-extruded dispersions in TRIS buffer pH 7.5.

TRIS/KCl Buffer:

Although the previous conclusions appear interesting, the structural differences of the hybrid self-assemblies are very small and many questions remain open. However, if the observed modifications are genuinely due to molecular recognition effects, as the spectroscopic and microscopic results seem to point out, these observations should be enhanced for higher ionic strengths, as it happens for the coupling of complementary poly or oligonucleotides. Some reports have appeared in the literature, where anionic or zwitterionic liposomes are able to condense DNA with the aid of bivalent cations, as already mentioned in Chapter 4[11-17]. However, encouraged from previous results on micelles and bilayers[18,19], we thought that it might be necessary only a slight increase in ionic strength to improve the adduct stability and there is no need for compensating stoichiometrically all the charges for nucleolipids thanks to molecular recognition between complementary bases.

On the basis of low toxicity in view of future drug delivery systems, potassium chloride salt represents a good choice. Therefore, the investigation of POPN/polyN systems was repeated in 0.1M TRIS buffer with the addition of KCl salt.

As a preliminary test, KCl was added in high concentration 0.5M. However, at this salt concentration liposomes of pure POPA show a precipitate by themselves, whereas POPG liposomes are still stable. The salt concentration was thus decreased to 0.1M where POPA liposomes appear stable for a long time.

In this buffer and ionic strength POPU molecules are organized in liposomes. As observable in Figure 5.14, perforated vesicles do not appear. And although many

liposomes have an elongated form, the sample is more homogeneous. The light scattering measurements record scattering intensity compatible with almost monodisperse vesicles (see Table 5.2). The average size (around 70 nm) of the particles obtained by analysing the Cryo-TEM micrographs agrees with LS experiments.

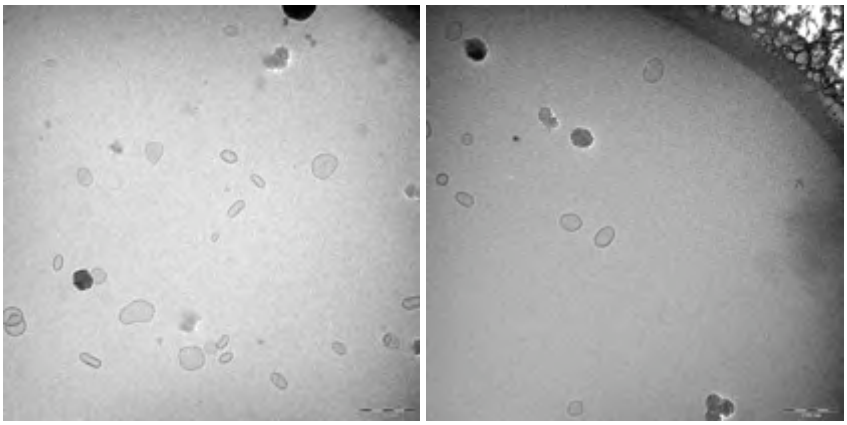

Figure5.14. Cryo-TEM micrographs of POPU liposomes in 0.1M TRIS and 0.1M KCl buffer.

However, these liposomes do not show any interaction with polynucleotides. Neither the diameters increase (Table 5.2) nor the absorbance nor the dichroic signals change (data not reported). The same behaviour was found out when POPU liposomes[20] were formed in phosphate buffer (data not shown). Therefore, it is clear that the capability of interaction with polynucleotides is missing for POPU molecules, when assembled in liposomes. The observed molecular recognition for unsalted TRIS buffer is likely due to the residual interaction of polynucleotides with perforated vesicles or small particles present in the POPU sample. These objects contain more energy than normal size vesicle due to the strain the molecules undergo when in these assemblies.

It is, in fact, possible to evaluate the minimum radius for vesicles to be formed spontaneously:

$$R_c = \frac{l_c}{\left(1 - \frac{v}{a_0 l_c}\right)} \qquad (5.4)$$

where l_c is the chain length according to Tanford[21] and the fraction inside the parenthesis is the packing parameter. For POPU molecule this number can be calculated to be about 6 nm, considering the area for polar head about 70 Å^2 as previously determined for in the current dissertation. However, the polar head dimension could be larger in solution than in low water content regime. A previous study[22] determined a value of 125 Å^2 for uridine derivative polar head, which would increase the diameter from 12 nm to 13 nm. These values can be considered close enough to dimension measured by Cryo-TEM, for the molecules in the assemblies

to be strained and thus contain a high level of energy. These aggregates are of course more susceptible to perturbation than normal 100 nm vesicles. Therefore, they might change their structure and in changing favour the interaction with polyN molecules.

The difficulties of POPU liposomes to complex polyN are not unexpected; we have attempted to intercalate ss-RNA in between the lamellar phases of this lipid, on the basis of the promising results already obtained for POPA lamellae, as discussed in Chapter 3. Even though we found out a modification of the POPU membranes affected by these polynucleotides, no structural peak of ss-RNA was found by SAXS. Therefore, it is possible that POPU bilayers follow a different kinetic in interacting with polyNs due to the more stable lamellae with respect to POPA both in low water content and in solution.

Table5.2. LS results for POPU liposomes with and without polyN in TRIS/KCl buffer

sample	d [nm]	poly	I [Kcps]
POPU	81	0.060	16.3
POPU + polyU	81	0.055	17.4
POPU + polyA	79	0.092	16.6
POPU + polyU co-extruded	79.5	0.06	16.2
POPU + polyA co-extruded	84	0.07	19.5

poly=polydispersity; parameters obtained by cumulat analysis.

Given the previous results, our attention has been focused on POPA liposomes, their interaction with polyNs and the comparison with POPG in the same buffers.

Light Scattering measurements on POPA liposomes report dramatic structural changes in salted TRIS upon polynucleotide addition (Figure 5.15 a). The hydrodynamic-radius (R_H) increases after one day from the preparation and keeps increasing, until a precipitate is visible for each investigated system. Obviously, POPA liposomes maintain the same radius and are stable for a long time, provided no polynucleotide is added; Figure 5.15 b, recorded after one week from sample preparation, highlights the noteworthy difference of R_H of POPA liposomes in relation to the other samples with polynucleotides.

Table 5.3 shows the measured hydrodynamic diameters of liposomes with and without polynucleotides for POPA and POPG lipids. It is obvious that there are many changes for POPA systems, as already remarked. Moreover, polyA and polyU interact in a different way with POPA, as well as they do in TRIS buffer. However, it is correct to observe that POPG/polyN co-extruded are slightly different with respect to pure POPG liposomes, and there are differences between different polynucleotides. UV and CD measurements, performed on the same samples, do not show spectroscopic changes with respect to pure polynucleotides in the same buffer (data not shown). Therefore, it is possible that salts aid the encapsulation of polyN inside POPG core, without modifying either polyN structure or polyN spectroscopic behaviour. It is worth reminding that DNA complexation is a key factor in gene-delivery.

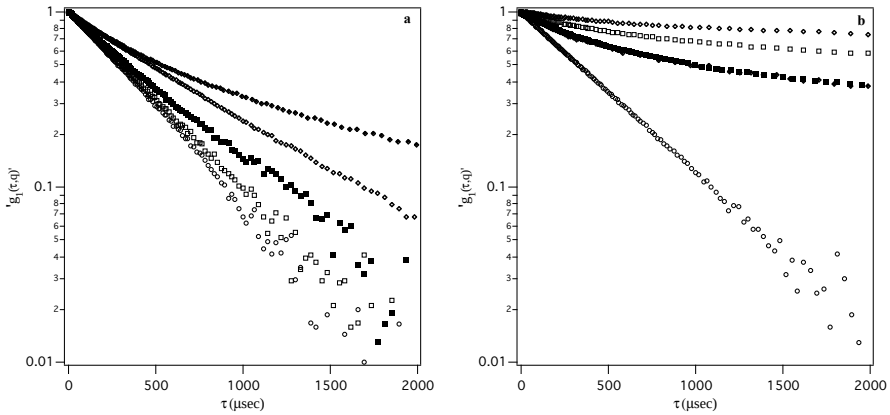

Figure5.15. a) Autocorrelation functions of POPA liposomes and polyN after one day from preparation. b) Autocorrelation functions of POPA liposomes and polyN after one week: POPA circles, POPA/polyU square, POPA/polyA diamond, POPA/polyU co-extruded full square and POPA/polyA co-extruded full diamond.

Table5.3. LS results for POPA and POPG liposomes with and without polyN after preparation in TRIS/KCl

sample	d [nm]	poly	I [Kcps]
POPA	90	0.074	23.6
POPA + polyU	95	0.096	20.8
POPA + polyA	145	0.170	44.4
POPA + polyU co-extruded	101	0.175	18.0
POPA + polyA co-extruded	163	0.210	32.4
POPG	99.9	0.09	13.0
POPG + polyU	102	0.093	13.2
POPG + polyA	100	0.096	12.8
POPG + polyU co-extruded	97	0.083	19.6
POPG + polyA co-extruded	105	0.075	20.0

poly=polydispersity; parameters obtained by cumulat analysis.

UV and CD measurements, performed one day after the sample preparation and therefore corresponding to the structures responsible of LS in Figure 5.15 a, point out that POPA liposomes and polyN display novel cooperative spectral features. Unfortunately, spectroscopic measurements on aged samples could not be performed because of the high scattering, which would have affected the results.

Remarkably, Figure 5.16 a,c highlights an important UV hypochromism when polyN are co-extruded with the nucleolipid, that is, when polyN is located both inside and outside liposomes. However, they behave in different way when SDS is added to these solutions. UV absorbance diverges for the two methods of sample preparation. In fact, the absorbance of the “POPA/polyU co-extruded” sample, increases less than polyU and POPA pure solution (solid line Figure 5.16a). On the other hand, “POPA/polyA co-extruded” absorbance increases by far more than the sum of the single pure solutions. These features might point out that the complexes have a different stability. In fact, “POPA/polyU co-extruded” sample could be not completely destroyed by SDS because of the stronger interaction among

complementary bases. On top of this, “POPA/polyA co-extruded” could absorb more than expected in UV due to a different polyA stacking effects. It is reasonable to consider that polyA secondary structure modification during the complexation with nucleolipid can retain a residual effect on the stacking interaction once added SDS. These observations, therefore, could effectively establish that a new superstructure was obtained by the molecular recognition between the nucleic acid bases.

On the basis of these data, it is easy to analyze the absorbance trend of Figure 5.16 b and d, where no evident change with respect to the simulated curve takes place. In these cases, where polyNs were added after the liposomes preparation, one might think that no interaction occurs; but this does not explain the structural modifications and the final precipitate. We are not currently able to explain the different structural and spectroscopic trend for “POPA/polyN added”. However, measurements carried out on POPG and POPU liposomes point out that no precipitation occurs when no interaction occurs.

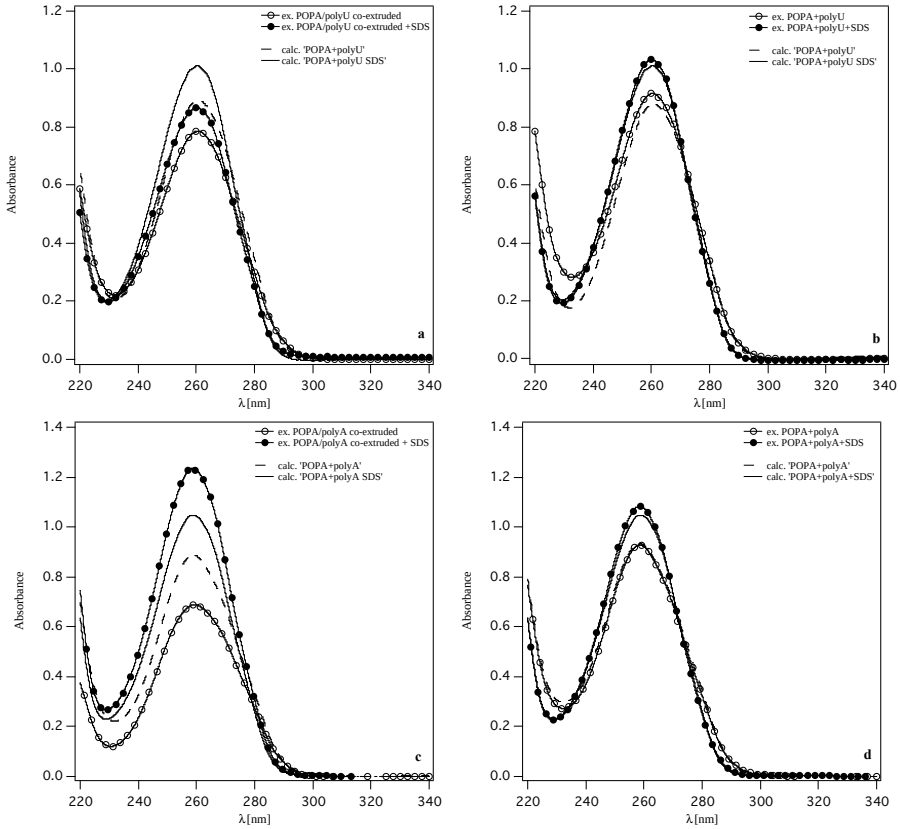

Figure5.16. a) Absorbance spectra of POPA and polyU co-extruded structures in buffer TRIS 0.1M 0.1M KCl with and without SDS 0.01M. b) Absorbance spectra of POPA liposomes and polyU with and without SDS 0.01M. c) Absorbance spectra of POPA liposomes and polyA co-extruded with and without SDS 0.01M. d) Absorbance spectra of POPA liposomes and polyA with and without SDS 0.01M.

CD experiments display similar signals already obtained for the same systems in TRIS buffer, highlighting again structural modifications of the nucleic bases (Figure 5.17). Interestingly, samples of polyN co-extruded with POPA vesicles report stronger modifications in CD spectra with respect to pure POPA liposomes, as already noted for samples in TRIS buffer, and perfectly in agreement with light scattering experiments.

Note: CD and UV measurements of samples in TRIS 0.1M KCl 0.1M with SDS have been carried out at 40ºC instead of room temperature because of the SDS cloud point.

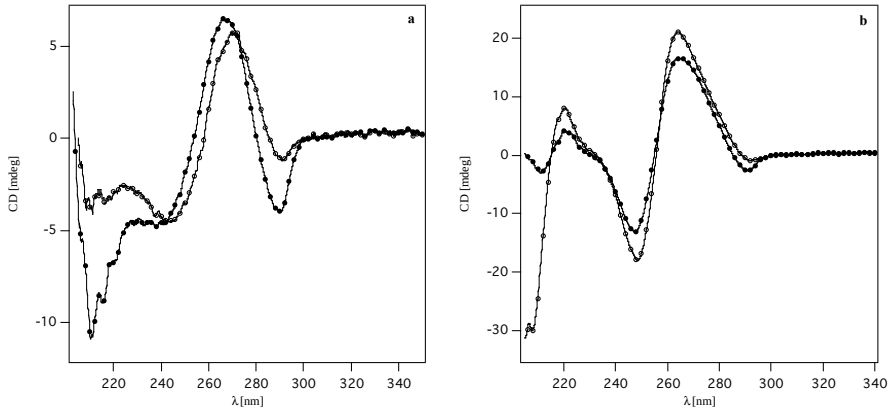

Figure5.17. a) Circular dichroism spectra of POPA and polyU hybrid structures in TRIS/KCl buffer. b) Circular dichroism spectra of POPA and polyA hybrid structures in TRIS/KCl buffer. POPA/polyN circles and POPA/polyN co-extruded full circles.

Phosphate Buffer:

To achieve further insights on these hybrid systems due to the noteworthy effect of the buffer, nucleolipids dispersions with and without polynucleotides have been also studied in phosphate buffer pH 7.5.

Dynamic light scattering measurements performed on POPA/polyN samples show that R_H increases with respect to the pure POPA liposomes. However, samples with polyA grow faster than polyU ones (Figure 5.18), confirming the trend already observed in TRIS/KCl.

Once again, a comparison with POPG/polyN systems confirms effects of polynucleotides over POPA lamellar structures, as reported in Table 5.4. POPG/polyN co-extruded samples display the same trend observed in TRIS buffer, where smaller particles were formed for polyN co-extruded with the lipid. Monitoring the kinetic of these samples highlights no evolution for POPG/polyN systems, whereas strong changes of light scattering autocorrelation functions indicate structural modifications for POPA/polyN. Aging processes are, though, different whether polyA are added to POPA liposomes already prepared or they are used to hydrated POPA lipidic films.

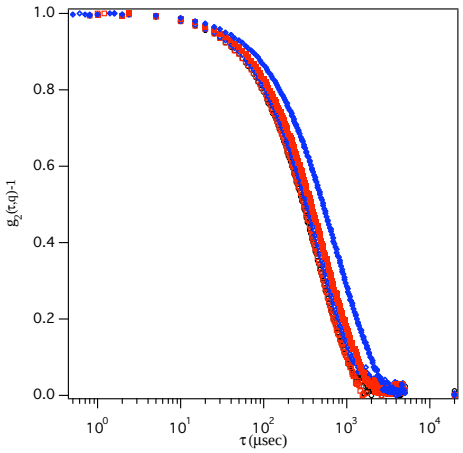

Figure5.18. Normalized autocorrelation functions of POPA liposomes and polyN after one day from preparation: POPA black circles, POPA/polyU red square, POPA/polyA blue diamond, POPA/polyU co-extruded red full square and POPA/polyA co-extruded blue full diamond.

Analysing the autocorrelation function for POPA/polyA systems after one week (Figure 5.19), it is possible to detect different growing mechanisms for the two preparation methods. CONTIN inversion or a quadratic cumulant fitting found only one relaxation time ascribable to a population of about 2600nm when polyA is simply added to POPA liposomes. On the other side, three different relaxation times were obtained by CONTIN inversion when polyA is both inside and outside POPA liposomes. The fastest may be assigned to liposomes without the polymer or still stable, the slowest, the third, which is the most populated relatively of the other, has an average dimension of 4500nm. Moreover, while POPA/polyA samples go on increasing till a precipitate is detectable, POPA/polyU hybrid structures are stable in solution; in fact, the dimension of its aggregate is still the same after one week.

Table5.4. LS results for POPA and POPG liposomes with and without polyN after preparation in PBS

sample	d [nm]	poly	I [Kcps]
POPA	91	0.065	57
POPA + polyU	96	0.070	57
POPA + polyA	99	0.109	57.5
POPA + polyU co-extruded	113	0.154	47.5
POPA + polyA co-extruded	150	0.206	62.5
POPG	99.5	0.09	18.3
POPG + polyU	100	0.085	19
POPG + polyA	101	0.095	18.6
POPG + polyU co-extruded	85	0.082	12.7
POPG + polyA co-extruded	95	0.090	13.5

poly=polydispersity; parameters obtained by cumulat analysis.

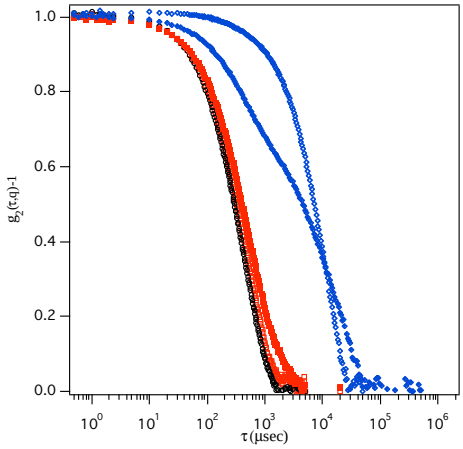

Figure5.19. Normalized autocorrelation functions of POPA liposomes and polyN after one week from preparation: POPA black circles, POPA/polyU red square, POPA/polyA blue diamond, POPA/polyU co-extruded red full square and POPA/polyA co-extruded blue full diamond.

Remarkably, UV and CD measurements report a similar trend of data already found for POPA/polyN in salted TIRS buffer. The CD spectra again show different arrangement of the nucleic bases of nucleolipids when they have interactions with polyN, stressing the stronger modification for samples where polyN is co-extruded with liposomes (Figure 5.20).

To understand how the previously found structural modifications affect POPA liposomes, Cryo-TEM investigations have been carried out on samples with and without polynucleotides and before and after liposome extrusion. Analysing the Cryo-TEM micrographs performed on POPA liposomes in phosphate buffer, it is visible a different arrangement with respect to the same molecules assembled as liposomes in TRIS buffer (Figure 5.21). The particles have not material inside the aqueous core and there are many vesicles with a thickness larger than expected (see arrows in Figure 5.21). These different features with respect to TRIS can explain the higher scattering intensity found in phosphate buffer solution (57 Kcps instead of 19 Kcps) in spite of the same molecule assemblies. Moreover, despite the same concentration and size, CD spectra of POPA in these two different buffers are slightly different (Figure 5.22).

Interestingly, this difference is utterly deleted by adding SDS (data not shown).

Amazingly, whether polyA is added to POPA liposomes or co-extruded with POPA, different assemblies occur. This confirms the previous light scattering study, where after a week it was possible to distinguish different populations of particles due to diverse assembly mechanisms in solution. Figure 5.22 shows some interesting micrographs for POPA liposomes where polyA was added. Three kinds of objects are detectable: (i) many liposomes, (ii) fibers and (iii) clusters of liposomes. On the other hand, POPA/polyA co-extruded samples show very unusual small objects and liposomes, which are attached together by an edge (Figure 5.23).

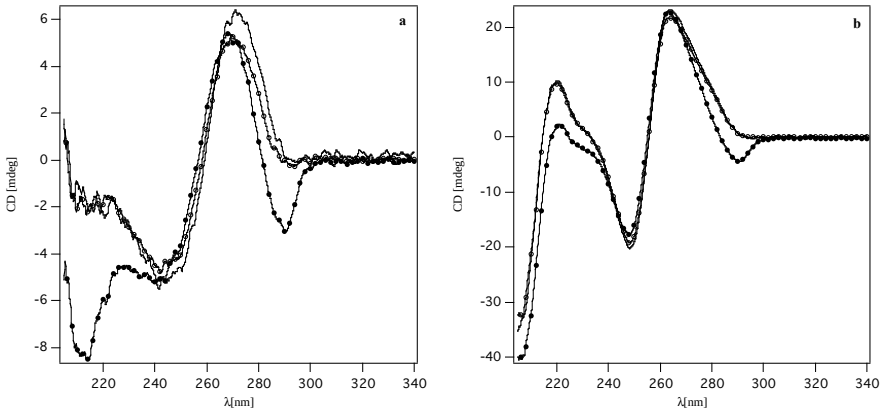

Figure5.20. a) Circular dichroism spectra of POPA and polyU hybrid structures in phosphate buffer. b) Circular dichroism spectra of POPA and polyA hybrid structures in phosphate buffer. POPA/polyN circles, POPA/polyN co-extruded full circles and computed spectrum of POPA + polyN single spectra solid line.

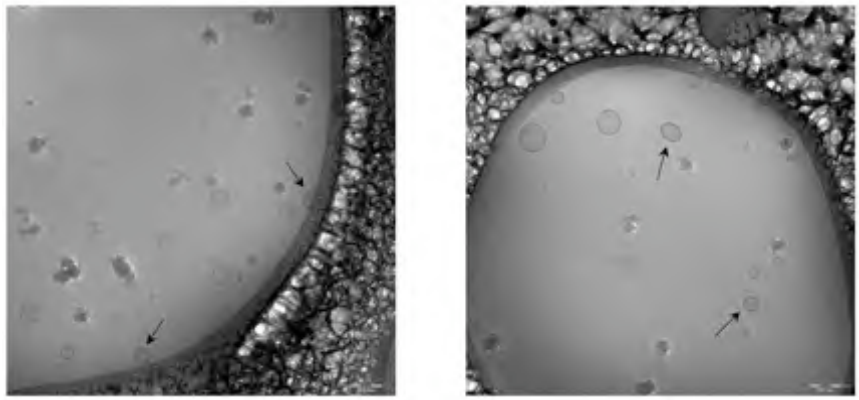

Figure5.21. Cryo-TEM micrographs of POPA dispersions 1 mM in phosphate buffer pH 7.5.

Despite the different aggregates found for the two methods of sample preparation, both systems highlight that interactions with polynucleotides lead to a modification of the structure of POPA bilayers. In the first sample, micrographs of Figure 5.23 indicate that liposomes are slightly larger and even asymmetric; that is, as reported by arrows A, liposomes have something over the membrane. A comparison with scattering measurements confirms that most of liposomes' radii grow due to a polymer coating. Moreover, owing to the low electronic contrast of nucleic acids, it is impossible to detect them by the electronic beam of Cryo-TEM instrument. Therefore, the long fibers are constituted by lipids, which gather the polymer within their lamellae, proving the interaction between nucleic bases, located both on the nucleolipid polar heads and on polynucleotides strands. We have to remind, for clarity, that fibers are probably not detectable by a typical 90 degrees dynamic light scattering due to the larger scattering intensity of liposomes,

which could shade them. However, the increased polydispersity measured by DLS with respect to sole POPA liposomes may be an indication of these structures. As in TRIS buffer, we found out that polyU and polyA have a different R_H; polyA has 90 nm and polyU abrout 150 nm. Both the R_H and the R_g for these polymers are similar in TRIS and PBS, accounting for likely differences in POPA/polyN systems that are due to the interactions occurring with nucleolipids and that are not dependent on the kind of the buffer solution.

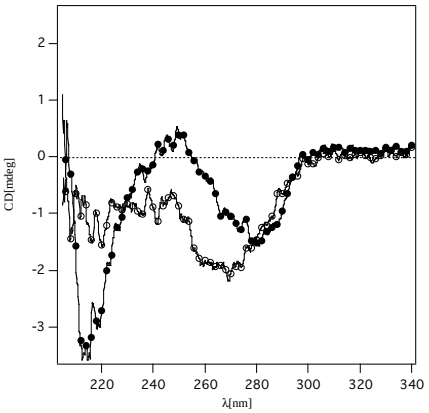

Figure5.22. Circular dichroism spectra of POPA liposomes in TRIS buffer (full circles) and POPA liposomes in phosphate buffer (open circles).

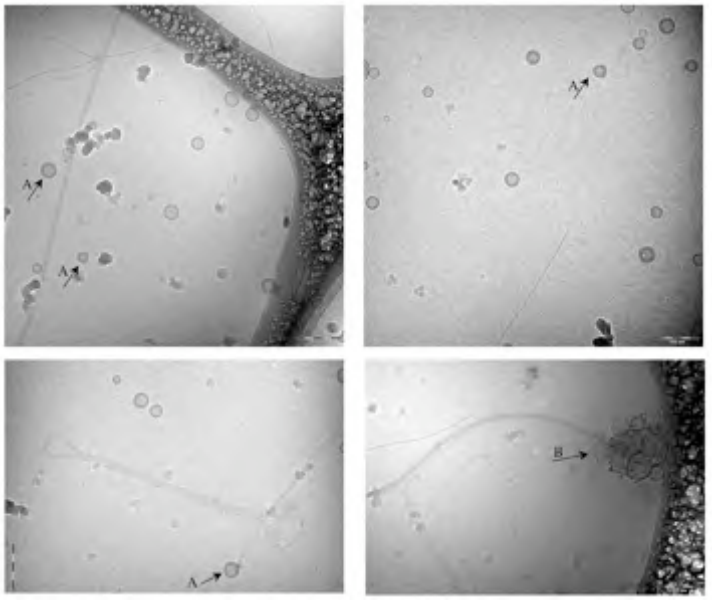

Figure5.23. Cryo-TEM micrographs of POPA/polyA dispersions in phosphate buffer pH 7.5.

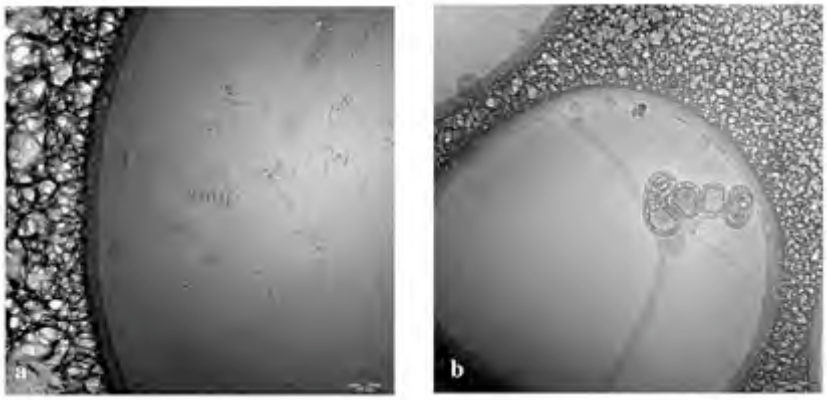

Figure5.24. a) Cryo-TEM micrographs of POPA/polyA co-extruded dispersions b) Cryo-TEM micrographs of POPA/polyA dispersions before extruding in phosphate buffer pH 7.5.

Figure 5.24 shows a very interesting sample because the flattening of the bilayers at the contact region of adjacent vesicles resembles a typical way of aggregation found studying CL-DNA by Cryo-TEM[23]. Moreover, in all of the samples with polyN the zone with the polymer within the bilayer are darker. This implies high electron density, which may be caused by locally accumulated polynucleotides in those regions. High electron dense regions are of course not resistant for a long period below the electronic beam of Cryo-TEM instrument[24]. At this regard, we found out that the electronic beam easily break down the structures shown in the pictures. The sample POPA/polyA has been also analysed before extruding. The density of these large assemblies of coated-liposomes was indicated by their high sensitivity towards the electron beam (Figure 5.24 b). Interestingly, before extruding POPA/polyA samples shows the same kind of structure found for the sample where polyA was added after extrusion. This confirms the interaction process among these molecules.

Interaction between polyU and POPA is confirmed by examining the micrographs of Figure 5.25 a,b. All of the methods of preparations outline structural modifications with respect to POPA liposomes in the same environments. As for polyA, when polyU is added to liposomes fibers, are formed, whereas polyU affects mainly the surface of the liposomes when it was used to hydrate POPA lipidic film. There is a different mechanism of interaction between POPA and polyU with respect to polyA, as long as diverse energies between complementary and not complementary nucleic bases take place. As in the previous case, high electron dense regions were found especially in the sample where the extrusion was not performed, highlighting again coating of polynucleotides on nucleolipid bilayers.

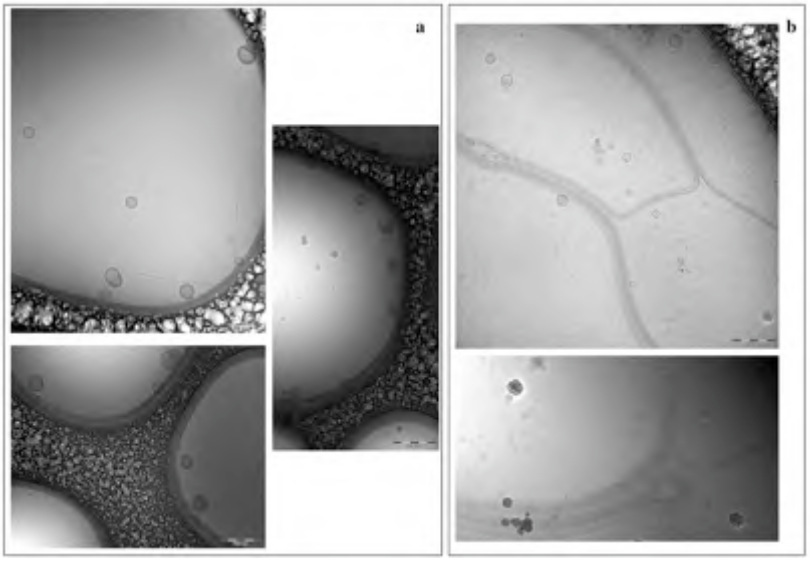

Figure5.25. a) Cryo-TEM micrographs of POPA/polyU co-extruded dispersions b) Cryo-TEM micrographs of POPA/polyU dispersions in phosphate buffer pH 7.5.

5.2 Effect of Oligonucleotides length on POPA liposomes

Analysing the results in the previous paragraph, we can conclude that the interaction between nucleolipids and polynucleotides is strengthened when polyN are both inner and outer of the bilayers. Polynucleotides are however very long polymers. It would be possible that the interaction when they are added after liposome preparation were in such a way driven by their capability of grouping several nucleolipid liposomes at the same time. An easy calculation (reported below as appendix) permits to evaluate that only strands longer than about 1000 bases would be able to connect more than one liposome simultaneously.

Owing to the relevant interest towards antisense oligonucleotides – strands usually made of 17-20 bases – in pharmaceutical field[25], an investigation has been performed to validate how or if the interactions between nucleolipids and nucleic acids single strands exist and it is driven by molecular recognition for shorter oligonucleotides as well.

The samples were prepared following the same methods already used for characterizing POPN/polynucleotides complexes.

Figure 5.26 reports the autocorrelation functions of POPA/oligos in phosphate buffer. The key of these measurements is that the complementary base oligonucleotides (50dT) have a bigger influence upon POPA liposomes with respect to non-complementary (50dA). This is a very interesting result, considering the previous study with polynucleotides, where it was found out a completely opposite trend. Considering the data in all the environments (TRIS, salted TRIS and PBS) it

seemed that no stronger effects between complementary bases for POPA/polyN systems occur. On the other hand, the way and the timing in which polyNs were added, seemed to be very important in determining stronger interactions.

As a matter of fact, oligonucleotides, which were co-extruded with POPA liposomes, affect the size of the vesicles by far more than when they are simply added to preformed liposomes solutions (Table 5.5).

Table5.5. LS results for POPA liposomes with and without Oligos in phosphate buffer

sample	d [nm]	poly	I [Kcps]
POPA	102	0.088	48
POPA + 50dT	179	0.174	73
POPA + 50dA	112	0.114	49
POPA + 50dT co-extruded	317	0.235	87
POPA + 50dA co-extruded	178	0.188	68

poly=polydispersity; parameters obtained by cumulat analysis.

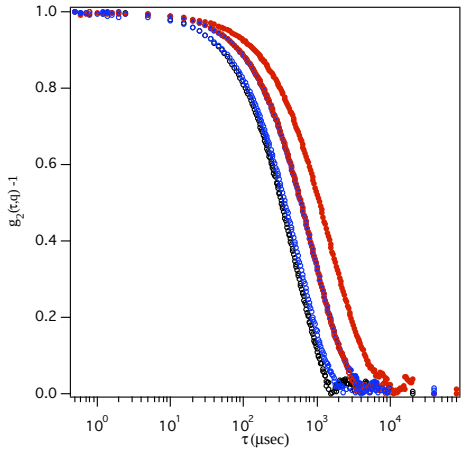

Figure5.26. Normalized autocorrelation functions of POPA liposomes and 50-mers in phosphate buffer solution: POPA black circles, POPA/50dT red circles, POPA/5dA blue circles, POPA/50dT co-extruded red full circles and POPA/50dA co-extruded blue full circles.

Spectroscopic measurements point out that adenosine bases on POPA headgroup interact with thymine bases of 50dT oligos. It is possible to observe hypochromism, which occur even when 50dA is used to hydrate the POPA lipidic film (Figure 5.27). This matches perfectly DLS data, confirming interactions are possible for not complementary strands as it was found out for polynucleotides by light scattering and Cryo-TEM analysis.

Circular dichroism analysis has been even performed highlighting different signals with respect to pure POPA and oligos in solution. Mainly, it is important to stress that the negative signal at 300 nm for both POPA and 50dT disappears. Remarkably, despite the different growth of hydrodynamic radii the same CD spectra is detectable for the two methods of sample preparation (Figure 5.28).

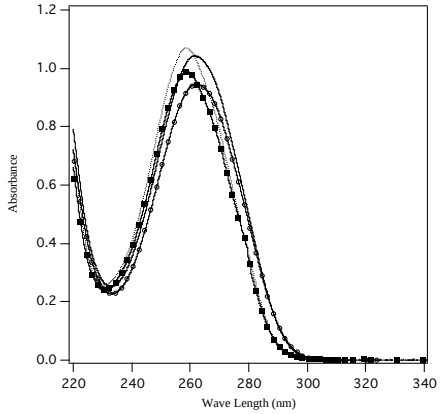

Figure5.27. Absorbance spectra of POPA and 50dT and 50dA co-extruded in buffer phosphate: circles POPA/50dT, square POPA/50dA, solid line simulated curve POPA liposomes and 50dT and dotted line simulated curve POPA liposomes and 50dT.

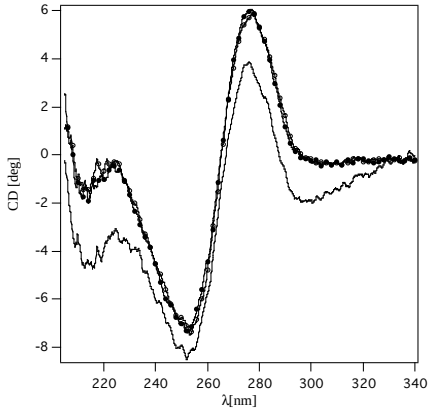

Figure5.28. CD spectra of POPA and 50dT hybrid structures in buffer phosphate: open circles POPA/50dT, full circle POPA/50dT co-extruded and solid line simulated spectrum of POPA liposomes and 50dT.

An equivalent study has been carried out in salted TRIS buffer. A light scattering investigation shows again a different trend with respect to polyN (Figure 5.29, Table 5.6). As in the case of POPA/oligos systems in phosphate buffer, in fact, 50dT affects more POPA liposomes than 50dA. This implies that complementary bases have a stronger interaction with respect to non-complementary as normally expected. Therefore, it is likely that other energetic contributes have to be taken into account for describing these particular systems when long polymer are concerned. A hypothesis is that polyA being more structured could trigger the interaction, in solution, such as for DNA, where cooperative effects are necessary for building up the double helix. Remarkably, in this buffer the R_H is smaller for "POPA/oligos co-extruded" with respect to "POPA/oligos added". This observation can find a confirmation in analysing circular dichroism spectra (Figure 5.30). In this figure, the stronger difference in

CD signals are detectable for the sample where 50-mers was simply added to pre-formed POPA liposomes.

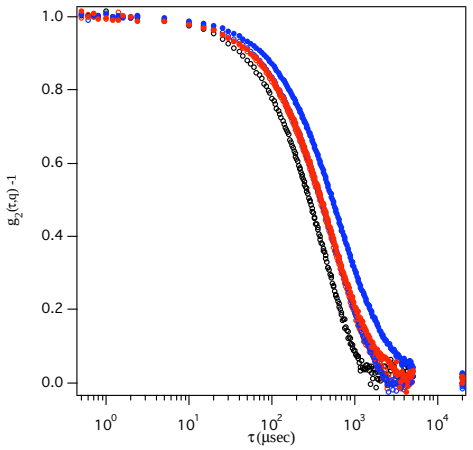

Figure5.29. Normalized autocorrelation functions of POPA liposomes and 50-mers in buffer TRIS 0.1M KCl 0.1M: POPA black circles, POPA/50dA red circles, POPA/5dT blue circles, POPA/50dA co-extruded red full circles and POPA/50dT co-extruded blue full circles.

Table5.6. LS results for POPA liposomes with and without Oligos in TRIS/KCl buffer

sample	d [nm]	poly	I [Kcps]
POPA	95	0.11	20
POPA+50dT	150		58
POPA+50dA	120		24
POPA + 50dT co-extruded	117	0.19	33
POPA + 50dA co-extruded	114	0.19	30.4

poly=polydispersity; parameters obtained by cumulat analysis.

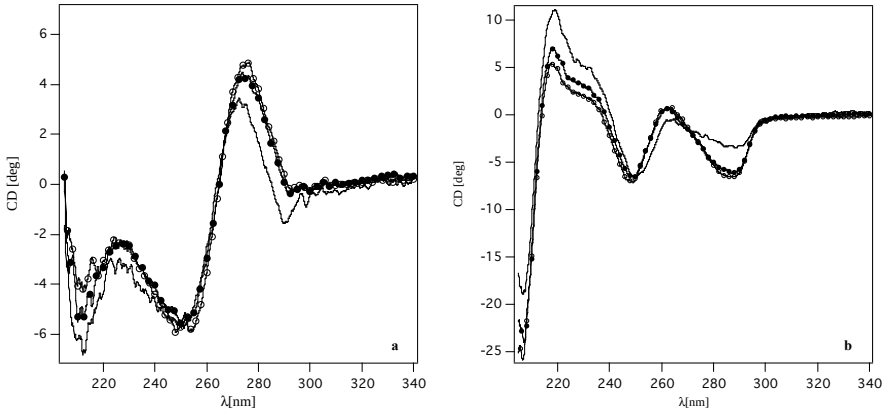

Figure5.30. a) CD spectra of POPA and 50dT hybrid structures in 0.1M TRIS 0.1M KCl. b) CD spectra of POPA and 50dA hybrid structures in 0.1M TRIS 0.1M KCl: open circles: open circles POPA/oligos, full circle POPA/oligos co-extruded and solid line simulated spectrum of POPA liposomes and oligos in solution.

UV spectroscopy (data not shown) indicates hypochromism for all the two methods of samples preparation and for complementary and not complementary bases, confirming the results obtained in phosphate buffer solution.

5.3 A Cryo-TEM investigation on Oligonucleotides and Nucleolipids Mixtures in solution

A Cryo-TEM investigation has been performed on POPN:POPC mixtures dispersion in water solution with and without addition of oligonucleotides. The necessity of this study was to answer the question of Chapter 3. Do the remarkable transformations obtained in lamellar phases when oligonucleotides were used to swell nucleolipids/POPC lipidic films, occur only in low water content, after drying and subsequent re-hydration, or do they occur before drying? That is, they take place in solution - they are thus visible in low water content - or *vice versa*.

In this study the solvent was pure water, so there is no influence or aid from buffer or ionic strength in the interaction between nucleolipids and oligonucleotides. For this reason, this analysis completes the study on the solvent effect in establishing the formation of hybrid structures between nucleolipids and oligonucleotides.

The samples were prepared without extruding to avoid possibly consequences due to the samples preparation as well. A comparison with POPG:POPC with and without oligonuclotides proves how the nucleic acid polar head of nucleolipids works in spite of the negative charge.

1:1 POPA:POPC dispersions appear in Cryo-TEM micrographs (Figure 5.31) to form mainly unilamellar vesicles. The interesting fact is that an untangled network of bilayers joins many of these vesicles, giving an explanation to the unexpected very high viscosity of these samples. This kind of structure is a novelty for POPC dispersion or mixture of lipids with long chains, which usually give vesicles in this environment and concentration (10mg/ml). The high viscosity and the web of bilayers are therefore due to POPA presence. These assemblies in solution can reasonably clarify the peaks separation observed in neutron diffraction that we have widely discussed in Chapter 2. In fact, we think that these nets of bilayers can be mainly made of POPA molecules determining clusters or rafts of this lipid when the infinite lamellar phase are formed by drying the dispersion over a glass for the neutron diffraction. An average bilayers spacing was measured from the micrographs and corresponds to around 60Å in good agreement with neutron diffraction (54 Å) considering a possible larger hydration in solution and even the Cryo-TEM resolution limit.

Adding warm (50ºC) aqueous solution of 50dT oligonuclotides to hydrate 1:1 POPA:POPC binary mixture instead of pure warm water, new structures appear in Cryo-micrographs (Figure 5.32). Fist of all, several multilamellar vesicles, not visible in the mixture without oligos, emerge (arrows D in Figure 5.32). The bilayer spacing of these multilamellar vesicles is around 53Å. Therefore, it is less thick

with respect to 1:1 POPA:POPC dispersion. On the other hand, the numerous fibers detectable in the micrographs are larger than 1:1 POPA:POPC bilayers, around 100 Å. This is very interesting because it matches closely the neutron diffraction measurements performed on the same sample at low water content. In that study, we found out two distinct lamellar phases having different spacing. And one of them, having larger bilayers spacing with respect to 1:1 POPA:POPC sample, was thought to be the membrane with the embedded oligonucleotides. Considering that POPA is an anionic lipid and has a larger area for polar head (~72 $Å^2$) with respect to choline headgroup of POPC (~60$Å^2$), it is possible that the multilamellar vesicles, as we imagined for the lamellae at smaller spacing in Chapter 3, is richer in POPC lipid.

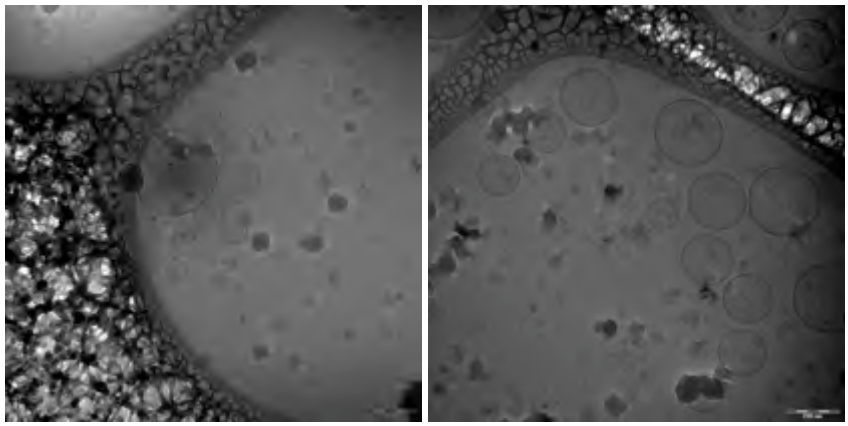

Figure5.31. Cryo-TEM micrographs of 1:1 POPA:POPC 10mg/ml in water.

As a result, the fibers, which, we think, encapsulate the 50dT oligonucleotides, are richer in POPA lipid. Many of these long fibers appear twisted in the micrographs (arrows B in Figure 5.32). Amazingly, despite the noteworthy similarity with the torsion in double helix DNA, the same kind of structure was found out by a recent investigation to be due to a different arrangement of adenosine polar headgroup in another nucleolipid derivative[26]. It is reasonably to presume that POPA changes its polar headgroup arrangement to form a complex with the complementary oligonucleotides. To confirm that strong interactions occur, there are present large aggregates that have no definite structure (arrows D in Figure 5.32).

Structures equivalent to the mixture without oligonucleotides are also detectable (see arrow A in Figure 5.32).

Remarkably, macroscopic differences were even found out during the samples preparation. The high viscosity, already discussed for POPA:POPC dispersion, vanished when 50dT oligonucleotides solution was added. This fact is proved by the loss of entangled bilayers network in the images of 1:1:1 POPA:POPC:50dT samples.

The same investigation performed on 2:3 POPA:POPC dispersions shows similar structures both in the samples with oligos than in the samples without

oligos. The only remarkable difference is that in this case any twisted structures was detectable in the mixtures with oligos, while several fibers even thicker than for 1:1 ratio were visible. Maybe a larger amount of POPC can explain this slight dissimilarity.

Even 1:1:2 POPA:POPU:POPC dispersion in water was investigated by Cryo-TEM. This system showed a larger separation of the Bragg peaks in neutron diffraction; that was assigned to the interaction between complementary bases of the nucleolipids POPA and POPU. As confirmation, the Cryo-TEM micrographs (Figure 5.33) display a wealthy of assembled structures already found for POPA:POPC mixture dispersions, though the general feature seems more emphasized. Moreover, some differences have to be mentioned: no pieces of lamellae inside the vesicles are visible, the entangled fibres are longer and resemble the fibres founded in the systems of POPA:POPC with oilgonucleotides, the micrographs highlight separated regions where are visible only unilamellar vesicles, as showed in Figure 5.33 A and some twisted fibers are detectable (arrows B in Figure 5.33).

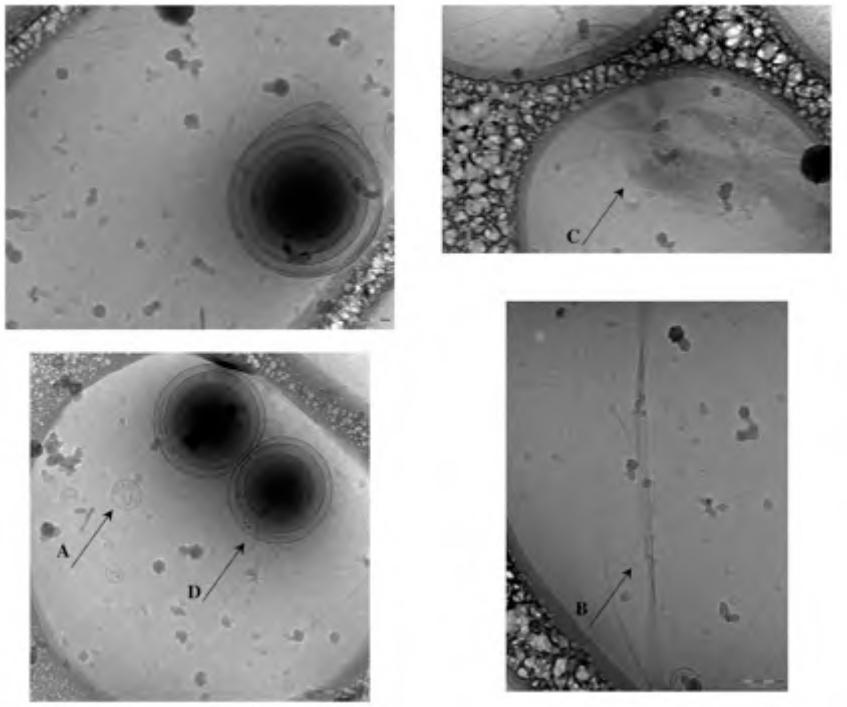

Figure5.32. Cryo-TEM micrographs of 1:1:1 POPA:POPC:50dT 10mg/ml in water.

This dissimilarity is likely due to the stronger interaction between complementary nucleolipids. H-bonding between A-U bases is added to the mere stacking between the adenosine bases in the dispersions where only POPA is present.

Adding complementary bases oligonucleotides (50d(AT)), new structures appear in Cryo-TEM images. Multilamellar vesicles are detectable (Figure 5.34 a) and several agglomerates of material show up (Figure 5.34 b). Furthermore, the disappearing of long filaments and of the unilamellar vesicles confirms that the interaction between nucleolipids mixtures and oligonucleotides occurs. The dense aggregates shown in Figure 5.34 b may give an indication that the interaction is slightly favoured or faster in this mixture where two different nucleolipids are present with respect to the systems with one nucleolipid. Remarkably, this matches perfectly the results of neutron diffraction in Chapter 3.

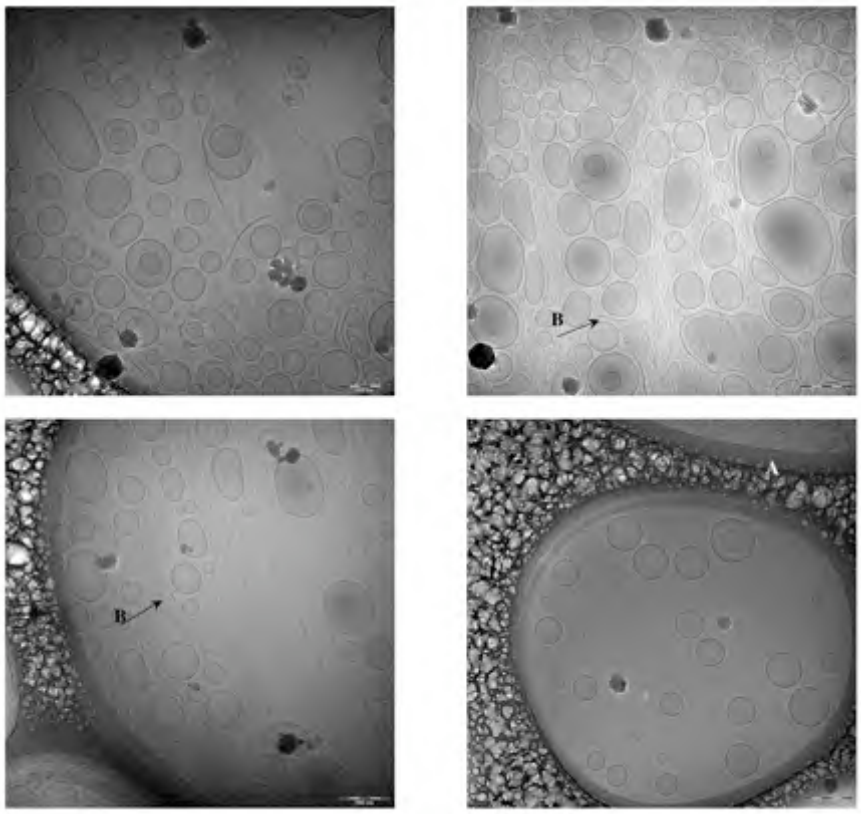

Figure5.33. Cryo-TEM micrographs of 1:1:2 POPA:POPU:POPC 10mg/ml in water.

As for POPA:POPC dispersion which was added oligonucleotides to, the appearing of these new structures explains presence of two lamellar phases in neutron diffraction experiments. This fact indicates that interactions take place in solution and then it is carried over into low water content regime.

To confirm this reasoning and to justify that no new lamellar phases shows up in neutron diffraction when oligonucleotides are added to POPG:POPC lipid mixtures, a Cryo-TEM investigation have been performed for these systems in water solution as well. Interestingly, 1:1 POPG:POPC water dispersion displays

multilamellar structures despite the average negative charge density on the bilayer plane (Figure 5.35). This is a strong difference with respect to 1:1 POPA:POPC dispersion where unilamellar structures indeed were found out. However, the difference in the solutions viscosity for these two systems supports the dissimilarity in the Cryo-TEM images. POPG:POPC water dispersion highlights the expected opalescence for these long chain lipid mixtures, as POPA:POPC dispersion does not.

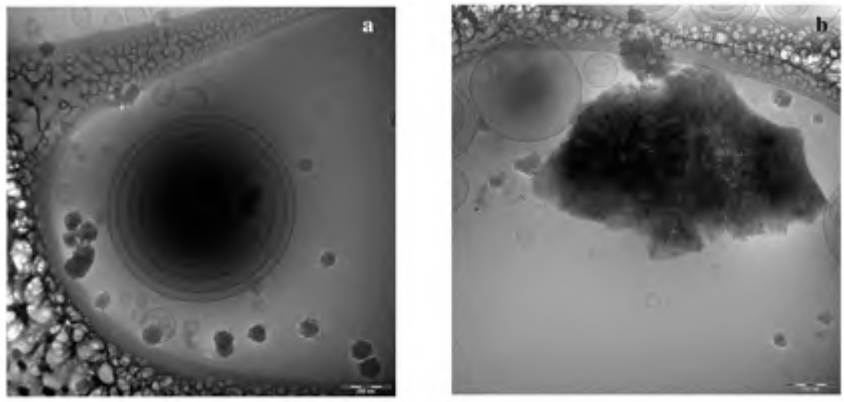

Figure5.34. a,b) Cryo-TEM micrographs of 1:1:2:2 POPA:POPU:POPC:50d(AT) 10mg/ml in water.

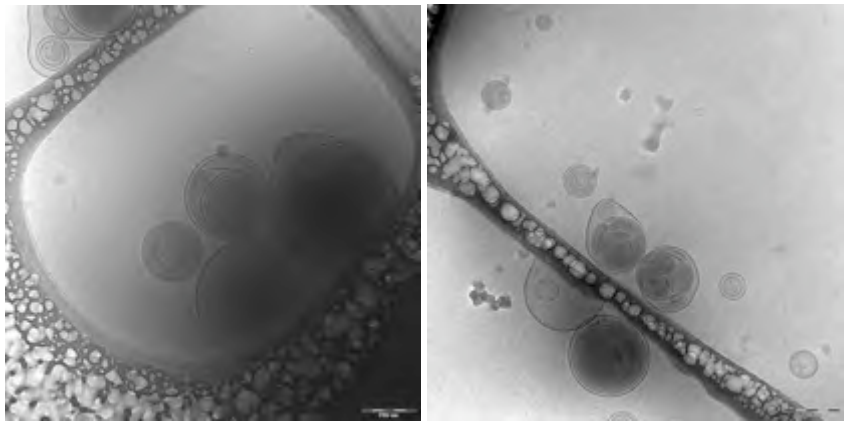

Figure5.35. Cryo-TEM micrographs of 1:1 POPG:POPC 10mg/ml in water.

When a warm aqueous solution of 50dT oligonucleotides was used to swell 1:1 POPG:POPC lipidic film (Figure 5.36). Multilamellar structures remain unperturbed by the oligo addition, even though more small unilamellar vesicles are present in the systems, indicating a destabilization in the multilamellar stacks. This is in agreement with the literature where no evidence of interaction between anionic lipid and nucleic acids was found without the aid of divalent cations[27]. Moreover, these images agree with our neutron diffraction results.

The previous results and the results obtained in this investigation confirm that molecular recognition capability of nucleolipids may be employed in design of new gene delivery vehicles.

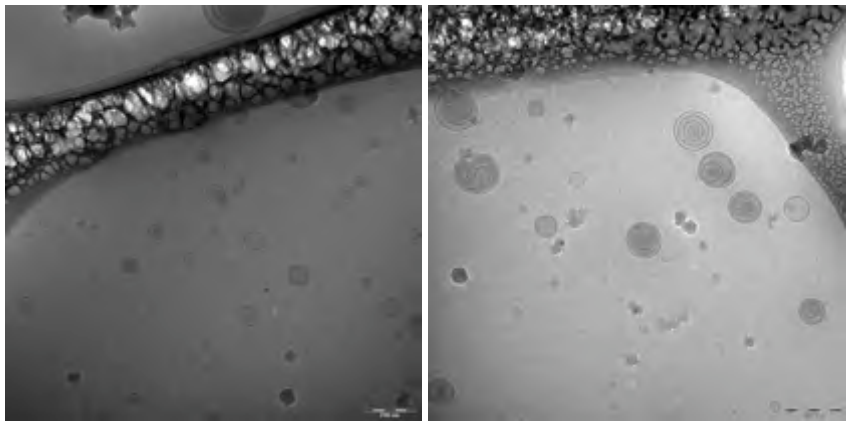

Figure5.36. Cryo-TEM micrographs of 1:1:1 POPG:POPC:50dT 10mg/ml in water.

Appendix:

$[lipid] = 0.5 mM$

$\langle d \rangle_{vesicles} \simeq 70 nm$

$d_{bilayer} = 40 Å$

$A_{polar-headgroup} \simeq 70 Å^2$

$$A_{vesicle} = 4\pi\left(\frac{\langle d \rangle_{vesicles}}{2}\right)^2 + 4\pi\left(\frac{\langle d \rangle_{vesicles}}{2} - d_{bilayer}\right)^2 = 2.74 \cdot 10^{-4}\, nm^2$$

$$N = \frac{A_{vesicle}}{A_{polar-headgroup}} = 39100$$

$$N_{vesicles} = \frac{N_{lipid-molecules}}{N} = 7.7 \cdot 10^{15}$$

Volume of vesicle at maximum packing, modelling vesicles as sphere, is:

$$V = \frac{4}{3}\pi r^3 \cdot N_{vesicles} \cdot \frac{\pi}{\sqrt{18}} = 1.02 \cdot 10^{21}\, nm^3$$

The total volume at maximum packing is: $10^{24} \cdot \frac{\pi}{\sqrt{18}}\, nm^3$

The volume occupied by each single object is:

$$V_d = \frac{V}{N_{vesicles}} = 9.6 \cdot 10^7\, nm^3$$

The radius of a sphere having the volume reported above is:

$R = 284\ nm$

therefore the distance between two sphere is: $2R - \langle d \rangle_{vesicles} / 2$

Considering that a nucleic base is about 6Å large, it is possible to calculate the number of bases (830) necessary to join two vesicles simultaneously.

Bibliography

(1) Algrem, M.; Edwards, K.; Karlsson, G. *Colloid Surface A* **2000**, *174*, 3-21.
(2) Riske, K. A.; Amaral, L. Q.; Dobereiner, H. G.; Lamy, M. T. *Biophys. J.* **2004**, *86*, 3722-3733.
(3) Hoffmann, H.; Thunig, C.; Munkert, U.; Meyer, H. W.; Richter, W. *Langmuir* **1992**, *8*, 2629-2638.
(4) Pabst, G.; Koschuch, R.; Pozo-Navas, B.; Rappolt, M.; Lohner, K.; Laggner, P. *J. Appl. Crystallogr.* **2003**, *36*, 1378-1388.
(5) Pabst, G.; Rappolt, M.; Amenitsch, H.; Laggner, P. *Phys. Rev. E* **2000**, *62*, 4000-4009.
(6) Bittman, R.; Blau, L. *Biochemistry* **1972**, *11*, 4831-4838.
(7) Parsegian, V. A.; Rand, R. P.; Rau, D. C. *Biophys. J.* **2000**, *97*, 3987-3992.
(8) Rand, R. P.; Parsegian, V. A. *Biochim. Biophys. Acta.* **1989**, *988*, 351-376.
(9) Lehtonen, J. Y. A.; Kinnunen, P. K. J. *Biophys. J.* **1994**, *66*, 1981-1990.
(10) Brahms, J. *J. Mol. Biol.* **1965**, *11*, 785-801.
(11) Uhrikova, D.; Hanulova, M.; Funari, S. S.; Khusainova, R. S.; Sersen, F.; Balgavy, P. *Biochim. Biophys. Acta-Biomembr.* **2005**, *1713*, 15-28.
(12) Bruni, P.; Pisani, M.; Amici, A.; Marchini, C.; Montani, M.; Francescangeli, O. *Applied Physics Letters* **2006**, *88*.
(13) McManus, J. J.; Radler, J. O.; Dawson, K. A. *J. Phys. Chem. B* **2003**, *107*, 9869-9875.
(14) Lu, D.; Rhode, D. G. *Biochim. Biophys. Acta.* **2001**, *1563*, 45-52.
(15) Spink, C. H.; Chaires, J. B. *J. Am. Chem. Soc.* **1997**, *119*, 10920-10928.
(16) Patil, S. D.; Rhodes, D. G. *Nucleic Acids Research* **2000**, *28*, 2439-2445.
(17) Patil, S. D.; Rhodes, D. G.; Burgess, D. J. *Aaps Journal* **2005**, *7*, E61-E77.
(18) Banchelli, M.; Berti, D.; Baglioni, P. *Angew. Chem.* **2007**, *47*, 3070 –3073.
(19) Milani, S.; Baldelli Bombelli, F.; Berti, D.; Baglioni, P. *J. Am. Chem. Soc.* **2007**, *129*, 11664-11665.
(20) Berti, D.; Bonaccio, S.; Barsacchi-Bo, G.; Luisi, P. L.; Baglioni, P. *J. Phys. Chem. B* **1998**, *102*, 303-308.
(21) Tanford, C. *J. Phys. Chem.* **1972**, *59*, 3020.
(22) Berti, D.; Franchi, L.; Baglioni, P. *Langmuir* **1997**, *13*, 3438-3444.
(23) Huebner, S.; Battersby, B. J.; Grimm, R.; Cevc, G. *Biophys. J.* **1999**, *76*, 3158-3166.
(24) Gustafsson, J.; Arvidson, G.; Karlsson, G.; Almgren, M. *Biochim. Biophys. Acta-Biomembr.* **1995**, *1235*, 305-312.
(25) Bennett, C. F. *Biochem. Pharma.* **1998**, *55*, 9-19.
(26) Baldelli Bombelli, F.; Berti, D.; Milani, S.; Lagi, M.; Barbaro, P.; Karlsson, G.; Brandt, A.; Baglioni, P. *Soft Matter* **2008**, *4*, 1-13.
(27) Filion, M. C.; Philips, N. C. *Biochim. Biophys. Acta.* **1997**, *1329*, 345-356.

Chapter 6

Complexes between Nucleolipid/liposomes and DNA

We have shown in the previous Chapter that single strands of DNA and/or RNA interact with nucleolipids/bilayered assemblies in solution. However, in dependence of the length of the polymer strand, different morphologies of complexes and different aggregates were found. In particular, it resulted that long strands of polynucleotides, having a secondary structure, might interact with non-complementary nucleolipid assemblies in some conditions of buffer and with some preparation methods. Therefore, it is possible that interactions may take place since other chemico-physical parameters have to be taken into account. Furthermore, we have proved by Cryo-TEM and Neutron Diffraction that stronger interactions occur between nucleolipids and oligonucleotides, when - in bilayered nucleolipid systems - H-bonding occurs between nucleic bases of complementary nucleolipid derivatives. It is worth reminding that cooperative effects are necessary to favour interactions, even between two negatively charged DNA single strands, whose strategy of interaction is ruled by million of years of evolution.

Since DNA solution and liposomes are both complex fluids with length scales in colloidal domain, a lot of parameters, both thermodynamic and kinetic, have to be considered. As reviewed in Chapter 4, concentration, temperature, ionic strength, surface charge and pH dramatically influence the morphology of complexes between cationic liposomes and DNA, as well as the kinetic of mixing and the order of mixing can give rise to path-dependent flocculation or precipitation.

While it is extensively acknowledged and reported that there are strong interactions between cationic liposomes and DNA thanks to electrostatic attractions among the charges, the interaction between DNA and neutral lipid or DNA and anionic lipids needs further investigation. Indeed, there are many cases where neutral and anionic liposomes have been showed not to affect DNA - as reported in this investigation for POPG as well -, but other results have to be mentioned. For instance, the interaction between DPPC and DNA has been proved[1], and it is a promising direction for understanding how genetic material can be efficiently

delivered into cells. However, the same authors were not able to reproduce the same interaction with neutral lipid DMPC and DNA, because of the different thermotropic state (fluid) of the lipid with respect to DPPC (gel) at room temperature.

As a result, if in principle it is possible to imagine encapsulation of double strand DNA within nucleolipids liposomes on the basis of our previous results on poly and oligonucleotides, more insights are necessary to explain which driving force are at the origin of this interaction.

A study on nucleolipids and ds-DNA (calf-thymus) has been carried out in different buffer solutions in the same way as for polynucleotides. The following paragraphs describe the results obtained, focusing on the structural characterization of the complex structures and on the kinetic of the complexation.

6.1 Structural and Spectroscopic investigation on Nucleolipids liposomes and ds-DNA

A study on nucleolipids liposomes and double strands DNA (from calf-thymus) has been performed in salted TRIS buffer (0.1M TRIS 0.1M KCl) and PBS where interesting results had been obtained on nucleolipids liposomes and polynucleotides. The sample preparation method was the same used for studying single strand nucleic acids; the correct amount of DNA solution was added to the already prepared liposomes or else a DNA buffered solution was used to hydrate the lipidic film.

POPA nucleolipids have shown stronger interaction with oligonuceotides and polynuceotides, both in solution and in the low water content regime; therefore, we have focus mainly on POPA nucleolipid in the investigation of the complexes with DNA, as described below.

A reference study with POPG/DNA systems indicates that DNA does not interact with “normal” anionic liposomes in those environments (salted TRIS and phosphate) at least without the aid of multivalent cations. It is indeed known that anionic lipids, such as POPG or DOPG can be used to destabilized lipoplexes, inducing DNA leakage[2-5].

Before describing the structural and spectroscopic data that were collected, it is worthwhile to stress that when DNA was co-extruded with nucleolipids we had to pass the sample solution through numerous polycarbonate membranes of different size (1µm, 800nm, 400nm, 200nm and 100nm). Otherwise the extrusion treatment was impossible because of the high pressure required or because of the extremely low speed of extrusion despite the low concentration of lipids. This is a very important feature because it could be an indication that large aggregate are forming. This procedure was necessary only for nucleolipids with DNA samples, given that simple POPA liposomes do not need this treatment. Interestingly, these steps are not required for preparing POPG/DNA co-extruded samples as well.

Light scattering experiments monitor differences between the samples prepared in different buffer solutions. However, the interaction - if it is measured in terms of diameter of particles or rate of particles growth - between ds-DNA and nucleolipids molecules results a fast phenomenon. In this scenario, the interaction might be defined as stronger with double strand DNA than with single strand oligonucleotides. These results are unexpected: in fact, if base pairing is the driving force, then coupling with single strands should be favoured over double strands. The hydrodinamic radii (R_H) increase for all samples containing DNA and nucleolipids and for both investigated buffers. However, some differences are detectable and the kinetic of particles growth is different using different buffer solutions (Table 6.1 and 6.2).

Table6.1. LS results for POPA 0.5mM liposomes with and without DNA 0.16 mg/ml in phosphate buffer

sample	d [nm]	poly	I [Kcps]
POPA after 2h	87	0.067	34
POPA after 1 day	103	0.125	53
POPA after 1 week	119	0.130	93
POPA+DNA after 2h	140	0.200	53
POPA+DNA after 1 day	303		76
POPA+DNA after 1week	1459		116
POPA+DNA co-extruded after 2h	250	0.200	110
POPA+DNA co-extruded after 3h	385	0.260	110
POPA+DNA co-extruded after 1day	2413		72

poly=polydispersity

Table6.2. LS results for POPA 0.5mM liposomes with and without DNA 0.16 mg/ml in TRIS/KCl buffer

sample	d [nm]	poly	I [Kcps]
POPA after 2h	88.0	0.090	16
POPA after 1 day	88.5	0.130	16
POPA after 1 week	90.0	0.150	15
POPA+DNA after 2h	94.0	0.140	19
POPA+DNA after 1 day	95.0	0.180	20
POPA+DNA after 1week	120.0	0.220	29
POPA+DNA co-extruded after 2h	80.0	0.150	21
POPA+DNA co-extruded after 1 day	92.5	0.220	23
POPA+DNA co-extruded after 3 days	#		22

poly=polydispersity, # bimodal distribution

Figure 6.1 summarizes the kinetic of DNA complexation highlighting the increase of relaxation times of the autocorrelation functions. After about 2 hours from the extrusion, the samples “POPA/DNA co-extruded” indicate that assemblies’ diameters are enormously larger than POPA liposomes. Even the polydispersity increases quickly. After three days it is, in fact, possible to see a precipitate. On the other hand, the samples where DNA was simply added to preformed liposomes highlights a slower kinetic of interaction between DNA and POPA liposomes; however, a precipitate appears after about ten days.

Just after few hours of the sample preparation, the autocorrelation curves for both the samples “added” or “co-extruded”, have a decay that cannot interpolated through cumulant analysis. This is an indication that the sample is a multimodal system. That is, there are different kinds of assemblies with detectably different particle size in solution. Thereby, a CONTIN inversion was applied to achieve an average distribution of the particles size in those samples.

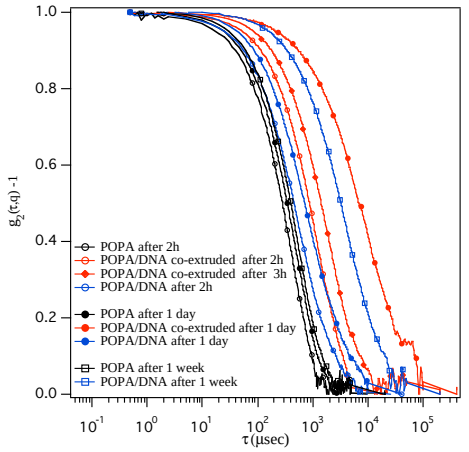

Figure6.1. Autocorrelation functions of POPA liposomes and DNA in buffer phosphate. The autocorrelation functions were normalized to assess the difference among the pure lipid dispersion (black) and the dispersion with DNA.

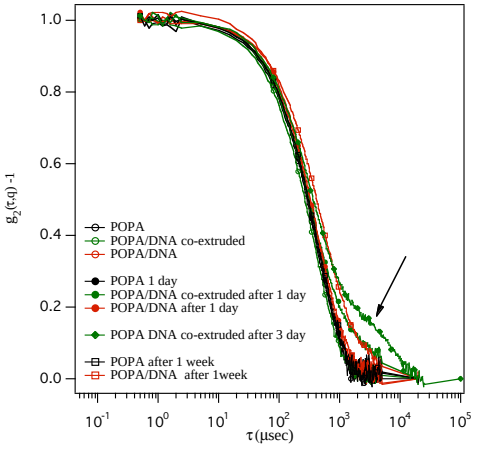

Figure6.2. Autocorrelation functions of POPA liposomes and DNA in TRIS/KCl buffer. The autocorrelation functions were normalized to assess the difference among the pure lipid dispersion (black) and the dispersion with DNA.

The interactions between DNA and liposomes of POPA in TBS (TRIS buffered saline) are less strong. The kinetic of complexation is slower than in buffer phosphate both for “POPA/DNA co-extruded” sample and for “POPA/DNA added”. It is possible that different growing mechanism occurs (Figure 6.2);

different types of assemblies might form due to the different buffer ionic strength. It is worth saying that DNA can be affected by monovalent cations in solutions[6-9]. Monovalent cations are not able to condense DNA, such as divalent[10,11], however, they play an important role in cell activity, especially Na^+ and K^+. Moreover, the deoxyribonucleic acid mobility changes in presence of monovalent cations, because they modify the H-bond structure of water[12]. It seems that the duplex rotation could be affected by the increase ionic strength and this is dependent on the nature of the cations. Moreover, the salt presence increases the melting temperature of DNA; that is, the double helix is stabilized. This stabilization could therefore decrease the interaction with DNA, giving an explanation of the different speed of interaction with nucleolipids liposomes.

As outlined by the arrows in Figure 6.2, for the sample where DNA was co-extruded with POPA after 3 days from preparation, two distinct decays appear in the autocorrelation function curve to point out that fast (small size) and slow (large size) assemblies are contemporaneously present in the dispersions. The Non Negative Least Squares (NNLS) analysis is shown in Figure 6.3. We choose to use this method for analysing this sample instead of CONTIN inversion because of the neat separation between the two distributions. The analysis reveals that there is a distribution of small particles whose hydrodynamic diameter is around 80-90 nm - possibly the particles that are not affected by DNA or not yet grown - and a distribution of large particles around 2000 nm.

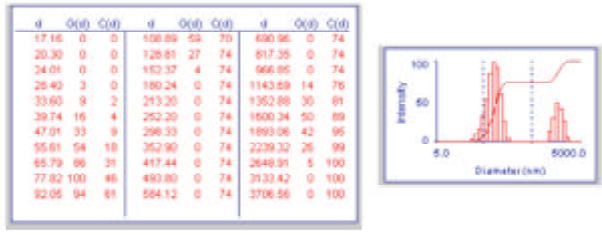

Figure6.3. NNLS fit result of POPA/DNA co-extruded 3 days old in TRIS/KCl buffer.

Interestingly, the scattering intensities are higher in phosphate buffer, as observed for POPA/polyN systems. However, the scattering intensities are neatly higher for samples with DNA in both the buffer solutions. Only the samples POPA/DNA co-extruded after 1 day records an intensity value lower than expected, considering even the large measured particles. This relies on the fact that probably the particles start precipitating.

UV spectroscopy highlights a tremendous hypochromism for all samples of POPA/DNA (Figure 6.4 a,b). Figure 6.4 collects some spectra recorded after a few hours from the samples preparation. Their results agree with the differences between the two buffer and methods of preparations observed with DLS. Hydrodynamic radii for POPA/DNA samples appear similar in salted TRIS buffer. On the other hand, the hydrodynamic radii are by far different in value for POPA/DNA in phosphate buffer. In fact, the dispersions have very different dimensions, depending on the preparation methods. Interestingly, the POPA/DNA

co-extruded samples in phosphate buffer presents a stronger hypochromism with respect to the other samples. This implies that the size of aggregate is an indication of the interaction between POPA liposomes and ds-DNA.

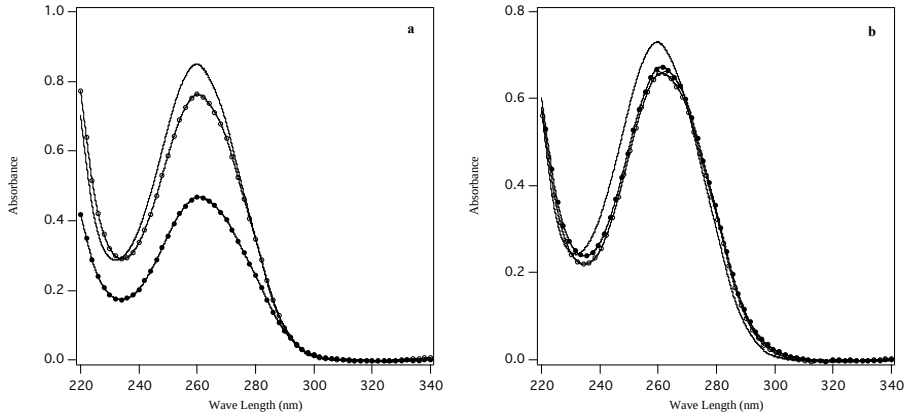

Figure6.4. a) Absorbance spectra of POPA and ds-DNA complexes in phosphate buffer. b) Absorbance spectra of POPA and ds-DNA complexes in 0.1M TRIS 0.1M KCl buffer: experimental spectrum of POPA/DNA circles, experimental spectrum of POPA/DNA co-extruded full circles and solid line computed spectrum of POPA liposomes + ds-DNA single spectra.

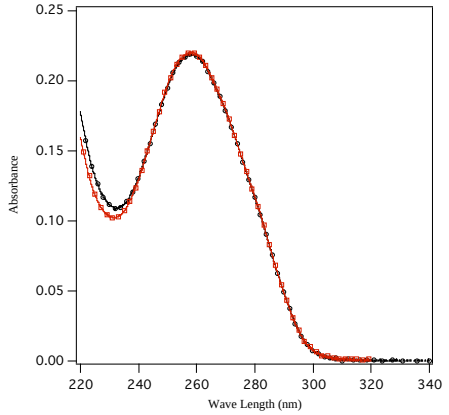

Figure6.5. Absorbance spectrum of ds-DNA (red line) and POPG/DNA (black line) dispersion in phosphate buffer.

The presence of hypocromism was unexpected for nucleolipids/DNA complexes. Nonetheless, this indicates that probably a component of interaction between nucleolipids and DNA is due to molecular recognition between the nucleolipids and DNA bases. At this stage, we have any further information to explain the mechanisms of this interaction, but stacking and/or H-bond of the nucleic bases occur. For the sake of clarity, any possible alterations in concentration due to extrusion processes have to be ruled out because hypochromism is detectable also for the samples prepared after the extrusion. Moreover, POPG/DNA samples

prepared following the same treatment than for POPA/DNA samples do not show difference in the DNA absorbance maximum (Figure 6.5).

To obtain further information on the structural modifications of these systems, we have performed a circular dichroism investigation. It is known that DNA is polymorphic: three structures at least exist in Nature, A-DNA, B-DNA and Z-DNA. These characteristics are caused by the particular conformation of the ribose moiety: B-form - the Watson-Crick structure - arranges 10.5 nucleotides per helix turn all in conformation *C2'-endo/anti*, A-form possess 11 nucleotides per turn all *C3'-endo/anti* and changes the structure making deeper the major groove while the minor groove becomes shallower. The Z-form displays much more changes with respect to the B-form (the most stable structure and common polymorph), there are 12 base pairs per helix turn, and the structure appears more slender and elongated. The DNA backbone takes on a zigzag appearance that results from the alternation of purines (*C3'-endo/syn*) and pyrimidines (*C2'-endo/anti*); thereby, it is more common when many CG residues are present. Therefore, every structure has a different CD spectrum[13]. Generally, B-DNA produces a positive band centred at 275 nm, a negative band at around 240 nm, which begins to be negative at around 260 nm, as reported in Figure 6.6 for calf-Thymus DNA in phosphate buffer solution pH 7.5. These bands are due to the overlap of the transitions present in all the bases. CD spectroscopy permits to assign the DNA secondary structures, but does not give the exact nucleotides sequence.

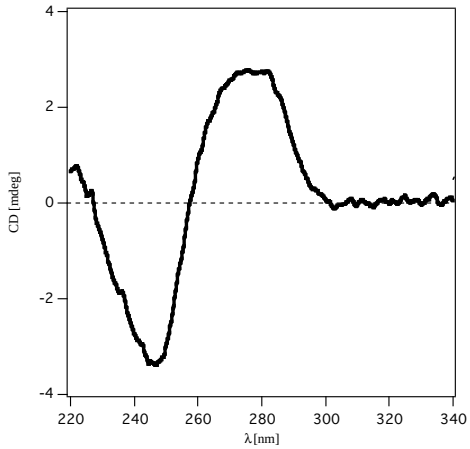

Figure6.6. CD spectrum of B-form of DNA concentration 0.16mg/ml in phosphate buffer.

Circular dichroism is also a useful technique to establish base pairing of a modified strand, which is mirrored by a change in secondary structure. This technique is useful when interactions between DNA and other molecules take place, therefore it is widely used in establishing liposome/DNA interactions[14-19].

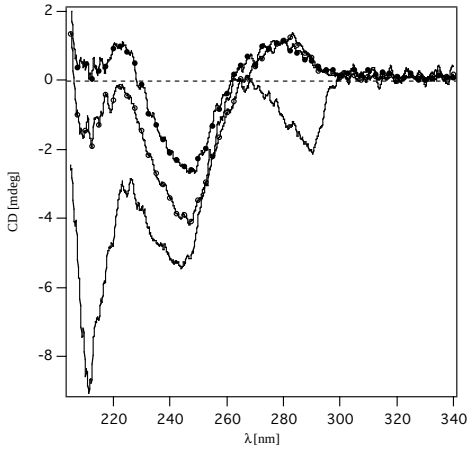

Figure6.7. CD spectra of POPA and ds-DNA complexes in phosphate buffer: experimental spectrum of POPA/DNA circles, experimental spectrum of POPA/DNA co-extruded full circles and solid line computed spectrum of POPA liposomes + ds-DNA single spectra.

Figure 6.7 shows the CD spectra of POPA/DNA systems in phosphate buffer. As for UV measurements, the spectra were recorded after a few hours from preparation to rule out any scattering interferences, which might occur for longer times. To detect DNA condensation or structural modifications is difficult in the case of nucleolipids/DNA complexes, since nucleolipids liposomes have a dichroic spectrum *per se*. However, the simulated spectrum, obtained from the pure spectra of ds-DNA and POPA liposomes in the same buffer, is dramatically different with respect to the experimental CD spectra of POPA/DNA. This proves the interaction, but it does not tell us which structural modifications these interactions cause.

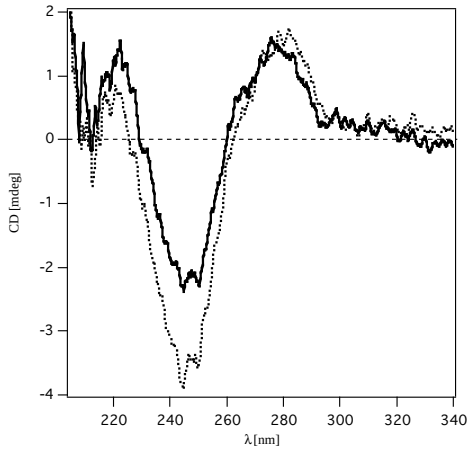

Figure6.8. CD spectra of POPA and ds-DNA complexes in phosphate buffer after 24h from the sample preparation: experimental spectrum of POPA/DNA dotted line, experimental spectrum of POPA/DNA co-extruded solid line.

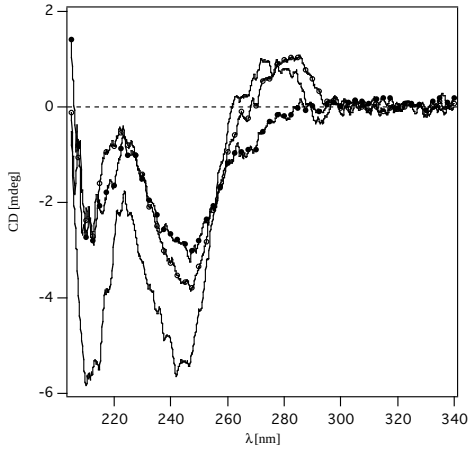

Figure6.9. CD spectra of POPA and ds-DNA complexes in TRIS/KCl buffer: experimental spectrum of POPA/DNA circles, experimental spectrum of POPA/DNA co-extruded full circles and solid line computed spectrum of POPA liposomes + ds-DNA single spectra.

However, some information can be obtained observing the results obtained after 24h from sample preparation (Figure 6.8). The sample where DNA was added, while increasing the hydrodynamic diameter, modifies the CD spectrum. After 24h this spectrum resembles the spectrum of POPA/DNA co-extruded after a few hours from sample preparation. The spectrum of POPA/DNA co-extruded does not show a time-dependence. All of these spectra look like the spectrum of B-DNA when the process of interaction occurs. Owing to the mild interaction and being the process non-stoichiometrically controllable, it is likely that not all the DNA added to the solution interacts with POPA liposomes or molecules.

Supporting the previous statement, a similar spectrum was also obtained for POPA/DNA in salted TRIS buffer (Figure 6.9), even though some variations exist between the two buffers. Some differences in the simulated spectrum allow for the different CD spectrum of POPA liposomes in these two buffers, as already described in Chapter 5.

6.1.1 Circular Dichroism on 50dAdT double strand

Circular dicroism and light scattering experiments have been also performed on samples of 50dA and 50dT single strands annealed to obtain 50dAdT double strands in both buffers solutions. Light scattering experiments (data not reported) confirm the measurements reported for calf-thymus. Therefore, larger particles with respect to POPA liposomes were obtained for ds-50dAdT added to POPA lipidic film. However, it is interesting to examine the circular dichroism spectra obtained as a function of aging and temperature for POPA/50dAdT (data have been collected only in salted TRIS buffer).

When solutions of 50dAdT are heated up 80ºC, the double strands show complete melting. The overlapping of their spectrum with the simulated spectrum

of 50dA and 50dT single strands at 80ºC both in UV and in CD spectroscopy (Figure 6.10) indicates this transition. On the other hand, when the POPA/50dAdT aged sample is heated at 80ºC in order to de-stack the bases, the dissimilarity with respect to simulated one are even stressed (Figure 6.11). Also the UV spectrum does not grow in terms of absorbance as much as the simulated one. UV spectra for POPA/50dAdT samples record a hypochromism that increases with the aging process, as well as for samples prepared from calf thymus DNA.

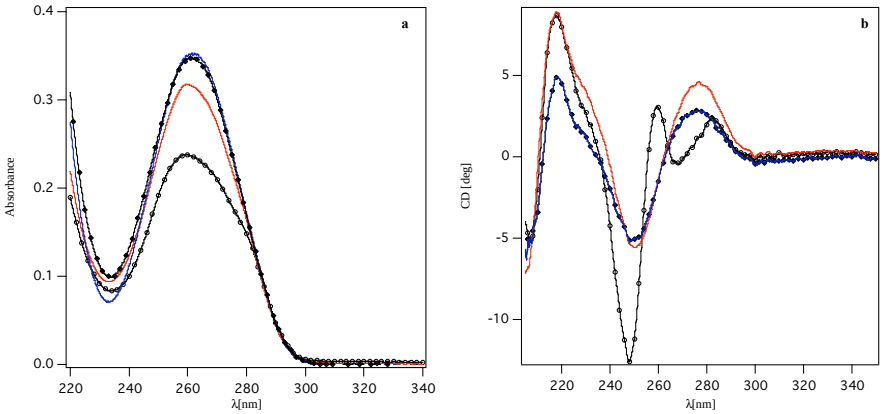

Figure6.10. UV (a) and CD (b) spectra ds-50dAdT in TRIS/KCl buffer: experimental spectrum of ds-50dAdT circles, red line computed spectrum of POPA liposomes + ds-50dAdT single spectra; experimental spectrum of 50dAdT full diamond at 80ºC and blue line computed spectrum of 50dA and 50dT single spectra at 80ºC.

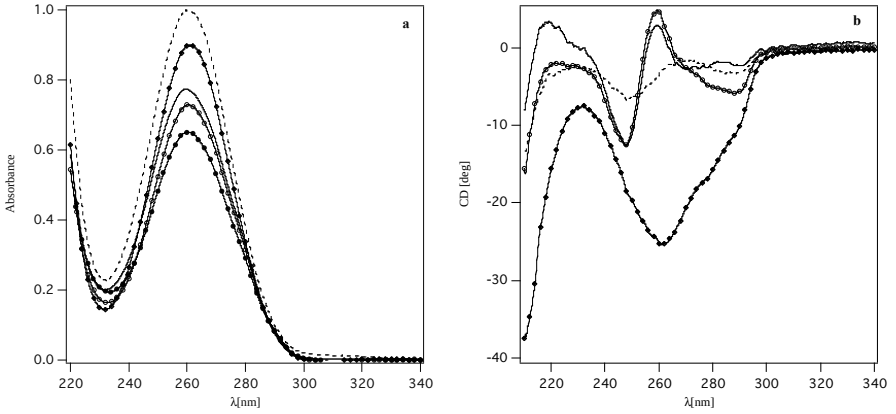

Figure6.11. UV (a) and CD (b) spectra of POPA and ds-50dAdT complexes in TRIS/KCl buffer: experimental spectrum of POPA/50dAdT circles, experimental spectrum of POPA/50dAdT aged sample full circles and solid line computed spectrum of POPA liposomes + ds-50dAdT single spectra; experimental spectrum of POPA/50dAdT full diamond at 80ºC and dashed line computed spectrum of POPA liposomes + ds-50dAdT single spectra at 80ºC.

Interestingly, the results of this investigation permit to conclude that the interaction with nucleolipids increases the stability of ds-DNA with respect to the temperature.

6.1.2 Detecting ds-DNA with molecular probes

The most common technique for measuring nucleic acids concentration is the reading of absorbance at 260 nm. In our case, though, we have problem with this measurement due to nucleolipid presence. Nucleolipids, as nucleic acids, absorb at 260 nm, making the evaluation of DNA concentration difficult for complexes nucleolipid/DNA, where hypochromism was effectively reported. However, there are many fluorescent probes that permit the evaluation of DNA concentration. These probes have been designed for several purposes, but certainly the necessity to distinguish between DNA and RNA is one of the most relevant reasons. It is commercially available an ultrasensitive fluorescent kit for quantifying DNA concentration in solution. This method was developed to minimize the fluorescent contributions of RNA and ss-DNA, likely present in solution. Thus, it is extremely useful in determining the amount of DNA that was not encapsulated or bound with nucleolipids in the nucleolipids/DNA samples.

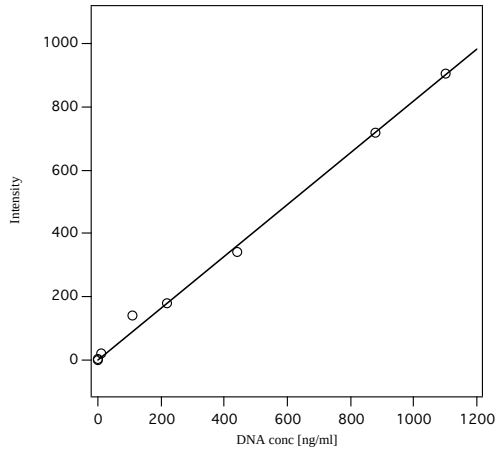

Figure6.12. Fluorescence emission intensity of PicoGreen (excited at 480 nm) vs concentrations of calf thymus DNA in 10mM Tris-HCl, 1mM EDTA pH 7.5.

This probe for ds-DNA, named PicoGreen, was purchased from Molecular Probes (Invitrogen). The calibration curve is reportes in Figure 6.12, where the fluorescence emission at 520nm is recorded after incubation of the samples for a few minutes.

Owing to the fast complexation kinetic of samples in phosphate buffer, only POPA/DNA systems in TRIS/KCl were investigated. Figure 6.13 shows the fluorescence intensity of PicoGreen, which was added to the POPA/DNA samples. Remarkably, the observed fluorescence intensities are smaller than the real ds-DNA

concentration used for preparing the complexes nucleolipid/DNA. In fact, about 825ng/ml should be the concentration for both DNA added to POPA liposomes and for DNA co-extruded with POPA, if there were no interaction between these molecules and all of the DNA were free in those solutions. This concentration should correspond in agreement with the standard plot of Figure 6.11 to about 680 fluorescence units. However, the value measured for the samples at 520 nm are by far smaller that the expected intensity value. Moreover, as expected, the samples where DNA was both inside than outside the liposomes, show larger complexation efficiency, being less the free DNA (about 141 ng/ml against 329 ng/ml) in this sample.

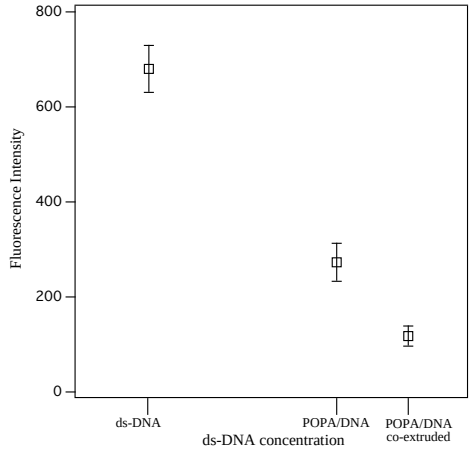

Figure6.13. Fluorescence emission intensity of PicoGreen (excited at 480 nm) vs ds-DNA concentrations in the sample "POPA/DNA added", in the sample "POPA/DNA co-extruded" and in ds-DNA aqueous solution (825ng/ml).

As a result, fluorescence measurements highlight and quantify that POPA nucleolipid is able to interact with ds-DNA, bringing a confirmation to the previous UV, CD and light scattering experiments.

6.2 Nuclolipoplexes by Optical Microscopy

In the previous paragraphs, we have shown that - unexpectedly - anionic nucleolipids were able to interact and to encapsulate DNA within their liposomes or lamellae. However, some differences between buffer solutions and methods of preparation can lead to different aggregates, having likely different morphologies and an optical growth kinetic. A microscopy study can show what structural differences are at the basis of these thermodynamic processes.

Optical microscopy was used due to the large size of the aggregates that appear after a few days from preparation. Moreover, this technique allowed us to observe precipitates from the POPA/DNA samples as well.

The micrographs of the precipitate from the sample POPA and DNA in phosphate buffer, display large structures, like twisted fibers or ribbons (Figure 6.14 a). To control if these structure were made of lipid lamellar phases, a cross polarization was used (Figure 6.14 b). As visible, the twisted ribbon shows strong birefringence, indicating lipid textures of nematic liquid crystal phases. Patches of material around the super-structure are not birefringent.

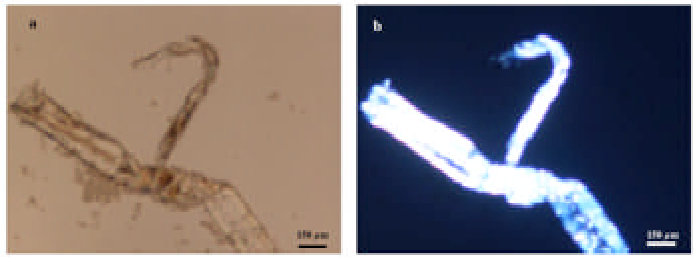

Figure6.14. a) optical micrograph of POPA/DNA co-extruded samples precipitate from phosphate buffer solution. b) the same image over cross-polarizer.

Different structures were found out for the samples in which DNA was added after preparation of POPA liposomes. No ribbons or well-defined fibres were visible under optical microscope. Figure 6.15 a,b shows a large structure of lipid liquid crystalline phases obtained after precipitation of that sample. Even in the "POPA/DNA added" precipitate there are many pieces of materials that do not display birefringence. These pieces are well detectable by means of phase contrast technique (Figure 6.15 c).

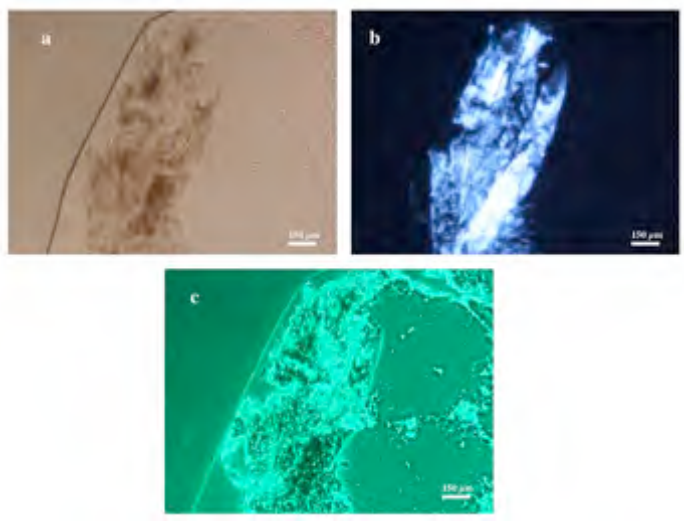

Figure 6.15. a) optical micrograph of POPA/DNA samples precipitate from phosphate buffer solution. b) the same image over cross-polarizer. c) the same image by phase contrast technique.

To check by fluorescence microscope the presence of DNA inside these lipidic textures, we have added a fluorescent dye (DAPI) for DNA. 4'-6-Diamidino-2-

phenylindole (DAPI) is known to form fluorescent complexes with natural double-stranded DNA. When DAPI binds to DNA, its fluorescence is strongly enhanced. DAPI binds to the DNA minor groove and it is stabilized by hydrogen bonds with acceptor groups such as AT, AU and IC base pairs. The samples were prepared adding DAPI to DNA buffer solutions before using them to hydrate POPA lipidic film or before addition to POPA liposomes. After two days from preparation, these dispersions where DLS detects large aggregated particles - within the range of detectability of optical microscopy -, were observed by optical and fluorescence microscope.

Figure 6.16 shows the micrographs for the sample POPA/DNA co-extruded in phosphate buffer. Interestingly, the same object that birefringes (Figure 6.16 a) under cross-polarized, is fluorescent (Figure 6.16 b) on selection of the wavelength of excitation. The object resembles the fibers already found in the precipitate, even though less twisted. It is worth stressing that these large structures were not detectable by DLS analysis – they are as large as dust and therefore settle.

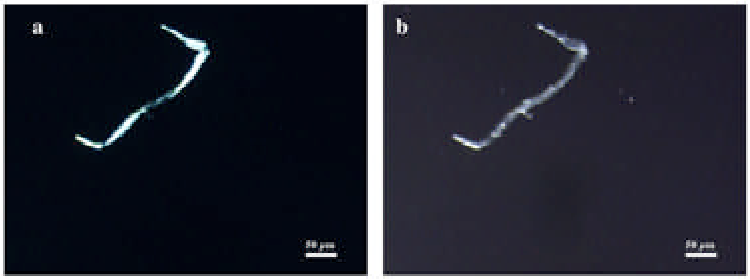

Figure6.16. a) optical micrograph of POPA/DNA/DAPI co-extruded in phosphate buffer over cross-polarizer. b) the same image by fluorescence microscopy.

Fluorescent and birefringent objects were found out for the sample where DNA was added to POPA liposomes, as well. In this case, other objects (see the arrows in Figure 6.17) close to the larger one were visible both under phase contrast and fluorescence, but they did not show birefringence.

Samples in salted TRIS contain similar structures that display birefringence and fluorescence (Figure 6.18). However, the sample where DNA was simply added, highlights very few objects of large dimensions in agreement with DLS where the polydispersity is even low (data not shown). These structures, as for POPA/DNA co-extruded sample, are smaller than the aggregates in phosphate buffers. Also the images of samples in TRIS/KCl display a wealthy of small particles that are active by fluorescence excitation, but they are not visible by cross-polarization.

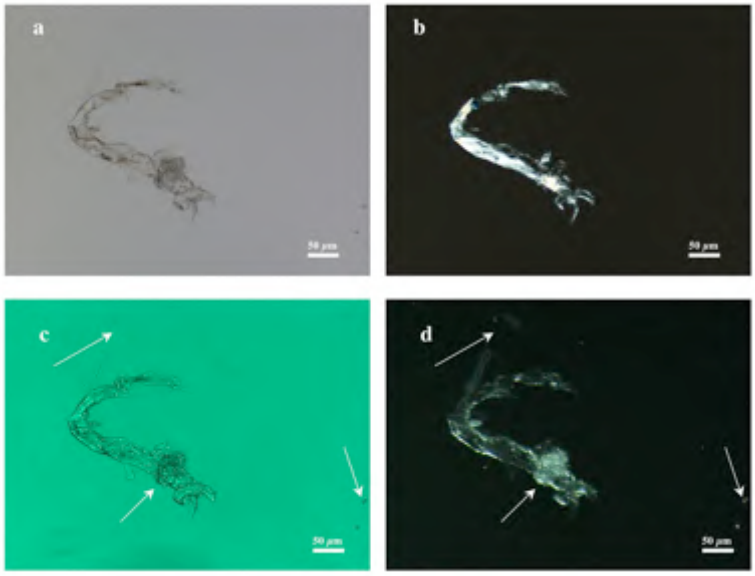

Figure6.17. a) optical micrograph of POPA/DNA/DAPI co-extruded in phosphate buffer. b) the same image over cross-polarizer. c) the same image by phase contrast. d) the same image by fluorescence microscopy.

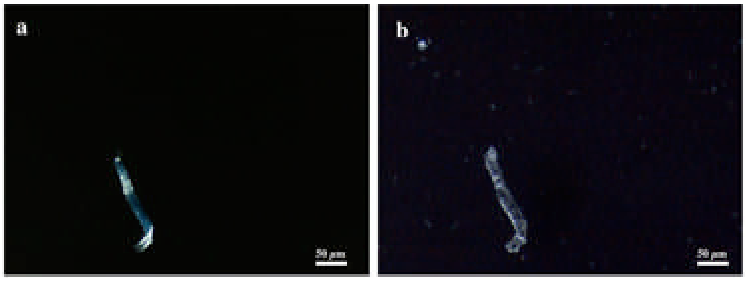

Figure6.18. a) optical micrograph of POPA/DNA/DAPI co-extruded in TRIS/KCl over cross-polarizer. b) the same image by fluorescence microscopy.

Bibliography

(1) Malghani, M. S.; Yang, J. *J. Phys. Chem. B* **1998**, *102*, 8930-8933.
(2) Caracciolo, G.; Pozzi, D.; Caminiti, R.; Marchini, C.; Montani, M.; Amici, A.; Amenitsch, H. *Appl. Phys. Lett.* **2007**, *91*, 143903.
(3) Caracciolo, G.; Pozzi, D.; Caminiti, R.; Marchini, C.; Montani, M.; Amici, A.; Amenitsch, H. *Appl. Phys. Lett.* **2006**, *89*, 233903.
(4) Caracciolo, G.; Pozzi, D.; Amenitsch, H.; Caminiti, R. *Langmuir* **2007**, *23*, 8713-8917.
(5) Koynova, R.; Wang, L.; Tarahovsky, Y.; MacDonald, R. C. *Bioconjugate Chem.* **2005**, *16*, 1335-1339.
(6) Bleam, M. L.; Anderson, C. F.; Record, M. T. J. *Proc. Natl. Acad. Sci.* **1980**, *77*, 3085-3089.
(7) Owczarzy, R.; Moreira, B. G.; You, Y.; Bahile, M. A.; Walder, J. *Biochemistry* **2008**, *47*, 5336-5353.
(8) Wissenburg, P.; Odijk, T.; Cirkel, P.; Mandel, M. *Macromolecules* **1995**, *28*, 2315-2328.
(9) Wissenburg, P.; Odijk, T.; Cirkel, P.; Mandel, M. *Macromolecules* **1994**, *27*, 306-308.
(10) Bloomfield, V. A. *Curr. Opin. Struc. Biol.* **1996**, *6*, 334-341.
(11) Bloomfield, V. A. *Biopolymers* **1997**, *44*, 269-282.
(12) Stellwagen, E.; Dong, Q.; Stellwagen, N. C. *Biopolymers* **2005**, *78*, 62-68.
(13) Rodger, A.; Norden, B. *Circular Dichroism and Linear Dichroism*; Oxford University: New York, 1997.
(14) Patil, S. D.; Rhodes, D. G. *Nucleic. Acids Res.* **2000**, *28*, 2439-2445.
(15) Patil, S. D.; Rhodes, D. G. *Nucleic. Acids Res.* **2000**, *28*, 4125-4129.
(16) Luciani, P.; Bombelli, C.; Colone, M.; Giansanti, L.; Ryhnen, J.; Sily, W. M. J.; Mancini, G.; Kinnunen, P. K. J. *Biomacromolecules* **2007**, *8*, 1999-2003.
(17) Ciani, L.; Casini, A.; Gabbiani, C.; Ristori, S.; Messori, L.; Martini, G. *Biophys. Chem.* **2007**, *127*, 213-220.
(18) Zuidam, N. J.; Hirsch-Lerner, D.; Margulies, S.; Barenholz, Y. *Biochim. Biophys. Acta-Biomembr.* **1999**, *1419*, 207-220.
(19) Prasad, T. K.; Gopal, V.; Rao, N. M. *Biochim. Biophys. Acta-Gen. Subj.* **2003**, *1619*, 59-69.

PART III

Chapter 7

Materials and Methods

7.1 Materials

POPC and POPG were purchased from Avanti Polar Lipids (Alabaster, AL) and their purity checked by thin-layer chromatography. The lecithins were used as received since no oxidation or lyso products could be detected. Adenosine, Uridine, SDS, Retinol (molecular structure chart 7.1), HCl, and NH_3 (33% aqueous solution) used in the synthesis and for experiments were purchased from Fluka (Buchs, Switzerland) such as KCl, Na_2HPO_4 and $NaHPO_3$ used for buffers preparation. TRIS buffer, MeOH and $CHCl_3$ were purchased from Sigma-Aldrich (St. Louis MO). Phospholipase D from *Streptomyces sp.* AA586 were bought from Asahi Chemical Industry (Tokyo, Japan). Polynucleotides acids (polyA, polyU) were acquired from Sigma-Aldrich, their molecular weight reported on the packages and measured by electrophoresis is around 800-1000kDa for both the polymers.

Deuterium oxide (>99.5%) for neutron diffraction measurements was provided by Euriso-Top, (Saclay, Gif sur Yvette, France).

Chart7.1. Chemical structure Retinol

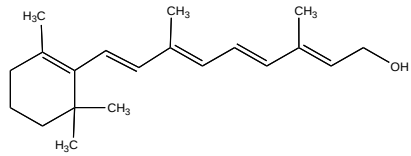

POPU and POPA were synthesized starting from the corresponding phosphatidylcholine in a two-phase system[1] according to a modification of the method proposed by Shuto and coworkers[2,3], and obtained as an ammonium salt. Separation from the by-products was achieved by silica-gel flash chromatography. Thin-layer chromatography and ^1H NMR were used to check their purity.

In some experiments, ammonium salts were converted in sodium salts for the needs described in the previous chapters. Ammonium salts were thus dissolved in

water and converted to sodium salts by titration adding the stoichiometric amount of 1M NaOH, followed by lyophilization.

All of the molecular structures for the nucleolipids, lipids and oligonucleotides used in this thesis are reported in chart 7.2.

Chart7.2. Chemical structures of lipids and oligonucleotides

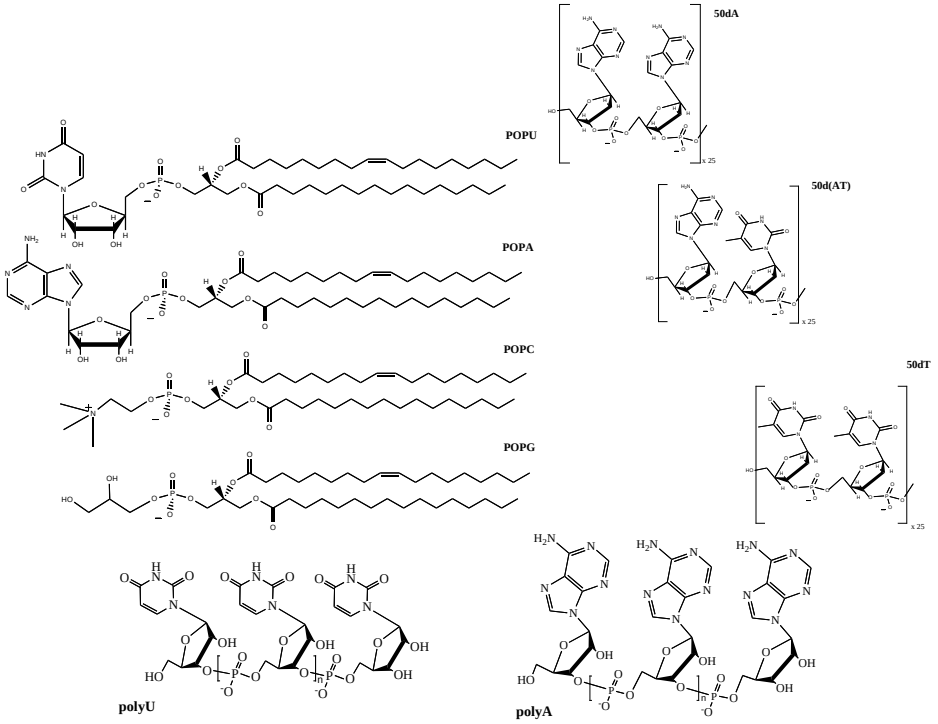

7.2 Sample Preparation

In low water content regime - Oriented samples for studying nucleolipid membranes:

About 20 mg of lipid lyophilized powder were dissolved in methanol/chloroform solution (4:1 v/v). The solution was deposited on a quartz microscope slide or a CaF_2 window for FTIR experiment using an artist airbrush. The slides were placed in a vacuum desiccator for 12 h in order to remove all traces of the solvent before re-hydration for 12 h at 37ºC in a K_2SO_4 saturated atmosphere (98% RH).

Assuming an average area for molecule of about 60 $Å^2$, about 700 bilayers were deposited.

In low water content regime - Oriented samples for studying nucleolipids membranes with helper lipids:

Oligonucleotides stock solutions were prepared by dissolving the lyophilized powders in water. For the preparation of the lipid mixtures proper amounts of POPC and anionic lipid (i.e., POPG, POPA) in chloroform/methanol stock solutions were mixed to get 1:1 and 2:3 mol/mol ratios. The organic mixtures were then dried under a nitrogen stream and allowed to dry overnight in vacuum desiccator. The dry bilayer stacks were swollen and suspended in warm (50ºC) aqueous solution (with or without oligonucleotides) by vigorous vortexing, followed by ten freeze-thawing cycles. Unilamellar liposomes are mandatory for obtaining well-ordered and uniform bilayers after dehydration. The high amount of anionic lipid guarantees unilamellar liposomes, without extrusion or sonication.

Oriented samples were obtained by spreading the dispersions onto quartz slides. The solvent was evaporated in a dust free environment at ambient relative humidity and temperature for 24h. Further drying of the lipid film was obtained leaving the slides in vacuum desiccator for at least 6h. Each sample was rehydrated before the measurement for 24h at 98% R.H. in the aluminium can used for neutron diffraction.

Each sample analyzed contained approximately 10 mg of lipid. The oligonucleotides amount was 1:1 mole ratio with respect to the nucleolipid headgroup (or POPG for the comparison experiment).

In low water content regime - Pastes:

About 10 or 20 mg of POPN sodium salt was weighted. The amount of solution (e.g., water or TRIS buffer 0.1M) required to obtain the correct lipid/water content was added by weighting and the sample homogenized by several cycles of centrifugation followed by freeze-thawing treatment to obtain a paste. A similar procedure has been used to add oligonucleotides. Oligonucleotides or polynucleotides dissolved in TRIS buffer were added to about 10 mg of liponucleoside sodium salt to obtain the wanted POPN/oligos ratio. The samples were homogenized by centrifugation and several cycles of freeze-thawing.

In the investigation of the hybrid systems, all of samples (with and without oligos) have been measured after preparation and after an annealing treatment. The annealing procedure consists of heating the samples at 50ºC and equilibrating them at 4ºC for about a week.

Pastes were sandwiched between CaF_2 windows or quartz slides in relation to the performed experiment (e.g., Infrared or Neutron Diffraction experiments).

In solution:

Lipid powders were weighted and then solved in a $CHCl_3$:CH_3OH 6:1 solution. A lipidic film was obtained evaporating the organic solvent under a stream of nitrogen and then the film was allowed to dry overnight. The lipidic film was further re-hydrated by a right amount of buffer solution to get the final concentration (usually 0.5 mM of lipid; differences in concentration are described in the texts). At the end, unilamellar liposomes were obtained by 10 freeze-thawing cycles and then by extrusion through polycarbonate membranes.

The samples were prepared in different buffers solutions: TRIS 0.1M buffer, Phosphate 0.1M buffer and TRIS 0.1/KCl 0.1M pH 7.5.

Polynucleotides, oligonucleotides or DNA were added to the lipid aggregated following two methods of sample preparation. In the first one, after swelling the lipidic film with the chosen buffer, liposomes were usually sized down by extrusion. After liposome preparation, a given amount of polynucleotides dissolved in the same buffer was added. In the second approach, the polynucleotide solution itself was used to swell the lipidic film and then the mixture was co-extruded.

7.3 Methods

7.3.1 Small Angle X-ray (SAXS and SAXD)

SAXS/SAXD experiments were performed on SAXS-WAXS Hecus X-ray system GMBH (Graz, Austria) containing 1024 channels. The working q-range was 0.05–6 nm^{-1} corresponding to Bragg's spacing of 120-1 nm. Cu Kα radiation of wavelength 1.542 Å was provided by a Seifert X-ray generator, operating at a maximum power of 2kW. The samples were mounted in kapton sample holder for pastes and in capillary for dispersions. To minimize scattering from air, the camera volume was kept under vacuum during the measurements. Temperature control within 0.1ºC was achieved using a Peltier element.

In a scattering experiment the scattering vector q is defined as the difference between the propagation vectors of the scattered (k_s) and the incident radiation ($\vec{k}_i$). For elastic scattering no change of the frequency occurs between incident and scattered radiation. Therefore, the scattered wavevector q is equal to $2\pi/\lambda$. This principle permit to obtained the common form of the scattering vector:

$$q = 4\pi/\lambda \sin\left(\theta/2\right) \tag{7.1}$$

The intensity scattered from a finite stack of unioriented bilayers is described by:

$$I(q) \approx \frac{\left\langle |f(q)|^2 s(q) \right\rangle}{q^2} \tag{7.2}$$

where q is the absolute value of the scattering vector, $f(q)$ is the form factor and $s(q)$ is the structure factor. The form factor characterizes the electron density distribution, and is given in the case of a layered structure by the Fourier transform of the electron density profile along z-axis:

$$f(q) = \int \rho(z) \exp(iqz)\, dz \qquad (7.3)$$

The structure factor accounts for the crystalline or quasicrystalline nature of the lattice of the bilayer stack in the lamellar phase.

The standard data analysis procedure consists in fitting the Bragg reflections with the appropriate structure factor multiplied by a constant form factor for each single peak. The electron density profile relative to the contrast electron density of the buffer is calculated by the Fourier synthesis, as described for Neutron diffraction experiments.

7.3.2 Neutron Diffraction Data Acquisition and Data Analysis

Neutron diffraction measurements were performed at the V1 membrane diffractometer (Berlin Neutron Scattering Centre, BENSC, Germany). The samples were placed vertically in an aluminum can at 98% relative humidity, adjusted by K_2SO_4 saturated aqueous solutions placed in a Teflon container at the bottom of the chamber. The temperature was controlled by a thermostat attached directly to this can. Contrast variation was achieved by changing the atmosphere composition, i.e., by varying the D_2O:H_2O ratio in the can (usually 8:92, 20:80, 50:50).

The diffraction intensity of the samples was measured with a rocking scan procedure, which consists in rocking the sample around the expected Bragg position θ by $\theta \pm 2^{o}$. The duration of each measurement around the Bragg position varied depending on the scattering intensity of the reflection, usually from 20 minutes to 6 hours.

The lamellar spacing d of each sample was calculated from the Bragg equation $n\lambda = 2d \cdot \sin\theta$ where n is the diffraction order and λ is the selected neutron wavelength (5.23 Å).

The structure factor amplitudes $|F(h)|$ were obtained from the square rooted integral of the Gaussian fit to the diffraction peak, followed by correction for absorption and Lorentz factor.

The absolute scattering length density (SLD) profile is given by

$$\rho(z) = \rho_0 + \frac{2}{d} \cdot \sum_{h=1}^{n} F(h) \cdot \cos\left(\frac{2\pi hz}{d}\right) \qquad (7.4)$$

where F is in units of the scattering length and ρ_0 is the average scattering length density per unit length of the bilayer. $F(h)$ are the scaled structure factors, and the sum describes the distribution of scattering length across the bilayer.

It is possible to obtain the real phase assignment by neutron diffraction following the isomorphous replacement method with the D_2O:H_2O exchange[4,5]. The structural functions are a linear function of the molar fraction of D_2O:H_2O, as shown in Figure 7.1. For all the data discussed in this thesis, only the scattering profile obtained at 8:92 D_2O:H_2O ratio was taken into account, because the

scattering length density of the water layer is zero at this contrast ratio[6]. At higher contrasts the large coherent scattering of the water layer hides that of the membrane.

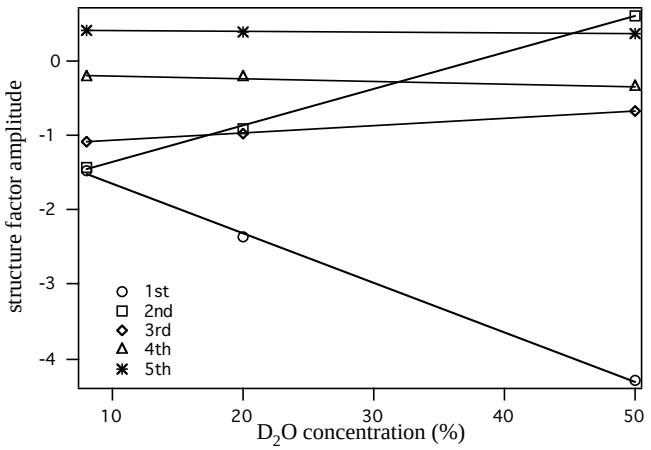

Figure7.1. Structure factor and its phase assignment using the D_2O/ H_2O exchange of a 1:1 POPG:POPC multilayers stacked mixture.

7.3.3 Light Scattering

DLS experiments were carried out on Brookhaven Instruments apparatus (BI 9000AT correlator and BI 200 SM goniometer). The signal was detected by an EMI 9863B/350 photomoltiplier, set usually at 90º with respect to the incident beam on the sample.

The light source was the second harmonic of a Nd:YAG diode laser (532 nm) Coherent Innova, linearly polarized in the vertical direction.

The autocorrelation function of the scattered light intensity was collected as time function. The data was analyzed according to the Siegert relation to get the field autocorrelation function $g_1(q,\tau)$:

$$C(q,\tau) = B\cdot[1 + a\left|g_1(q,\tau)^2\right|] \qquad (7.5)$$

As it is known, the field autocorrelation function $g_1(q,\tau)$ is related to the $g_2(q,\tau)$, which is the autocorrelation function of the scattered intensities in the approximation of Gaussian distribution:

$$g_2(q,\tau) = 1 + \left|g_1(q,\tau)\right|^2 \qquad (7.6)$$

The autocorrelation function describes the kinetic of the scattered intensity fluctuations that of course are dependent on the particle size. The variations in concentration, caused by the Brownian motions of the particles, provoke these fluctuations.

For more clarity of the figures the reported data were processed following a further normalization so that all the curves had the values between 0 and 1. So the field autocorrelation functions $g_1(q,\tau)$ were subtracted for their min value and then divided for the difference between their max and min values:

$$'g_1(q,\tau)' = (g_1(q,\tau) - g_1(q,\tau)_{\min})/(g_1(q,\tau)_{\max} - g_1(q,\tau)_{\min}) \qquad (7.7)$$

7.3.4 Fourier Transform Infrared Spectroscopy (FTIR)

Transmission:

IR spectra were collected with a Nexus 870 spectrophotometer (Thermo Nicolet, Paris.) equipped with a pyroeletric detector (DTGS-TEC). The samples were squeezed in two CaF_2 windows. All of the transmission spectra have been performed at room temperature with 2 cm^{-1} resolution and averaging 250 scans.

Linear Dichroism:

All of the IR spectra were carried out in a Nexus 870 spectrophotometer (Thermo Nicolet, Paris.) equipped with a liquid nitrogen cooled mercury cadmium telluride (MCT) detector. The resolution was 4 cm^{-1} and an average of 1500 scans was collected at room temperature. VLD, Vibrational linear dichroism measurements were achieved by using a static linear polarizer (Graseby Specac) or a photoelastic modulator (Hinds instrument PEM90). The experimental setup is sketched in Figure 7.2.

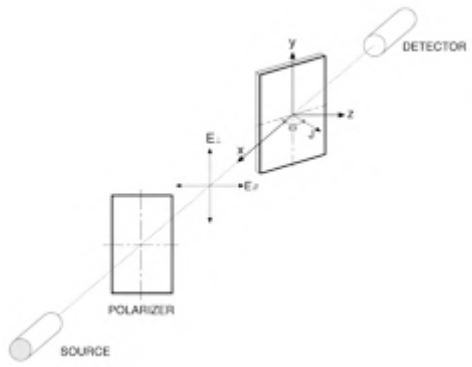

Figure7.2. Schematic drawing of the experimental FTIR setup; the polarized IR beam impinges the sample at an angle ⊥(90) or ω with respect to the bilayer normal.

Linear dichroism (LD) is the difference in adsorption of light polarized parallel and perpendicular with respect to an orientation direction. The intensity of the LD signal is related to the oscillatory strength of a transition and to the polarization of the transition with respect to the orientation axis. The LD signal and the dichroic ratio (D) are different from zero when the sample has a non-random orientation.

The dichroic ratio can be expressed as follows:

$$D = \frac{A_p}{A_s} \tag{7.8}$$

while the LD signal has the following definition:

$$LD = A_p - A_s \tag{7.9}$$

where A_p and A_s are the absorbance in the parallel and perpendicular direction, respectively[7-9].

Lipids membranes have linear dichroism equal to zero when the incoming beam is coincident with the membrane normal, however they yield linear dichroic signal when the sample orientation is varied[7]. Accordingly with the experiment setup showed in the figure, when the polarization is perpendicular, the angle between the incident light and the bilayer is 90° and it yields the absorbance spectrum, A_s. Rotating the sample with respect to the parallel-polarized light, the angle between the incident beam and the bilayer normal results ω. Table 7.1 shows typical angles at which we collected the measurements.

Table7.1. Sample setup parameters during FTIR measurements

ω*	$\cos^2(90-\omega)$
0	0.0
20	0.1
30	0.2
35	0.3
40	0.4
45	0.5
50	0.6
55	0.7

* rotation angle

If the z-axis of the molecular frame is chosen as coincident with the direction of a dipole transition, for a particular vibrational transition and uniaxial distribution, a relation between the dichroic ratio D and the order parameter S is given:

$$D = 1 + \frac{3S\cos^2(90-\omega)}{(1-S)n^2} \tag{7.10}$$

where n is the refractive index of lamellar liquid crystalline phase.

The order parameter associated to a given transition dipole can be calculated, provided n is known. The refractive index used for the calculations is n=1.4[7].

Upon ω variation the dichroic difference increases for oriented samples. As an example, the plot for CH_2 asymmetric stretching vibrations of POPA bilayers is reported (Figure 7.3).

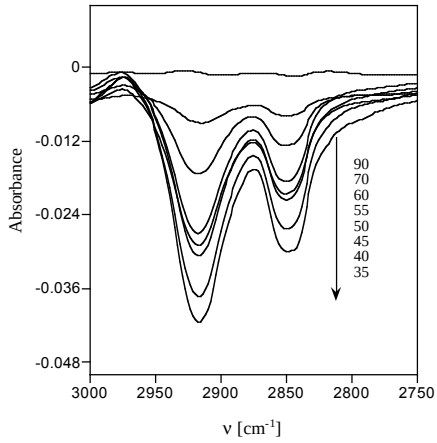

Figure7.3. D-1 vs. $\cos^2(90-\omega)$ for CH_2 asymmetric stretching vibrations of POPA.

7.3.5 UV and Circular Dichroism

Circular dichroism measurements were carried out on JASCO J-600 spectropolarimeter, using a 0.1 cm path length Hellma quartz cells.

Linearly polarized light is polarized in a certain direction (that is, the magnitude of its electric field vector oscillates only in one plane, similar to a sine wave). In circularly polarized light, the electric field vector has a constant length, but rotates about its propagation direction. Hence it forms a helix in space while propagating. If this is a left-handed helix, the light is referred to as left circularly polarized, and vice versa for a right-handed helix.

The electric field of a light beam causes a linear displacement of charge when interacting with a molecule, whereas its magnetic field causes a circulation of charge. These two motions combined result in a helical displacement when light impinges on a molecule. Since circularly polarized light itself is chiral, it interacts with a chiral molecule. In a CD experiment, equal amounts of left and right circularly polarized light impinge a sample. One of the two polarizations is absorbed more than the other one, and this wavelength-dependent difference of absorption is measured, yielding the CD spectrum of the sample.

Due to the interaction with the molecule, the electric field vector of the light traces out an elliptical path while propagating, thus it is defined elliptically polarized. The parameter describing this phenomenon is the ellipticity, θ, expressed in degrees. The molar ellipticity $[\theta]$, instead is given by the relation:

$$[\theta] = \frac{100\theta}{cl} \tag{7.11}$$

where c is for sample concentration and l is the path length of the quartz cell in cm^3.

Nucleic acid bases are not optically active molecules themselves; however, the ribose and deoxyribose sugars are asymmetric and being the bases attached to these sugars, the sugar can induce a CD in the absorption bands of the chromophoric bases. Moreover, the stacking interactions between the bases in a polynucleotide or DNA strand can increase the CD signals, usually low for a single base.

UV Absorbance spectra were collected with a Perkin-Elmer Lambda 900 spectrophotometer in the range 500-200 nm.

7.3.6 Cryo-TEM and Optical Microscopy

The Cryo-TEM pictures were obtained in the laboratory of Prof. Katarina Edwards in the Laboratory of Physical Chemistry, Uppsala University, Sweden. The Cryogenic Transmission Microscopy investigations were performed with a Zeiss EM 902A Transmission Electron Microscope (Carl Zeiss NTS, Oberkochen, Germany). The instrument was operating at 80kV and in zero loss bright-field mode. The method for sample preparation was in agreement with the procedure used in the Prof. Edwards's lab[10,11]. Thin sample films were prepared under well-controlled temperature (25 °C) and humidity conditions. Excess liquid was thereafter removed by means of blotting with a filter paper, leaving a thin film of the solution on the grid. Immediate after blotting the sample was vitrified by quickly freezing to 108 K in liquid ethane before being transferred to the microscope for examination. Samples were kept below –165°C and protected against atmospheric conditions during both transfer to the TEM and examination.

An Inverted Optical microscope (DIAPHOT 30, Nikon Co.) has been used to collect optical images. This instrument is provided of a cross polarizer and it is attached to a digital camera (Nikon Digital sight US-U1). Florescence images have been obtained thanks to an EPI-Fluorescence (Nikon) device fitted to this microscope.

7.3.7 Differential Scanning Calorimetry (DSC)

Thermal experiments were performed with Differential Scanning Calorimetry DSC-Q1000 (TA Instrument) using heating and cooling rates of 5ºC/min and 0.5°C/min. At least two runs were recorded for each sample. The range available for this instrument is from –90ºC to 400ºC, generally the measurements were carried out in a range of –15-40ºC.

Samples purity, after thermal analysis, was checked by TLC in order to verify possible lipids degradation.

Hermetic aluminium pan were used for these measurements.

Bibliography

(1) Berti, D.; University of Florence, Florence, 1997.
(2) Shuto S; Ueda S; Imnamura S, F. K., Matsuda A, Ueda T. *Thetrahedr. Letter* **1987**, *28*, 199.
(3) Shuto S; Ueda S; Imnamura S; Fukukawa K; Matsuda A; Tsujino M; T, U. *Chem. Pharm. Bull* **1988**, *36*, 209.
(4) Franks, N. P. *J. Mol. Biol.* **1976**, *100*, 3450-3358.
(5) Franks, N. P.; Lieb, W. R. *J. Mol. Biol.* **1979**, *133*, 469-500.
(6) Dante, S.; Hauss, T.; Dencher, N. A. *Biochemistry* **2003**, *42*, 13667-13672.
(7) Holmgren, A.; Johansson, L. B. Å.; Lindblom, G. *J. Phys. Chem.* **1987**, *91*, 5298-5301.
(8) Johansson, L. B. Å.; Lindblom, G. *Quarterly Reviews of Biophysics* **1980**, *13*, 63.
(9) Nillson, A.; Holmgren, A.; Lindblom, G. *Chem. Phys. Lipids* **1994**, *71*, 119.
(10) Bellare, J. R.; Davis, H. T.; Scriven, H. T.; Talmon, Y. *J. Electron Microsc.* **1988**, *10*, 87-111.
(11) Almgren, M.; Edwards, K.; Karlsson, G. *Colloid Surface A* **2000**, *174*, 3-21.

Chapter 8

Concluding Remarks

This investigation has been focused on the investigation of the interactions between negatively charged nucleolipids and nucleic acids (e.g., single strand oligonucleotides or double strand DNA). We have proved that it is possible to obtain hybrid structures built from associative interactions between these assemblies, despite the same charge of partners. We have highlighted that the formation of these assemblies, nucleolipids/oligonucleotides, relies on the same principles that lead a single strand of nucleic bases to pair with a complementary strand of bases notwithstanding the fact that they are both negatively charged. Molecular recognition, namely H-bonding and π-stacking between nucleolipid polar heads and nucleic acid bases, is thus the driving force of the interaction between these molecules. This evidence has been inferred from spectroscopic investigations through several techniques. The behaviour of nucleolipids in binary phases and the morphologies of their assemblies are very important parameters in determining further interaction with oligonucleotides. At this regard, it appears that adenosine derivatives can favour the embedding of oligos within the lamellar phases thanks to the stronger, compared to uridine derivatives, stacking interactions between the polar heads; a consequence of which is a not well-ordered lamellar phase[1,2].

In the first part of this work, a low water content regime has been studied to better highlight the interactions and to avoid effects arising from the choice of the buffer and concentration. Remarkably, nucleolipid membranes can encapsulate oligonucleotides in this environment. The formation of a new phase[3], termed L_{α}^{c} in analogy with lipoplexes, arising from oligonucleotides' ordering, has been detected only for POPA nucleolipid lamellae and complementary oligos, whereas POPU membranes seems to be too ordered and structurally without defects to give rise to a structural transformation that guarantees the oligonucleotides order.

The same behaviour was found analysing mixed membranes of nucleolipids with POPC, where molecular recognition between the bases of the nucleolipids in the sample without oligos, favours further interactions with oligos especially for the mixture containing both complementary nucleolipids (POPA/POPU/POPC)[4]. This feature was stressed both in the low water content regime by neutron diffraction

experiments and in solution analysing the dispersions by Cryo-TEM. The effect of the helper lipids was investigated. The morphology of POPA lamellae is affected by the presence of the neutral lipid, as it happens to cationic lipids-DNA systems. However, it is the nucleolipid nature to rule the interaction with oligonucleolipids, even if interesting similarities with neutral lipids and DNA bound by divalent cations deserve further investigations.

A different behaviour in determining the morphology of the final assembly was found out for different lengths of oligonucleotides. In particular, short 50-mers favour the interactions with nucleolipids made of complementary base both in solution than in low water content regime. However, if in low water content regime also complementary polynucleotides (long strand of hundred bases) interact with nucleolipids, whereas no interactions were detectable for non-complementary, in solution other features have to be taken into account to explain why polyadenilic acids affects so deeply POPA liposomes structures. Probably, this can be understood based on the cooperative effects that are necessary also to pair nucleic bases. Following this rationale, the interaction between nucleolipids liposomes and double strands DNA should be favoured, as it actually results. As a consequence, a precipitate was always found out after a few days from the sample preparation. This fact is remarkable not only because a precipitate is a demonstration that a strong interaction - tremendous structural transformations - takes place between partners (i.e., nucleolipids and DNA), but also that this system so different with respect to lipoplexes, where electrostatic forces are involved, follows similar steps in DNA complexation of lipoplexes.

The analysis of the dispersions is made difficult by the presence of buffers and possible differences in sample preparations. For example, it is difficult to understand why single strands of bases interact with nucleolipids liposomes in such a different way if TRIS or phosphate buffer are used. Nonetheless, a possible explanation of the slower kinetic of complexation in TRIS/KCl buffer than in phosphate buffer when double strands DNA and nucleolipids systems are concerned, can be found in the stabilization of double strands by salt presence. Anyway, the difficulty in understanding buffer effects is unexpected, because lipoplexes as well are enormously affected by buffer and sample preparation procedures; for examples different efficiency of DNA transfection were discovered *in-vitro* and *in-vivo* because of the serum components. However, we have shown that the experimental conditions can be tuned to obtain different morphologies of the final assembly, pointing out that many parameters can be changed for designing an efficient gene delivery system.

Florescence measurements indicate that nucleolipids liposomes can yield a good efficiency in DNA encapsulation. OligoGreen is withdrawn in interacting with double strand DNA when DNA is complexed by nucleolipids, proving thus that the nucleolipoplex might protect DNA while in transit.

In this investigation, we have also showed that this kind of hybrid structures can be formed only if the anionic lipid is a lipid with molecular recognition capability. All of the experiments were in fact performed for POPG anionic lipids and nucleic acids as well, showing that no interactions or assemblies between these

molecules and the same charged nucleic acids occur. No spectroscopic changes (UV and CD) were reported between POPG and nucleic acids with respect to nucleic acids in solutions. Moreover, dynamic light scattering experiments display no modifications in the hydrodinamic radii in solutions containing these molecules; the contrary often was reported for nucleolipids. In the low water content regime, we found out that oligonucleotides produce an osmotic stress upon the POPG membranes. POPG:POPC mixed membranes are slightly affected by oligonucleotides as proved by neutron diffraction, but the dispersions analyzed by Cryo-TEM show the same structures (multilamellar) both in the samples with and without oligonucleotides.

In conclusion, this study shows for the first time that it is possible to obtain hybrid systems between anionic lipids and nucleic acids without the mediation of divalent cations. It is worth reminding that observing molecular recognition in nucleolipids eases the interaction with complementary oligos and likely with DNA. This is an important guideline for the design and preparation of hybrid systems between nucleolipid/oligonucleotide.

It is the similitude between these systems, called nucleolipoplexes, and more common lipoplexes despite the different driving force of interaction to be a really remarkable result. This study, consequently, introduces a new paradigm in the research of strategies for delivering DNA or antisense oligonucleotides into the cells.

Bibliography

(1) Milani, S.; Baldelli Bombelli, F.; Berti, D.; Dante, S.; Hauss, T.; Baglioni, P. *Biophys. J.* **2006**, *90*, 1260-1269.

(2) Milani, S.; Baldelli Bombelli, F.; Berti, D.; Dante, S.; Hauss, T.; Baglioni, P. *J. Phys.: Condens. Matter* **2008**, *20*, 104212.

(3) Milani, S.; Baldelli Bombelli, F.; Berti, D.; Baglioni, P. *J. Am. Chem. Soc.* **2007**, *129*, 11664-11665.

(4) Milani, S.; Berti, D.; Dante, S.; Hauss, T.; Baglioni, P. *Langmuir* **in press**.

ACNOWLEDGMENTS

First and foremost I would like to thank my supervisor, the leader of the CSGI group, Prof. Piero Baglioni for giving me the opportunity to work in his group and to carry on the research on nucleolipids. I deeply thank Dr. Debora Berti for guiding my research, for the help and for the fruitful discussions that have increased my knowledge in this field.

I thank Prof. Katarina Edwards for the Cryo-TEM measurements and Dr. Silva Dante and Dr. Thomas Hauss for their help during the neutron diffraction experiments. I wish also to thank Prof. Michael F. Brown for the interesting conversations on biophysical chemistry.

Many thanks to all my fellow researchers and colleagues in the CSGI laboratories.

I am wholly grateful to my family for patience and support.

I acknowledge the CSGI (Consorzio Interuniversitario per lo sviluppo dei Sistemi a Grande Interfase), the Ministro dell'Istruzione, dell'Università e della Ricerca and the European Commission under the 6th Framework Programme for funding the research.